Defining the Functions and Regulation of *Clostridium difficile* Toxins A and B Enzymatic Activities in Cellular Intoxication

By

Nicole Marie Chumbler

Dissertation

Submitted to the Faculty of the

Graduate School of Vanderbilt University

in partial fulfillment of the requirements

for the degree of

DOCTOR OF PHILOSOPHY

in

Chemical and Physical Biology

May, 2015

Nashville, Tennessee

Approved:

Paul E. Bock, Ph.D.

Timothy L. Cover, M.D.

Brandt F. Eichman, Ph.D.

Lawrence J. Marnett, Ph.D.

D. Borden Lacy, Ph.D.

To my parents

Terry and Jayne Chumbler

Your love and support are unwavering.

and

to my best friend

Melissa Farrow

This would not have been possible without you.
I am forever grateful.

I love you all.

ACKNOWLEDGEMENTS

I am extremely grateful to Dr. Borden Lacy for the opportunity to work in her lab. She allowed me to follow the unexpected observations we made very early in my graduate career, which led us down new paths and to interesting discoveries. Borden's boldness and willingness to challenge 30 year old dogma required trust, and I am very honored and so thankful she could find it in me. Borden has made me a better scientist and a better speaker by forcing me to examine my data from every point of view. This was the project of a lifetime, and I could not have dreamed of a more fascinating one. I am so thankful to have been allowed to work on it.

This dissertation would not have been possible without the support, guidance, and mentorship given to me by Dr. Melissa Farrow. Melissa taught me to trust my data, how to think about it in a productive way, how to ask the right questions, and design experiments to answer them. She helped make me a better scientist than I ever thought I could be, and I cannot fully express my profound appreciation of her trust and support of both me and my data. I am also truly thankful for Melissa's friendship. Her love and kindness have largely contributed to my emotional, mental, and physical health. She and her family are now my family, and their love and support have meant the world to me.

I also greatly appreciate other members of the Lacy lab, particularly Ramya Chandrasekaran. Her humility and willingness to learn from others is refreshing, as is her eagerness to help and work as a team. I am so thankful for her attitude and friendship. Stacey Seeback crystallized the 1-1832 truncation of TcdA, and the structure has provided unforseen insights into toxin activity. Dr. Rory Pruitt was instrumental in introducing the Lacy lab to *C. difficile*. The early training I received from him was crucial to the development and understanding of my project. The entire Lacy lab has contributed in some way to my growth as a scientist, professional, or person, and I am grateful.

I am also greatly indebted to our amazing collaborators. Dr. Jim Goldenring, Dr. Lynne Lapierre, and Dr. Jeff Franklin were instrumental in the development and success

of our colonic explant model, which has been invaluable to the success, validity, and acceptance of our work. Dr. David Giedroc (Indiana University) and John Lisher performed the ICP-MS experiments we used to determine the function of zinc in the toxins. Dr. Erik Farquhar (Brookhaven National Labs) performed the XANES experiment in which we discovered zinc was the coordinated metal in TcdA.

The Vanderbilt University High Throughput Screening Facility was immensely helpful in conducting our small molecule inhibitor screen, particularly Dan Dorset and Michelle Williams. Dr. David Aronoff and Dr. Bruno Trindade performed mouse experiments, which helped us to make huge leaps forward in our identification of the target and function of our lead compound. Dr. Dena Lyras (Monash University) graciously shared her *C. difficile* isogenic knockout strains with us, which will be important in the delineation of the contribution each toxin makes to disease.

I would also like to thank Dr. Ben Spiller for his constant enthusiasm, challenging discussion, and valuable suggestions regarding my work. Likewise, I would like to thank the members of my committee: Dr. Paul Bock, Dr. Tim Cover, Dr. Brandt Eichman, and Dr. Larry Marnett. They have provided helpful scientific suggestions and have challenged me to become a better speaker.

I am also very thankful for the funding sources that have provided for this project: the VICB Pilot Project Funding, the National Institutes of Health NIAID, and the Chemistry Biology Interface training grant.

Finally, this would not have been possible without the love and support of my family and friends. My parents have supported all of my endeavors and aspirations physically, emotionally, and financially, and I would not have succeeded without them. My sister has been a much needed source of relaxation, fun, and distraction during my time in graduate school. All of my friends at Immanuel Church have supported me with constant prayers, encouragement, and reminders that this work was done to bring glory to God.

TABLE OF CONTENTS

LIST OF TABLES

Table Page

LIST OF FIGURES

LIST OF ABBREVIATIONS

aa	Amino acids
AC	Adenylate cyclase
ANOVA	Analysis of variance
APD	Autoprocessing domain
ATP	Adenosine triphosphate
BME	β-mercaptoethanol
BoNT	Botulinum neurotoxin
CDI	*Clostridium difficile* infection
CDTab	*Clostridium difficile* binary toxin
CHO	Chinese hamster ovary
CPE	Cytopathic effect
CROPS	Combined repetitive oligopeptides
CSPG4	Chondroitin sulfate proteoglycan 4
CT	Computed tomography
DAPI	4’,6-diamidino-2-phenylindole
DHP	Dihydropyridine
DTT	Dithiothreitol
EDTA	Ethylenediaminetetraacidic acid
ELISA	Enzyme-linked immunosorbent assay
EM	Electron microscopy
EPNP	1,2-epoxy-3-(pnitrophenoxy)propane
FDA	Food and Drug Administration
GAPDH	Glyceraldehyde 3-phosphate dehydrogenase
GDP	Guanosine diphosphate
GTD	Glucosyltransferase domain
GTP	Guanosine triphosphate
GT	Glucosyltransfer
H&E	Hemotoxylin and eosin
HMGB1	High-mobility group protein B1

HRP	Horseradish peroxidase
IACUC	Institutional Animal Care and Uses Committee
ICP-MS	Inductively coupled plasma mass spectrometry
ICU	Intensive care unit
InsP6	Inositol hexakisphosphate
LCT	Large Clostridial toxins
LDH	Lactose dehydrogenase
MLD	Membrane localization domain
NADPH	Nicotinamide adenine dinucleotide phosphate
NOX	NADPH oxidase
PCR	Polymerase chain reaction
PMC	Pseudomembranous colitis
ROS	Reactive oxygen species
SV40	Simian virus 40
TcdA	Clostridium difficile toxin A
TcdB	Clostridium difficile toxin B
TcdC	Clostridium difficile toxin C
TcdD	Clostridium difficile toxin D
TCEP	Tris(2-carboxyethyl)phosphine
Tcnα	Clostridium novyii α toxin
TcsH	Clostridium sordellii hemorrhagic toxin
TcsL	Clostridium sordellii lethal toxin
TeNT	Tetanus toxin
TpeL	Clostridium perfringens large cytotoxin
TPEN	N,N,N',N'-tetrakis(2-pyridylmethyl)ethane-1,2-diamine
UDP	Uridine diphosphate
VcRTx	Vibrio cholerae MARTX
VRE	Vancomycin resistant entercocci
VU HTS	Vanderbilt University High Throughput Screening
XANES	X-ray absorption near edge structure
YAMC	Young adult mouse colonic

CHAPTER I

INTRODUCTION

Clostridium difficile

Clostridium difficile is a Gram positive, spore-forming, anaerobic bacterium that is commonly found in the soil and can also colonize the colon of many mammals, including humans and livestock. *C. difficile* was discovered in 1935 when Ivan Hall and Elizabeth O'Toole isolated the bacteria from the stool of healthy infants [7]. *C. difficile* remained a poorly understood organism for many years, considered part of the normal flora of infants. Today, *C. difficile* is known as one of the most threatening nosocomial pathogens, making the mechanisms of pathogenesis important areas of investigation. *C. difficile* is an opportunistic bacterium as it is usually outcompeted by normal intestinal bacteria. Infection typically occurs after a perturbation, most often broad spectrum antibiotics, to the colon and its normal, healthy flora. *C. difficile* is inherently resistant to many commonly used antibiotics, including erythromycin, clindamycin, tetracycline, and moxifloxacin, allowing it to flourish in the absence of its non-resistant competitors [9]. Once *C. difficile* has colonized the colon, it can, like many *Clostridia* species, secrete large exotoxins that cause disease symptoms collectively known as *Clostridium difficile* infection (CDI).

Clostridium difficile Infection

Epidemiology

C. difficile is the most common cause of nosocomial diarrhea and was classified as one of the most urgent threats to patient health in 2013 by the Center for Disease Control with almost 500,000 infections and more than 29,000 deaths in 2011 [12]. Both

prevalence and mortality rates have more than doubled since 2007. Though a very small percentage of the population (3%) is asymptomatically colonized, most *C. difficile* infections occur in health care facilities [13,14]. An average of 30% of patients test positive for *C. difficile* at a given time in healthcare facilities across the country. It should be noted that prevalence and incidence vary drastically based on both geographic and demographic factors [9]. High incidence and easy transmission of the bacteria in hospitals and nursing homes is attributed to the production of hardy and resilient spores and the emergence of an epidemic strain, NAP1/027. Because spores are resistant to most cleaning solutions, an estimated 20-43% of hospital surfaces are contaminated, leading to overwhelming infection rates [9]. One study showed that of 399 patients testing negative for *C. difficile* upon admittance to the hospital, 21% tested positive for colonization over the course of their hospital stay. While most of these patients remained asymptomatic (63%), 37% developed CDI symptoms [15]. The NAP1/027 strain is thought to contribute to increased incidence and also more severe disease, with an overall mortality rate of 17% [9]. The epidemic strain has been shown to have increased toxin production [16], higher rates of sporulation [17,18], and increased antibiotic resistance [19].

Major risk factors for developing CDI symptoms have been identified as antibiotic therapy, advanced age (≥ 65 years), renal insufficiency, immunosuppression, comorbidities, presence of nasogastric tubes, recent gastrointestinal procedures, use of proton pump inhibitors, ICU admission, and duration of hospital stay [20]. The most understood of these is prior antibiotic therapy. An average of 96% of all CDI patients were on antibiotic therapy prior to the manifestation of symptoms [9]. The length of hospitalization is another well documented risk factor. Patients hospitalized for more than one week had a 15-45% chance of acquiring CDI, according to one study [21]. The opposite correlation is also well documented. CDI has been shown to lengthen hospital stays by an average 4-5 days, increasing costs of each stay by an additional $2,000-$14,000 [22,23]. CDI presents a significant burden to the United States healthcare system which has been estimated to surpass $4.8 billion each year [24-26].

Symptoms

C. difficile is most commonly ingested in the form of spores which can germinate in the duodenum in response to bile salts. The mechanisms of sporulation and germination are not well understood, though glycine and taurocholic acid have been implicated as components of bile that can initiate germination [27]. Colonization of the colon and risk of infection are greatly increased in patients that have received antibiotic therapy. Virtually every antibiotic has been associated with CDI. Clindamycin, fluoroquinolones, penicillins, and cephalosporins are commonly associated with and considered risk factors for developing symptomatic CDI [28-31]. Disease symptoms typically appear 4-9 days into antibiotic treatment and can span a wide range of disorders from diarrhea to potentially lethal fulminant colitis and toxic megacolon [32]. The most common symptoms include diarrhea, crampy abdominal pain, fever, and leukocytosis [32]. Pseudomembraneous colitis (PMC) is the most common complication of CDI [33]. PMC is described as severe inflammation accompanied by raised plaques (pseudomembranes) along the colonic mucosa. The plaques are usually small in size and contain fibrin, mucin, necrotic epithelial cells, and dead neutrophils [34]. Although rare, severe cases of CDI are described as fulminant colitis and/or toxic megacolon and are increasing in incidence (3-8% and 0.3-4%, respectively) [9,35]. These complications are often difficult to diagnose because of their sudden onset and consequently have alarmingly high death rates associated with their occurrence (30-90% and 38-80%, respectively). An estimated 20% of fulminant colitis patients present with abdominal pain in the absence of diarrhea [32]. Similarly, toxic megacolon is a condition in which the colon becomes paralyzed, ceasing peristalsis, and alleviating diarrheal symptoms. This allows for the accumulation of digestive gases leading to extreme dilation and swelling of the colon. Toxic megacolon can lead to bowel perforation and multi-organ failure, often resulting in death [33].

Diagnosis

There are many tests available to determine whether or not a patient is infected with *C. difficile*. The gold standard is a cell cytotoxin assay in which stool filtrate is applied directly to tissue culture cells and assessed for cytopathic effects (CPE) in 24 to

48 hours. This test is considered to be both sensitive and specific though quite time consuming. Several enzyme-linked immunosorbent assays (ELISA) have been developed for the detection of toxins secreted by *C. difficile* in stool. These are very specific but lack sensitivity. The return time for these assays can be as short as 6 hours, but there is a risk of false-negatives. *C. difficile* can also be cultured from the stool of infected patients. Though the turnaround time is quite long (2-5 days), this method of testing is specific, sensitive, and allows strain identification. Polymerase chain reaction (PCR) to detect the presence of toxin genes is another very sensitive and specific diagnostic test. This test is more expensive than others and can detect the presence of *C. difficile* in asymptomatic patients. Latex agglutination assays, which detect the presence of glutamate dehydrogenase, are also used to diagnose *C. difficile* because they are quick, easy, and inexpensive. This test, however, is not specific or sensitive to the presence of pathogenic *C. difficile* [9,33].

In addition to biochemical and microbiological tests, computed tomography (CT) scans are often used to rule out other causes of abdominal pain and to assess the severity of disease. Endoscopy is used to assess the colonic mucosa and diagnose pseudomembranous colitis. This procedure also allows the collection of stool samples for further testing. Most diagnostic guidelines discourage the use of a single test for accurate diagnoses [9,33].

Treatment

Upon CDI diagnosis, the preferred course of treatment includes stopping the initial antibiotic therapy and beginning oral metronidazole in cases of mild to moderate CDI. Symptoms resolve within 10 days in approximately 60% of patients. Metronidazole is preferred to vancomycin because of its lower cost and reduced risk of selecting for vancomycin-resistant entercocci (VRE). Metronidazole, however, has been reported to have a higher failure and recurrence rate than vancomycin. Vancomycin and early surgical intervention are recommended for the treatment of severe or complicated CDI. Subtotal or total colectomy is often required and can reduce mortality rates [9,33].

Some alternative treatments are proving to be quite effective. Fidaxomicin was approved for use as a CDI therapy in 2011, and has since been shown to be noninferior

to vancomycin in terms of cure rates and led to fewer recurrent infections than vancomycin in a number of studies [36-39]. Fidaxomicin is a particularly useful therapeutic in cases where the original antibiotic cannot be discontinued [40]. It is fairly specific to *C. difficile* and thought to be significantly less disruptive to the normal gut microbiota, making it a good option for the treatment of recurrent CDI [41-43]. Although considered investigational by the US Food and Drug Administration (FDA), fecal microbiota transplants have been effective in the treatment and prevention of recurrent CDI [44-46]. In this procedure, stool from a healthy donor is instilled in the gastrointestinal tract of a patient with CDI, thus replenishing the healthy, diverse microbiota that normally outcompete *C. difficile* [44]. In 2013, purified bacteria were lyophilized into pill form as "synthetic stool" as a more appealing alternative to fecal transplants. Limited data show some success with the synthetic stool in patients not responding to antibiotics [47].

Even less data support the use of other antibiotics (rifaximin, nitazoxinide, and tigecycline) as adjunct therapies in recurrent cases [48,49]. Teicoplanin has been shown to be noninferior to vancomycin, but is currently not approved for use in the United States [50]. Surotomycin and cadazolid are currently in Phase 3 clinical trials. There are also three human monoclonal antibodies with neutralizing activity against the toxins in Phase 3 clinical trials for use as a therapy to prevent recurrent CDI.

Recurrence

An estimated 20-30% of CDI patients will have at least one recurrent infection. Approximately 25% of patients will have their first recurrence within the first 30 days after clearance and after the second recurrence, the rate of recurrence more than doubles [51]. The mechanism of recurrence is not well understood, but it is well documented that the recurring infection can be caused by the same strain or a completely different strain (45%) from the original *C. difficile* infection [35]. Predicting which patients are at greater risk of recurrence has been quite challenging. Several studies have identified advanced age as the major risk factor. Studies have also correlated previous use of fluoroquinolones, antibiotic and proton pump inhibitor use after initial clearance, and insufficient immune response to higher incidence of

recurrence [52]. The recommended treatment for recurrent infections is a vancomycin taper. In high risk or multiple recurrent patients, a vancomycin pulse is frequently pursued along with adjunct therapies mentioned above. The high incidence of recurrence remains a difficult problem contributing to high mortality rates (10% increase compared to primary infections) and highlights the need for more effective therapeutics [9,33].

Virulence Factors of *C. difficile*

Many factors are thought to contribute to the virulence of *C. difficile*. Flagella [53,54], fimbrae [55], capsule [55], paracrystalline S-layer [56,57], adhesins [58], extracellular enzymes [59], cyclic diguanylate [60], and exotoxins [61-64] have all been implicated as virulence factors. Most, however, are poorly understood and their functions in disease pathogenesis are highly speculative. The functions of the exotoxins in disease are well accepted and the focus of many research efforts. *C. difficile* secretes three large toxins: a binary toxin (CDTab) [61,62], and the main virulence factors, toxin A (TcdA), and toxin B (TcdB) [65]. While CDTab has been shown to contribute to virulence, it is not present in all pathogenic isolates [66]. TcdA and TcdB have been clearly implicated as virulence factors, as purified toxins can replicate pathogenic hallmarks in animal models [67-69]. Additionally, TcdA and TcdB can be detected in the stool of patients and animals exhibiting disease symptoms, and antibodies recognizing TcdA have been isolated from CDI patients [70-73]. Notably, $TcdA^{-}TcdB^{+}$ strains have been isolated but portions of TcdB have been mutated to more closely resemble TcdA [74,75]. No $TcdA^{+}TcdB^{-}$ strains have been isolated thus far. Most recently, genetic knockouts of the toxins in the bacteria further implicate TcdA and TcdB as the main virulence factors and mediators of disease caused by *C. difficile* [63,64]. Understanding how *C. difficile* toxins cause disease has been delayed in part because of both the inability to manipulate *C. difficile* genetically and the absence of a recombinant expression system for the toxins. Much of the early work on TcdA and TcdB was performed using native toxin, which is not easily or abundantly purified. Both

of these problems are becoming less of an issue with the development and exploitation of genetic manipulation tools, like the ClosTron system [76,77], and the *Bacillus megaterium* expression system [78].

Pathogenicity locus

The genes encoding TcdA and TcdB are within the chromosome on what is known as the pathogenicity locus. The pathogenicity locus consists of 5 genes. The genes *tcdA* and *tcdB* encode the toxins; *tcdC* and *tcdD* encode two regulatory proteins; and *tcdE* encodes a holin-like protein [79-81]. Little is known about TcdE, though it has been hypothesized that it may form pores in *C. difficile* through which the toxins are secreted [80]. TcdC is a negative regulator and TcdD a positive regulator of toxin expression [79]. *C. difficile* strains of the epidemic ribotype NAP1/027 have a deletion in the *tcdC* gene that is thought to result in increased toxin production [16]. *In vitro*, TcdA and TcdB are expressed in stationary phase and correlate with a decrease in TcdC and an increase in TcdD expression [81]. Temporal expression of toxins *in vivo* is not well understood.

TcdA and TcdB are AB toxins

TcdA and TcdB are broadly classified as AB toxins. The A portion of the protein has enzymatic activity that is typically responsible for the function of the toxin and damage to host cells. The B portion binds to the host cells and delivers the A portion of the toxin into the cytosol (Figure 1.1). Many pathogenic bacteria secrete AB toxins including *Bacillus anthracis*, *Corynebacterium diptheriae*, and some of the *Clostridia* species. A subclass of AB toxins, termed AB5 toxins, is similar in function secreting 5 subunits of the B portion of the toxin, forming a pentamer. Pathogens that secrete AB5 toxins include *Vibrio cholerae*, *Bordetella pertussis*, and *Shigella dysenteriae*.

Large Clostridial Toxins (LCTs) are a subgroup of AB toxins secreted by some *Clostridia*. In addition to TcdA and TcdB from *C. difficile*, this group includes hemorrhagic (TcsH) and lethal (TcsL) toxin from *C. sordellii*, α-toxin (Tcnα) from *C. novyi*, and large cytotoxin (TpeL) from *C. perfringens*. The original domain assignments and much of the mechanism of toxin function was predicted for TcdA and TcdB based

upon homology to other LCTs and AB toxins. TcdA and TcdB consist of four functional domains and were thought to intoxicate cells via identical mechanisms, both resulting in apoptosis of the host cell. The enzymatic A portion of the toxins was identified as the N-terminal region and shown to glucosylate Rho-family GTPases. The C-terminal B portion of the toxins includes three domains with functions ascribed as autocleavage, pore-formation/delivery, and host cell receptor binding (Figure 1.1).

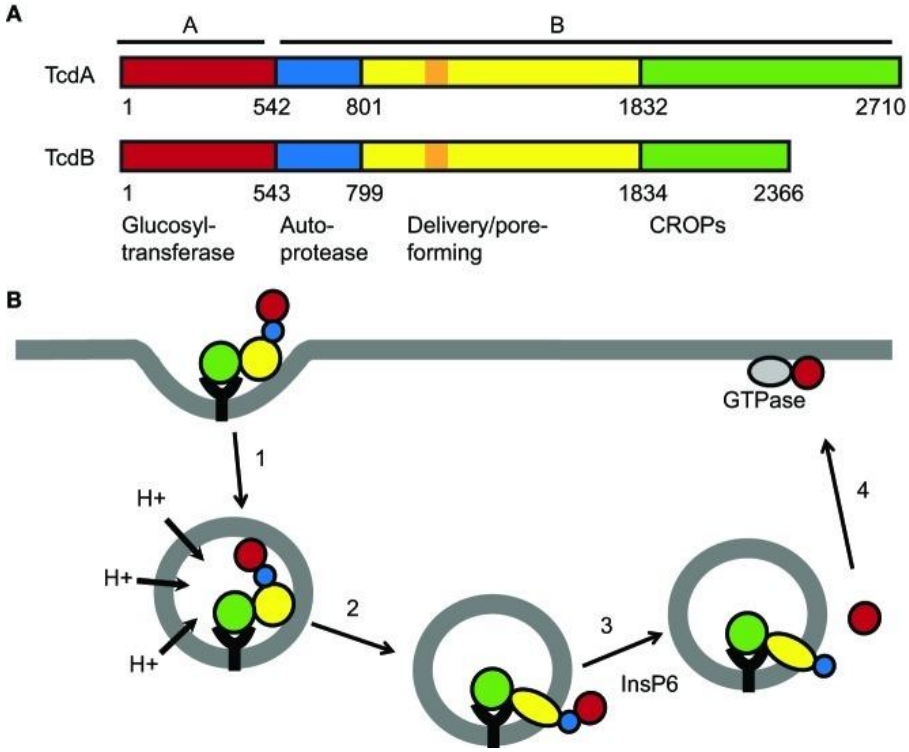

Figure 1.1. TcdA and TcdB primary structure and mechanism of cellular intoxication. A, TcdA and TcdB are homologous AB toxins consisting of four domains. The enzymatic A component is an N-terminal glucosyltransferase domain (GTD) (red). The B component, involved in delivery of the GTD into the cell, has three identified domains: combined repetitive oligopeptides (CROPs) (green), "delivery" or pore-forming (yellow), and autoprotease domains (blue). The orange box represents the hydrophobic region of the delivery domain that has been proposed to form part of the transmembrane pore (amino acids 956–1128 of TcdB). B, The delivery process is divided into four main steps that are mediated by each of the four domains. (1) The toxin binds to the surface of the cell and is internalized by receptor-mediated endocytosis. (2) Acidification of the endosome triggers the formation of a pore through which the GTD is translocated. (3) The GTD is released into the cytosol by InsP6 dependent autoproteolysis. (4) The GTD glucosylates Rho family GTPases at the cell membrane [6].

Host cell receptor binding

Host cell receptor binding was predicted to occur through the highly repetitive C-terminal portion of the toxin referred to as the CROPS (combined repetitive oligopeptides) domain, consisting of many 19-24 amino acid short repeats and 31 amino acid long repeats. TcdA CROPS contains 32 short repeats and 7 long repeats, while TcdB is significantly shorter with 19 short repeats and 4 long repeats [82,83]. This domain is defined as residues 1832-2710 and 1834-2366 in TcdA and TcdB, respectively [8]. Together, these repeats were shown to form cell wall binding motifs that could likely bind sugars [84,85]. TcdA CROPS was first shown to bind α-Gal-(1,3)-β-Gal-(1,4)-β-GlcNAc, which is not expressed in the human colon [86,87]. TcdA was later shown to bind human I, X, and Y blood antigen as well as glycosphingolipid [87,88]. Notably, these sugars contain the β-Gal-(1,4)-β-GlcNAc identified previously, but the functional relevance of these sugars as ligands in the colon have not been demonstrated. Structural studies have noted that the sugar binding pockets of TcdB have the opposite electrostatic charge of TcdA, providing structural evidence for the decreased affinity of TcdB for α-Gal-(1,3)-β-Gal-(1,4)-β-GlcNAc [8].

Two host cell proteins have been implicated in TcdA binding. Sucrose-isomaltase was identified as a potential receptor for TcdA in the ileum of rabbits [89]. Binding was inhibited by galactosidase, suggesting that the interaction between sucrose-isomaltase and TcdA was mediated by an unidentified glycosyl modification. Unfortunately, sucrose isomaltase cannot be the receptor facilitating TcdA induced pathology in humans as it is not expressed in the human colon [89]. The heat shock protein gp96 has also been identified as a potential host cell receptor for TcdA [90]. Consistent with previous data, gp96 is also predicted to be glycosylated, though the specific moieties remain unidentified.

Recently, chondroitin sulfate proteoglycan 4 (CSPG4) has been identified as a potential host cell receptor for TcdB [91]. Yuan *et al*. demonstrated that genetic knockout of the protein resulted in loss of CPE in tissue culture models. They also demonstrated direct interactions between residues 1500 and 1851 of TcdB and CSPG4. In a CSPG4 genetic knockout mouse, however, mice continue to die when injected

intraperitoneally with purified TcdB. These data suggest the potential for multiple receptors mediating toxin entry.

While the mechanism of host cell entry is not understood, both TcdA and TcdB are thought to enter cells via clathrin-mediated endocytosis [92]. Interestingly, it has also been shown that the CROPS domains of both toxins are not the only domains interacting with the surface of host cells. Truncations lacking the CROPS in both TcdA and TcdB have been shown to enter and induce cytopathic and cytotoxic effects, albeit with reduced potency [93,94]. These data lend further evidence to multivalent binding capabilities of the toxins. Identification of toxin receptors relevant to human disease and mechanism of toxin entry remain important areas of ongoing investigation.

Delivery

After binding and internalization, the toxin must deliver its enzymatic A portion into the cytosol. Based largely on analogy to other AB toxins, it is thought that TcdA and TcdB accomplish this translocation event with a pH sensitive conformational change in the endosome upon which the toxin forms a pore in the endosomal membrane. This function was ascribed to the central, hydrophobic one-third of the toxins.

Though evidence for the formation of a pore has yet to be shown, other aspects of the proposed model of translocation have been supported. TcdB was shown to undergo a conformational change in response to low pH using fluorescent probes and protease digests [95]. TcdB was also shown to form channels through which large ions, Rb^+, could pass both on cells and artificial lipid bilayers in response to low pH [96,97]. The hypothesis that this function is pathologically relevant was supported in tissue models with the pharmacological proton pump inhibitor, bafilomycin A1 [95,96]. Bafilomycin specifically targets the V-ATPase responsible for the acidification of endosomes [98]. Pretreatment of cells with the inhibitor prevented the CPE caused by TcdB. TcdA was also shown to form channels in cells and lipid bilayers. *In vitro* bilayer experiments revealed a requirement for cholesterol in TcdA channel activity [97].

Identification of the residues involved in pore formation has been difficult. A cluster of particularly hydrophobic residues in the middle of the delivery domain (aa 958-

1130 in TcdA and 956-1128 in TcdB) have been implicated as potential pore forming residues [82,85]. Genisyuerek *et al*. attempted to identify essential residues by investigating a series of TcdB truncations. They found that a fragment consisting of residues 1-1500 contained the complete translocation machinery necessary for cell intoxication. They noted that residues 830-1025 were sufficient to allow channel activity in lipid bilayers, though they were careful to acknowledge that channel activity and translocation machinery are not necessarily the same [99]. There are only two studies to date that identify specific residues involved in pore formation. One study identified two residues, E970 and E976, as residues that when mutated prevented channel activity in lipid bilayers and CPE on tissue culture cells [99]. The most recent study by Zhang *et al*. identified four residues with a 99% reduction in toxicity and no detectable channel activity. Based on striking homology to diphtheria toxin, they proposed a similar model in which TcdB inserts a double-hairpin into the endosomal membrane. The authors acknowledge that the model does not address the outstanding question of whether or not TcdA and TcdB form oligomeric pore structures [100]. These data present an exciting new avenue for investigation of the mechanism of pore-formation and translocation and how it relates to intoxication.

Autocleavage

LCTs are synthesized and secreted as single polypeptide chains. As in other AB toxins, however, the enzymatic A subunit was thought to be released into the host cell cytosol. It was, therefore, assumed that the LCTs undergo a cleavage event that releases the A subunit after translocation into the cytosol. The N-terminal A subunit of TcdB was shown to be released into the host cell in 2003 [101]. A couple of years later, the cleavage site was identified as the amide bond between residues Leu543 and Gly544 [102]. This proteolytic event was also shown to be dependent upon a host cell factor, presumably a protease. Reineke *et al.* instead identified host cell inositol phosphates as the essential activator mediating the apparent autoproteolysis. Inositol hexakisphosphate (InsP6) was shown to be the most efficient activator, though InsP3 and InsP4 were also effective. In the absence of host cell lysate, purified InsP6 was sufficient to induce TcdB autoprocessing [103].

The autoproteolysis of TcdB was first attributed to aspartyl protease activity using epoxy-3(p-nitophenoxy)propane (EPNP) which specifically modifies protease active aspartates. EPNP was shown to inhibit autoprocessing in TcdB and Asp1665 was identified as the covalently modified residue [103]. This report was quickly contradicted and the autocatalytic activity of TcdA and TcdB was demonstrated to be dependent upon cysteine protease activity [104]. Based on homology to the *Vibrio cholerae* MARTx (VcRTx) toxin, an AB toxin also shown to have cysteine protease autoprocessing activity, the autoprocessing domain (APD) was identified and localized to the region directly C-terminal to the enzymatic A subunit released into the host cell. These observations were confirmed with site-directed mutagenesis of the proposed catalytic site residues (Cys698, His653 and Asp587 in TcdB) and cysteine protease inhibitors that covalently modify the catalytic cysteine [104].

Since this report, many studies have been conducted to define the function of this domain and its activity in the context of cellular intoxication. If the enzymatic A domain must be released into the cytosol to target its host cell proteins, one would predict that the autocleavage activity of the APD would be essential for toxin function within the cell. To try to test this hypothesis, APD point mutants were tested using a number of cell based readouts, most often looking for CPE [3,32,103-105]. In these assays, autoprocessing was found to be essential for the CPE mediated by TcdA and TcdB.

Glucosyltransfer

The N-terminal 63 kDa enzymatic A subunit released upon InsP6-dependent autocleavage is a glucosyltransferase capable of modifying Rho family GTPases [106-110]. The GTPase targets of LCTs are known to regulate essential cellular processes including cell cycle progression, cellular adhesion, cytokinesis, secretion, and cytoskeletal maintenance [111]. The glucosyltransferase domain (GTD) of TcdA and TcdB hydrolyzes a UDP-glucose molecule and transfers the glucose to a threonine in the switch one region of the small GTPases [106]. The GTDs of TcsH and TcsL also use UDP-glucose as a substrate [110]. Tcnα uses UDP-GlcNAc, and TpeL can use either UDP-glucose or UDP-GlcNAc [112,113]. The toxins preferentially modify the

GDP bound state of GTPases, locking the enzyme in the inactive conformation and preventing its association with downstream effectors [106,109]. This inactivation leads to profound cytoskeletal rearrangements resulting in cell rounding (CPE). The inactivation has also been thought to cause loosening of tight junctions, prevention of cell proliferation, and ultimately an apoptotic cell death [20,114-120].

It is thought that the GTD is likely targeted to the plasma membrane, where its substrates are most often found. The membrane localization domain (MLD) was determined to be included within the first 70 residues of TcdA and TcdB, again based largely on homology to VcRTx [121]. *In vitro* experiments have demonstrated that the *C. difficile* toxins can modify RhoA, RhoB, RhoC, RhoG, Rac1, Cdc42, and TC10 [83,122]. TcdA can additionally glucosylate the Ras-like proteins Rap1A and Rap2A [123]. TcsH and Tcnα also modify Rho family proteins [112,124] while TcsL and TpeL preferentially modify the Ras family proteins H-Ras, Ral, and Rap [113]. Interestingly, they can glucosylate Rac but not Rho proteins. Clinically isolated $TcdA^{-}TcdB^{+}$ strains have been shown to be conserved in every domain of the prototypical TcdB except the GTD. There are a number of residue differences that are thought to contribute to the GTPase substrate shift to those of TcsL instead of TcdB [125-127]. The mechanism of substrate recognition is not well understood, but it has been well documented that modification of different substrates leads to different cellular effects.

The glucosyltransferase (GT) activity of TcdA and TcdB is thought to be essential to toxin function, eventually leading to host cell apoptosis. This has been demonstrated by a number of groups in a number of cell lines most often using CPE as the readout for toxin function. There are many reports showing mutagenesis of essential residues that result in defective GT activity *in vitro* result in loss of CPE. These studies and the implications of their findings on the function of the GTD in tissue culture models are discussed in more detail in the next section.

Pathological Functions of TcdA and TcdB

Animal models

TcdA and TcdB have been studied in several animal models including mice, rats, hamsters, and rabbits. They have been shown to have different effects depending on the model system and method of intoxication. In most models, TcdA has a more profound effect, inducing fluid accumulation and inflammation, whereas TcdB has little effect [67,68]. The rabbit ileal loop, for example, has been used extensively as a model system for understanding the relative functions for the toxins in tissue damage and fluid secretion. In this model, TcdA induces fluid accumulation, inflammation, and extensive tissue damage, whereas TcdB has no effect [68]. Notably, when the toxins are injected intraperitoneally, TcdA and TcdB kill the animals with similar potencies [128]. Also, TcdB has been reported to be 100-10,000 times more potent than TcdA in tissue culture models [123,129-131]. These observations led to the distinctions of TcdA as an enterotoxin and TcdB as a potent cytotoxin because of its potency in tissue culture models. The lack of potency exhibited by TcdB in animal models resulted in a hypothesis that TcdA acted as the main virulence factor, disrupting the colonic epithelium and causing disease symptoms while providing TcdB with access to other tissues [65]. Lyerly *et al*. provided supporting evidence of this idea with experiments showing that hamsters died when intoxicated with TcdB in conjunction with sublethal doses of TcdA or if first subjected to intestinal damage. In this pathogenic model, TcdB was acting as an accessory virulence factor, which is inconsistent with the isolation of $TcdA^{-}TcdB^{+}$ clinical strains [75]. Also inconsistent with this model are data describing the effects of TcdA and TcdB in human colonic explants and xenografts. TcdB was found to be at least 10 times more potent against colonic explants, and both toxins induced necrosis and inflammation in the xenograft model [132,133].

In 2009, two studies reported the first genetic manipulations of *C. difficile*. Both reports demonstrated the construction of *tcdA* and *tcdB* knockouts in otherwise isogenic 630*erm* strains. Lyras *et al*. showed that the $TcdA^{-}TcdB^{+}$ strain killed hamsters with the same potency as the $TcdA^{+}TcdB^{+}$ strain. The $TcdA^{+}TcdB^{-}$ strain, however, showed a

significant loss in virulence, implicating TcdB as the major virulence factor [63]. Kuehne *et al*. reported soon after that both TcdA and TcdB were essential for virulence, demonstrating a loss in virulence for both $TcdA^{-}TcdB^{+}$ and $TcdA^{+}TcdB^{-}$ strains [64]. There have been two further reports involving studies with knockout strains, however, the interpretation of these data remain somewhat unclear [134,135]. The requirement for one toxin over the other in disease pathology is a point of contention within the field.

In addition to gross pathological effects, cytokine release has also been investigated in response to TcdA and TcdB in both animal and tissue culture models. TcdA has been shown to result in the production of IL-1, IL-6, IL-8, tumor necrosis factor, intestinal secretory factor, transforming growth factor β, substance P, and macrophage inflammatory protein 2 [119,136-140]. The cytokine profile has not been as extensively characterized in response to TcdB, though IL-1, IL-6, and IL-8 secretion have been reported [133]. Importantly, IL-8 is known to recruit and activate neutrophils at sites of infection [141]; neutrophil infiltration is a hallmark of CDI.

Tissue culture models

TcdA and TcdB were thought to intoxicate and induce cell death by identical mechanisms (Figure 1.1). They are often used interchangeably and rarely compared directly in the same study using tissue culture models. Both toxins have been reported to have a number of effects on a number of different tissue culture cell lines. The most obvious and commonly used readout for intoxication with TcdA and TcdB is CPE. The toxins are also known to kill cells. Unfortunately, the terms cytopathicity and cytotoxicity have been used interchangeably to describe cell rounding without the use of true viability readouts. Many studies have described the cell death induced by both TcdA and TcdB as apoptotic, though the pathway leading to apoptosis has been unclear [9,20,21,142-149]. The apoptotic pathways of both TcdA and TcdB have been described as both p53-dependent and p53-independent as well as both caspase-dependent and caspase-independent [115,150-152]. One study reported an absence of apoptotic markers when cells were intoxicated with higher concentrations of TcdB, suggesting a necrotic cell death [21].

The development of a recombinant expression system made it possible to begin dissecting the contributions of different domains and enzymatic activities to toxin function. Most extensively studied were the enzymatic activities of the GTD and APD. In several studies, essential residues were mutated rendering the toxins deficient in their glucosyltransferase functions and assessed the impact of these mutations in cells. The majority of reports concluded that the GT activity of both toxins was required to achieve apoptosis. Assay readouts included CPE, caspase activation, cell proliferation, and DNA fragmentation. Similarly, the contribution of the APD enzymatic activity was determined to be essential for the induction of apoptosis after intoxication with both TcdA and TcdB. The readouts used in these reports included CPE, caspase activation, and Rac1 modification. A publication by Kreimeyer *et al.* determined that the autoprocessing activity of TcdA was not essential to cytotoxicity but was a determinant of potency [105].

The variation among studies including the cell types, assays, toxins, toxin concentrations, observations, and terminology have resulted in confusion and seemingly conflicting ideas about the mechanism of cellular intoxication. These complications have made it difficult to extrapolate data acquired in these model systems to relevance in disease pathology. It highlights the need for rapid and convenient model systems that accurately and consistently recapitulate the observations made in human disease.

Structural Insights into TcdA and TcdB

One goal of the Lacy laboratory is to determine the structures of the toxins. Our lab has been successful in determining the crystal structures of individual domains of TcdA as well as a low resolution electron microscopy derived 3-dimensional reconstruction of the holotoxin. The structural insights gained from these and other studies are described in more detail.

Electron Microcopy of TcdA holotoxin

Our lab captured images of the TcdA and TcdB holotoxins using negative stain electron microscopy (EM) (Figure 1.2) [5]. In collaboration with Dr. Melanie Ohi, Dr. Rory Pruitt used random conical tilt to reconstruct a 3-dimensional structure of the toxin at ~20 Å resolution. The TcdA structure consists of a globular head domain with two tails, one long tail and one short tail, protruding from the base of the head. The 2-dimensional negative stain images of TcdB look very similar to TcdA, differing in the length of the long tail (Figure 1.1) [5].

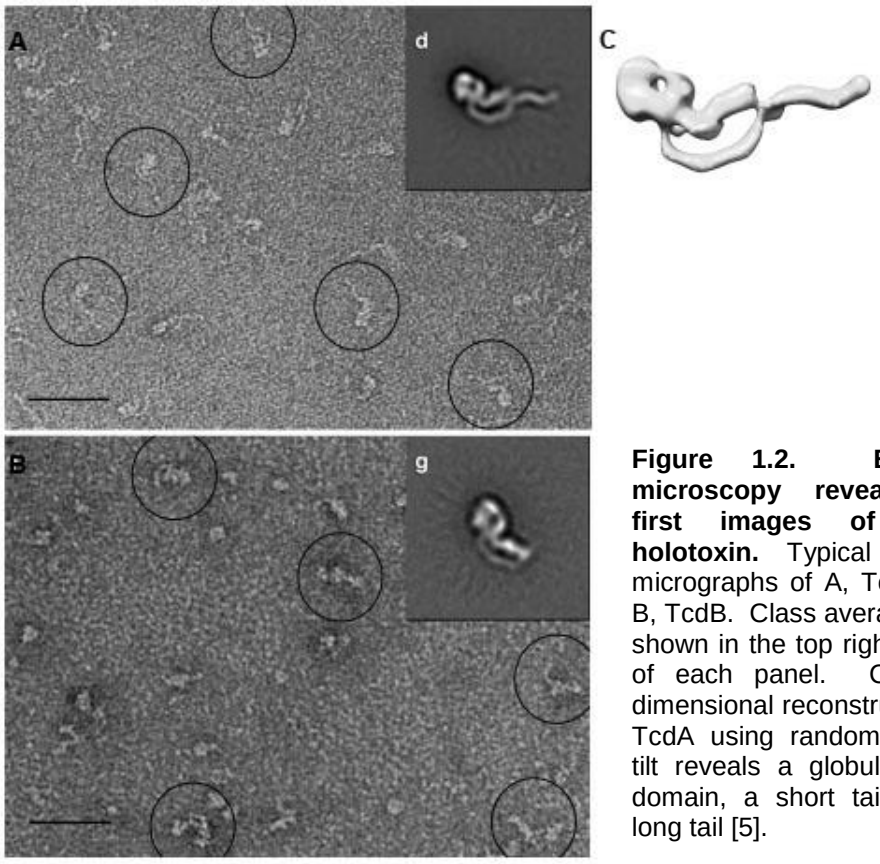

Figure 1.2. Electron microscopy reveals the first images of TcdA holotoxin. Typical electron micrographs of A, TcdA and B, TcdB. Class averages are shown in the top right corner of each panel. C, A 3-dimensional reconstruction of TcdA using random conical tilt reveals a globular head domain, a short tail and a long tail [5].

The Ng laboratory published a model of the TcdA CROPS domain based on their determination of the crystal structure of a small fragment from this repetitive domain [8]. They predicted the entire domain would adopt an elongated serpentine-like structure (Figure 1.3A) [8]. This prediction and electron micrographs of the CROPS domain

alone (878 aa) allowed the identification of the CROPS domain as the long tail in the holotoxin structure (Figure 1.3) [5]. The localization of the CROPS domain to the long tail is consistent with the observation that the long tail is significantly shorter (532 aa) in the TcdB structure. The CROPS domain appears to interact with at least two other parts of the protein. There is contact between the base of the head domain and the N-terminal portion of the CROPS and there may also be contact at the tip of the short tail and the middle of the CROPS domain (Figure 1.3) [5]. Determining the location of the GTD, APD, and delivery domain will be important in understanding the function of the interactions observed with the CROPS domain.

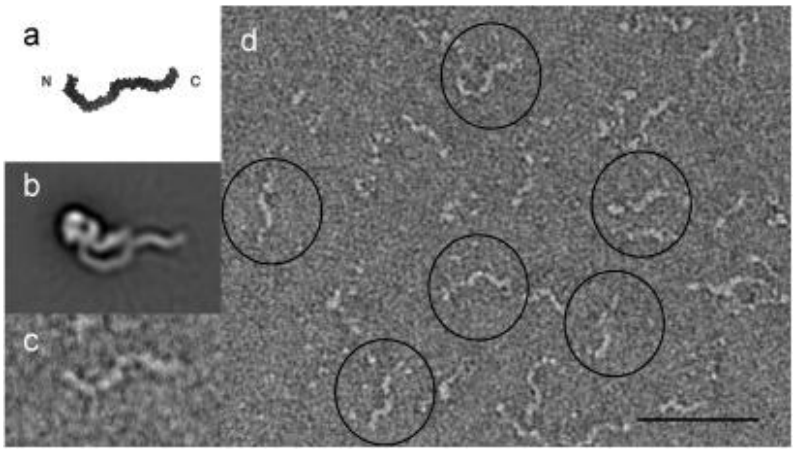

Figure 1.3. Localization of the CROPS with the TcdA holotoxin structure. A, Proposed model of TcdA CROPS domain [8]. B, EM average of negative stained TcdA. C, Negative stained particle of TcdA CROPS. D, Typical electron micrograph of TcdA CROPS [5].

The EM structure of TcdA also provided insight into the conformational change that is thought to occur upon encountering the low pH of the endosome. A second structure was generated from TcdA particles exposed to acidic pH (Figure 1.4) [5]. There is a significant rearrangement of the positions of the short tail and globular head. At pH 4.5, the short tail is no longer positioned somewhat parallel the CROPS, but is rotated out creating a more elongated structure (Figure 1.4) [5]. Determining a high resolution structure of the holotoxins and identifying the location of the domains remains a high priority for further study.

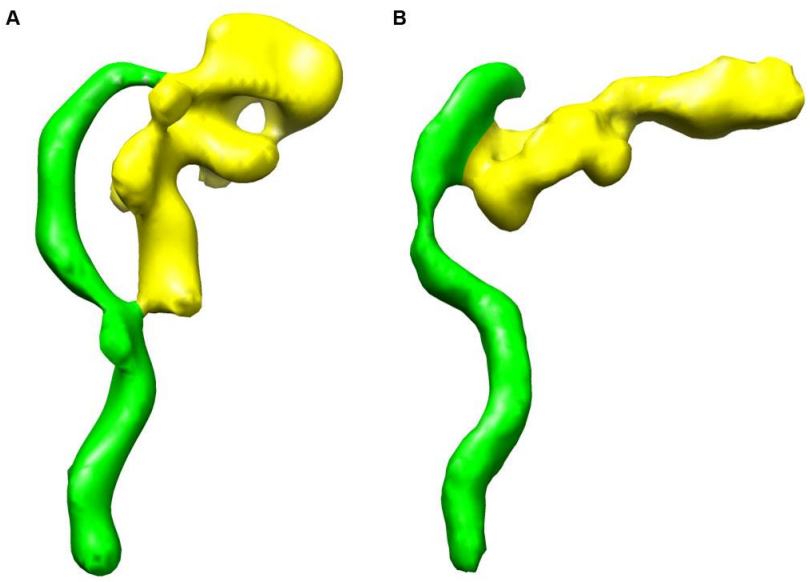

Figure 1.4. Structural evidence of a pH-induced conformational change of TcdA. 3-dimensional reconstruction of TcdA at A, pH 7.0 and B, pH 4.5. Both structures were achieved using random conical tilt. The CROPS domain is colored green [5].

Crystal structures of the glucosyltransferase domains

The crystal structure of the TcdB GTD was determined in 2005 by Reinert *et al*. The GTD was crystallized in the presence of the UDP-glucose substrate, which was found to be hydrolyzed within the active site of the protein [153]. In addition to mechanistic insight, the structure revealed a core Rossman fold that is common among glycosyltransferase A (GT-A) family members. The GTD consists of four α-helical bundles in addition to the core GT-A fold [153]. The most N-terminal bundle is thought to be involved in membrane localization [121,154]. The function of the other α-helical sub-domains is hypothesized to include GTPase substrate binding, though data supporting this hypothesis are minimal [10]. The structure revealed residues involved in binding UDP-glucose and the metal cofactor, Mn^{2+}, which when mutated demonstrated significant enzymatic deficiencies [10,153]. Among these essential residues are those involved in binding UDP-glucose (Tyr284, Asp286, Asp270, Asn394, S518 and Trp520) and Mn^{2+} binding, Asp288. Trp520 forms a hydrogen bond with the glycosidic oxygen

of UDP-glucose and is thought to be involved in hydrolysis and transfer of the glucose to the GTPase target (Figure 1.5B) [10].

The structure of the TcdA GTD was determined in both the apo and UDP-glucose bound states (Figure 1.5A) [2]. The major difference between the apo and substrate bound structures was the position of Trp519 (Trp520 in TcdB). The residue hydrogen bonds with the glycosidic oxygen in the UDP-glucose bound structure but is 10 Å away from the active site in the apo structure (Figure 1.5C) [2]. A similar loop movement has been described in mammalian glycosyltransferases as a "lid" covering the substrate upon binding [155]. This loop movement may be a function of mechanistic efficiency for the enzyme.

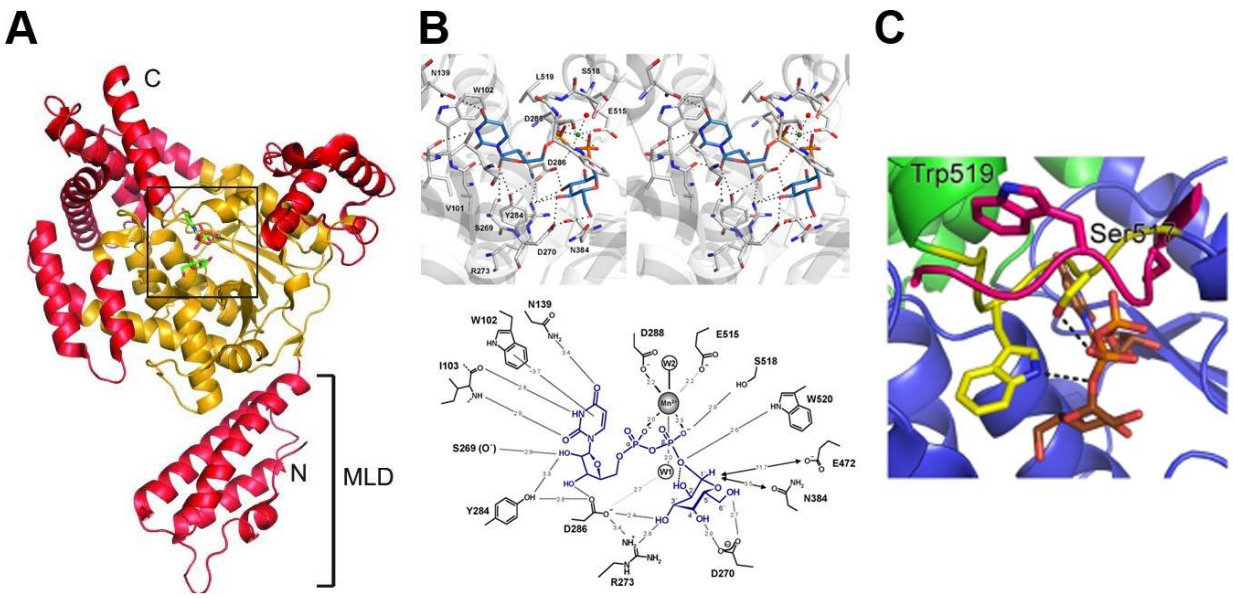

Figure 1.5. Structures of TcdA and TcdB GTD. A, The putative membrane localization domain (MLD) is highlighted toward the N-terminus of the TcdA GTD. The active site is highlighted in the box [2]. B, The active site of TcdB identifying residues that bind the UDP-glucose substrate. The active site is shown in 3-dimensions (upper panel) with the substrate in blue sticks and in 2-dimensions (lower panel) for clarity [10]. C, An illustration of the Trp519 movement observed upon UDP-glucose binding. Shown in pink is the apo position. The substrate-bound position is colored yellow [2].

The TcdA holotoxin glucosyltransferase activity has been described as 100 times less efficient than that of the TcdB holotoxin [123] and was thought to contribute to the even greater discrepancy in potency described between the toxins in tissue culture models [123,129-131]. When comparing the structures of the GTD active sites, however, the only noticeable difference was that the UDP-glucose is hydrolyzed in the TcdB GTD structure and intact in the TcdA structure [2]. Otherwise, the structures are nearly identical, providing no obvious structural or mechanistic basis for the difference in potency. Pruitt *et al*. went on to show that the activities of the isolated domains are very similar to each other and enhanced compared to their activities in the context of the holotoxin [2]. These observations are reasonable with respect to the proposed mechanism in which the GTD is translocated from the endosome, autoproteolyzed, and trafficked to the membrane where it can modify its target GTPases in the host cell.

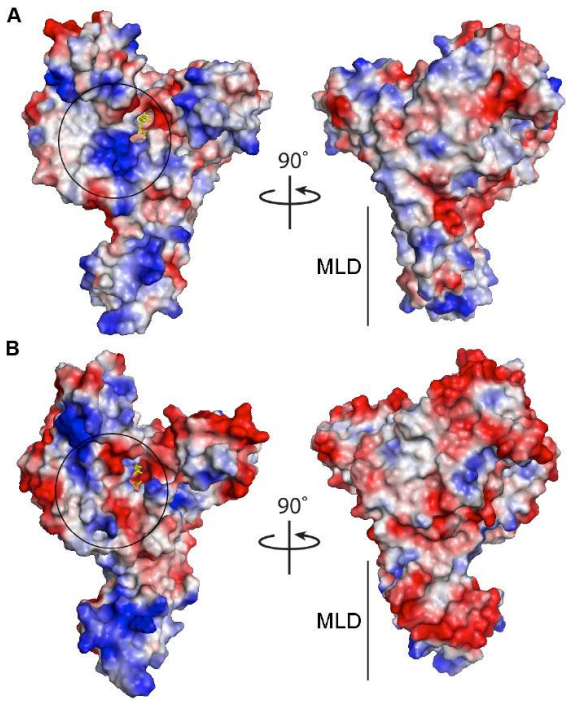

Figure 1.6. Surface electrostatic charges of TcdA and TcdB are different. Though the overall structures are highly similar, A, TcdA and B, TcdB differ in their surface-exposed charged residues. Positively charged residues are colored blue. Negatively charged residues are colored red [2].

Though there was little difference in the overall structure of the GTDs, there was a striking difference between TcdA and TcdB in the electrostatic potentials on the surface of the putative GTPase binding sites [2]. TcdA has a highly positively charged pocket, whereas TcdB has a highly negatively charged group of surface residues

(Figure 1.6). Pruitt *et al*. hypothesized that this difference could be the structural basis of the reported difference in substrate specificity between TcdA and TcdB [2]. Efforts to control substrate specificity through the targeted mutagenesis of these surfaces, however, have been unsuccessful.

Crystal structures of the autoprocessing domains

The structures of the autoprocessing domains of both toxins have also been determined [3,4]. Prior to the determination of the structures, the domain was described as a cysteine protease using both site-directed mutagenesis of active site residues (C700, H655, and D589 in TcdA) and pharmacological inhibitors [104]. Additionally, it was also known that the activity of the protease was dependent upon a host cell factor, inositol hexakisphosphate (InsP6) [4,103,156]. Upon the elucidation of the structure of the TcdA APD, two important observations were made (Figure 1.7). First, InsP6 was bound in a basic pocket containing six lysine and two arginine residues, similar to the VcRTx APD structure [4,157]. InsP6 was bound on the protein face opposite the active site, suggesting an allosteric mechanism of activation. Allostery was proposed to be communicated through what was termed the β-flap (Figure 1.7A) [4]. This mechanism of activation was confirmed and investigated in more detail in later studies [158]. The second important observation was that the active site residues were not in a conformation typical of a cysteine protease triad (Figure 1.7B) [4]. In a typical cysteine protease, the nucleophilic cysteine is activated by a residue that is hydrogen bonded, typically a histidine [159,160]. The structure revealed an active site conformation in which the Cys700 was > 6 Å from His655 and > 10 Å from Asp589 [4]. Though this conformation had been observed in the structure of VcRTx [157], it suggested an atypical mechanism of proteolysis.

Puri *et al*. determined the structure of the TcdB APD in the presence of covalent inhibitors and the allosteric activator, InsP6. The dipeptide inhibitors were substrate mimics covalently bound to the catalytic cysteine, thus providing insight into the conformation of the substrate bound protease [3]. The similarity to the structure of the substrate bound VcRTx protease domain was quite striking [1]. Again, both structures revealed an atypical active site conformation in which the substrate lies between the

catalytic cysteine and the histidine [1,3]. These observations further suggested a unique mechanism of proteolysis.

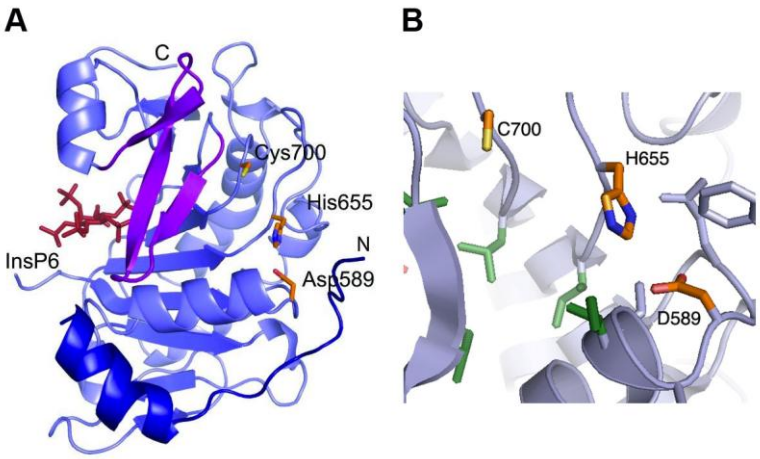

Figure 1.7. The structure of the TcdA APD reveals and allosteric InsP6 binding site and an unusual active site conformation. A. The TcdA APD (residues 543 to 809). The active site residues are colored orange; InsP6 is colored red; and the β-flap is colored purple. B, The TcdA APD active site is in an unusual conformation for cysteine protease activity [4].

Comparison of the TcdA and TcdB APD structures again revealed no obvious structural or mechanistic reason for differences in toxin potency as they were nearly identical. Notably, it has been reported that TcdA requires high concentrations of reducing agent, such as dithiolthreitol (DTT), in addition to InsP6 before autoprocessing could occur [104]. TcdB, however, can initiate autoprocessing with the addition of InsP6 only [102,103]. The resulting assumption was that a disulfide bond [104], present in TcdA and not in TcdB, must be reduced before cleavage could occur. While this difference in autoprocessing efficiency could potentially explain the differences in potency in cells between the two toxins, no investigations were made to formally test either of these hypotheses.

Research Objectives

At the outset of this project, one of my goals was to conduct a high throughput small molecule inhibitor screen for compounds that protected cells from TcdB-induced cell death. As a primary mediator of CDI, we wanted to target TcdB for the development of new, more effective therapeutics. We conducted a cell-based, high throughput small molecule inhibitor screen to identify compounds that provided protection from TcdB-mediated cell death. We expected to find compounds that inhibited the enzymatic activities of TcdB as they were thought to be essential for TcdB induced apoptosis. The GTD and APD both presented attractive binding sites for inhibitors in their active and allosteric sites. We also recognized that compounds could be inhibiting any step of the cell death pathway, including binding the host cell receptor, pore formation, or downstream effects of GTPase modification. Through the course of conducting the screen and developing controls for inhibitors we predicted we would find against the GTD and APD activities, we made some surprising discoveries.

In Chapter II, I present data demonstrating TcdB induces necrosis. We employed a number of necrotic markers, including rapid ATP depletion, lactose dehydrogenase (LDH) release, and high-mobility group protein B1 (HMGB1) relocalization as well as the absence of apoptotic markers such as active caspase-3 to support our claims. Activated caspases were nearly undetectable in response to TcdB in our tissue culture models. TcdA induced low levels of caspase activation at high concentrations 48 hours post-intoxication in our cell lines. Using site-directed mutagenesis, we went on to show that the autoprocessing and glucosyltrasferase activities of TcdB are not required to induce the necrotic cell death we were observing at nanomolar concentrations of toxin. Because the necrotic phenotype was occurring at higher concentrations than what is typically used in CPE assays, we also provided evidence that nanomolar concentrations of toxin are pathologically relevant using a colonic explant model. This work provided a mechanism of cell death that could explain the underlying pathology of the necrotic lesions, typical of CDI. This work also

highlighted the unlikelihood that the autoprocessing activity of TcdB would be a viable drug target.

In collaboration with Dr. Melissa Farrow, we went on to define the mechanism of necrosis induced by TcdB as being dependent upon the assembly and activation of the NADPH oxidase (NOX) complex and subsequent reactive oxygen species (ROS) production. With this new understanding of how cells were dying, we were able to return to the small molecule inhibitor screen with new, relevant, and testable targets for inhibition in mind. We have chosen to focus on one compound, 0049, as a representative of the major class of compounds that came out of the screen as confirmed hits. Our progress on this ongoing work is presented in Appendix I.

In the experiments performed in Chapter II, we made the perplexing observation that TcdA-induced cell death was detectable only at high nanomolar concentrations of toxin 48 hours post-intoxication. Reports of TcdA activity on tissue and in animal models had indicated that TcdA was a more potent toxin than what we were observing in our tissue culture models. We sought to understand why our observations in cells were not an accurate reflection of pathological activity of TcdA. Young adult mouse colonic (YAMC) epithelial cells express a temperature dependent simian virus 40 (SV40) T-antigen that disrupts p53. These cells provide a unique tool in that they are an easily carried cell line at the permissive temperature where p53 is disrupted and are a relevant primary cell line at the non-permissive temperature where the cells can undergo normal apoptosis. We exploited this cell line to investigate the effects of TcdA and TcdB intoxication side by side in the same cell line using the same assay readouts. In Chapter III, we clearly demonstrate that TcdA is a potent cytotoxin, inducing cell death to levels similar to TcdB. Cell death induced by TcdA is apoptotic and dependent upon the p53 pathway and glucosyltransferase activity. We were also able to show that TcdB induces a concentration dependent bimodal profile of cell death. At higher concentrations, TcdB induces glucosyltransferase independent necrosis, as previously described, and at lower concentrations, TcdB induces a p53, glucosyltransferase dependent apoptotic cell death. These observations were recapitulated in our colonic explant model. This work highlights the need to work in model systems capable of undergoing normal apoptosis when studying the cell death pathway induced by TcdA

and the concentration-dependence of TcdB phenotypes. The data presented in Chapter III provide the opportunity to coalesce the field's observations that have appeared to be conflicting in recent years.

Another goal of my project was to understand the difference in TcdA and TcdB autoprocessing activity. As presented in Chapter IV, we discovered that TcdA autoprocessing is regulated by the coordination of zinc ions. TcdA coordinates at least 3 zinc ions, two for which we have defined functions. One zinc ion acts as a regulator of autoprocessing; its presence inhibits autoprocessing and its removal allows autoprocessing to occur normally. Interestingly, this zinc ion is not present in TcdB, and once removed from TcdA, by chelators or low pH *in vitro*, autoprocessing can occur as efficiently as in TcdB. The second zinc was unexpectedly localized to the active site of the APD. We demonstrated that autoprocessing is dependent upon the presence of this zinc ion, suggesting the enzymatic mechanism of autoprocessing of both toxins is that of a zinc protease, not a cysteine protease as previously described. The data presented here represent two novel zinc dependent mechanisms for the functions of *C. difficile* toxins.

Together, these data have advanced our understanding of the mechanisms by which TcdA and TcdB intoxicate and kill cells. The insights presented here can help direct drug discovery efforts and development of more effective therapeutics to combat CDI. Our ongoing work to understand the mechanistic aspects of cell death induced by *C. difficile* toxins and our ideas for future experiments are discussed in Chapter V.

CHAPTER II

CLOSTRIDIUM DIFFICILE TOXIN B CAUSES EPITHELIAL CELL NECROSIS THROUGH AN AUTOPROCESSING-INDEPENDENT MECHANISM

Introduction

Clostridium difficile is a gram-positive, spore-forming anaerobe that infects the colon and causes a range of gastrointestinal disorders including diarrhea, pseudomembranous colitis, and toxic megacolon [65,161]. This is a major healthcare concern as the number and severity of *C. difficile*-associated disease (CDI) cases have increased dramatically in recent years [162]. Two large toxins, TcdA and TcdB (308 kDa and 270 kDa, respectively), are recognized as the main virulence factors of *C. difficile* [63,64]. The C-terminal portion of these toxins is responsible for delivering an N-terminal glucosyltransferase domain (GTD) into the host cell [102,163]. The GTD inactivates Rho family GTPases including Rho, Rac1, and Cdc42 [109,110].

While there are numerous studies that report the effects of toxin-mediated glucosylation in cells, a consensus as to the conclusion of these reports, taken together, has been difficult due to differences in cell types, toxin concentrations, and assay methods. In addition, it appears that TcdA and TcdB can elicit different effects under similar conditions [68,164]. In all reports, both toxins can induce a cytopathic effect characterized by cell rounding. In many reports, these cells go on to die by apoptotic mechanisms, but the time course can be up to 48 hours [9,20,115,143-145,150,151]. It has been noted, however, that apoptosis cannot be detected in cells treated with higher concentrations of TcdB [142]. In at least one study, the absence of apoptosis in cells treated with TcdB has led to suggestions of a necrotic mechanism of cell death [21].

The mechanism of GTD delivery for TcdA and TcdB involves binding a host cell receptor [82,165], uptake by endocytosis [92,166], pH-dependent pore formation [95-97], translocation across the endosomal membrane, host-factor dependent

autoprocessing [103], and release of the GTD into the host cell cytosol [101]. Release is thought to allow the GTD access to the Rho-family GTPases tethered to the plasma membrane surface. An N-terminal sub-domain within the GTD is thought to serve as a membrane localization domain [121].

The autoprocessing function of the toxins is mediated by a cysteine protease domain (CPD) that follows the N-terminal GTD [104]. Inositolphosphates, predominantly inositol hexakisphosphate (InsP6), have been identified as the host factors responsible for inducing autoprocessing [103]. The InsP6-bound structures of the TcdA and TcdB CPDs reveal a positively charged InsP6-binding pocket that is distinct from the catalytic active site [3,4]. InsP6 binding is thought to trigger conformational changes that permit the formation of the substrate-binding pocket and alignment of the catalytic residues [158]. The three catalytic amino acids Asp587, His653, and Cys698 (TcdB sequence) and the P1 substrate recognition site, Leu543, have been shown to be important for *in vitro* processing activity by genetic mutation [104]. Mutation and chemical modification of these residues has also been shown to prevent activity in various cell based assays [3,32,35,103,104]. For this reason, TcdB autoprocessing activity and GTD release have been considered important in the toxin mechanism, an idea which suggests that the CPD could serve as a useful target for novel small molecule inhibitor discovery.

The objective at the outset of this project was to conduct a high-throughput screen for small molecules that inhibit TcdB-mediated cell death. Our first step toward exploring this potential was to evaluate apoptotic and necrotic markers as cell death indicators. In observing a necrotic response to TcdB, we decided to specifically focus on the question of whether the assay would be able to detect inhibition of TcdB autoprocessing. We constructed mutant TcdB proteins with deficiencies in either the autoprocessing or glucosyltransferase activities and tested their effects on cell viability. Our unexpected observation that the mutants killed cells rapidly and at concentrations comparable to wild-type led us to investigate the role of autoprocessing and GTD release in cell death and cell rounding in greater detail. In this report, we provide evidence that epithelial cells and porcine colonic tissue challenged with TcdB undergo a rapid, necrotic cell death that is not dependent on autoprocessing and GTD release.

Methods

Ethics statement

This study was performed in strict accordance with the recommendations in the Guide for the Care and Use of Laboratory Animals of the National Institutes of Health. Animal husbandry and experimental procedures related to the porcine colonic explants were performed in accordance with the Vanderbilt University Institutional Animal Care and Use Committee (IACUC) policy. Discarded colon tissues were obtained from pigs following euthanization at the end of IACUC-approved animal use protocols. Animal husbandry and experimental procedures related to the generation of the anti-TcdBGTD monoclonal antibody were performed in accordance with the Washington University Animal Studies Committee policy, approval number 20100113.

Expression of recombinant proteins

Single amino acid point mutations were made in the TcdB autoprocessing active site (C698S, C698A, H653A, and D587N), the cleavage site (L543A), and the glucosyltransferase domain (D270N, D270A, Y284A, N384A, and W520A) using the QuickChange mutagenesis protocol (Stratagene). The template for mutagenesis and clone for the production of wild-type TcdB was a *B. megaterium* expression vector encoding the strain 10643 of TcdB [5]. A similar clone was used for expression of recombinant TcdA [5]. Plasmids for expressing TcdA, TcdB, and TcdB point mutants were transformed into *B. megaterium* according to the manufacturer's instructions (MoBiTec, Göttingen, Germany). 1 L of LB was inoculated with 35 mL overnight culture and 10 mg/L tetracycline and grown at 37 °C and 230 rpm. At an OD_{600} of 0.3, expression was induced with 5 g of D-xylose. Cells were harvested after 4 h by centrifugation and resuspended in 20 mM Tris, pH 8.0, 500 mM NaCl and protease inhibitors. Cells were lysed by French press, and lysates were centrifuged at 48,000 g for 25 min. The proteins were purified by Ni-affinity chromatography, Q-sepharose anion exchange chromatography, and gel filtration chromatography in 20 mM HEPES, pH 6.9, 50 mM NaCl.

Protein purification from C. difficile

Proteins were expressed and purified as previously described [65].

Cell death assays

HeLa and Caco2 cells (cultured in DMEM, 10% FBS, 5% CO_2 and MEM, 10% FBS, 5% CO_2, respectively) were seeded in a black 384-well plate at a concentration of 3,000 or 1,000 cells/well, respectively. HeLa cells were intoxicated the next day, and Caco2 cells were intoxicated 36 h later. After intoxication, the cells were incubated at 37 °C, 5% CO_2 for either 2.5 h (HeLa) or 18 h (Caco2). The amount of ATP (cell viability) was assessed with a luminescence-based indicator, CellTiterGlo (Promega). LDH release was assessed with a luminescence-based indicator, CytoToxGlo (Promega). Caspase-3/7 activation was determined using a fluorescent indicator, Apo-One (Promega). Staurosporine (Sigma, 1mM) was used as a positive control for caspase-3/7 activation. Plates were read in a Biotek Synergy 4 plate reader.

HMGB1 release

HeLa cells were seeded into a tissue culture treated chamber slide at 2 $x10^4$ cells per well and incubated overnight. Cells were synchronized at 4 °C and intoxicated with 10 nM TcdB for 1 h. Cells were then shifted to 37 °C for 1 h. Media was removed from the cells, and the cells were washed with PBS. They were fixed with 4% paraformaldehyde at room temperature for 10 minutes and quenched with 1 mM glycine. Cells were permeated with 0.2% Triton X-100 in PBS for 5 minutes, washed in PBS, and blocked for 30 minutes in PBS, 2% BSA, 0.1% Tween 20. Cells were stained with a monoclonal antibody against HMGBI (Abcam, ab77302), and an Alexa Fluor 488 anti-mouse antibody (Invitrogen, A11001). Cells were visualized with an LSM 510 Confocal microscope.

In vitro cleavage assay

1 uL InsP6 stock solution (100X) or buffer was added to 200 nM TcdB or TcdB autoprocessing mutant and incubated for 2 h at 37 °C. The reactions were stopped with

the addition of loading buffer and boiling and analyzed by Coomassie stained SDS PAGE.

Anti-TcdBGTD antibody generation

Genomic DNA of *C. difficile* clinical isolate 630 was obtained from American Type Culture Collection, and the region encoding residues 1 to 549 of TcdB, which is known to encode the substrate binding and enzymatic domains of the toxin, was amplified in frame with a carboxy-terminal (His)6-tag using upstream primer :5'-CCGGATGTACAGTTGAGGGGGTAAAATGAGTTTAGTTAATAGAAAACAGTTAG -3' and downstream primer 5'-GGTCCTCAATGATGGTGATGGTGATGAAGATTATCATCTTCACCAAGAGAACC -3'. The resulting product was cloned into plasmid pcDNA3.1 (Invitrogen, Carlsbad CA) and sequenced to ensure fidelity of the amplified product. The gene was then released with restriction enzymes BsrG1 and AgeI and cloned into similarly digested vector pHIS1525 (MoBiTec), placing the gene under control of a xylose-inducible promoter. Recombinant protein was expressed in *B. megaterium* and purified by sequential nickel affinity and gel filtration chromatography. Two mice were immunized bi-weekly by intraperitoneal injection with 100 □g purified TcdB-GTD. Three days after the third vaccination, splenocytes were harvested and fused to P3X63Ag8.6.5.3 myeloma cells using polyethylene glycol 1500 [167]. Hybridomas producing anti-TcdB-GTD MAbs were identified by ELISA, subcloned by limiting dilution, and purified by protein G immunoaffinity chromatography.

Cell based cleavage assay

HeLa cells were synchronized by cooling to 4 °C and then intoxicated with 10 nM TcdB, autoprocessing mutant, or buffer. The cells were returned to 4 °C for 1 h, and then shifted to 37 °C for 50 min. The cells were harvested and lysed, samples were boiled, and proteins were separated by SDS PAGE. Samples were analyzed by Western with primary antibodies specific for the TcdB GTD, unglucosylated Rac1 (BD, 610650), total Rac1 (Millipore, clone 23A8), and GAPDH (Santa Cruz Biotechnology, sc-25778). Binding of an anti-mouse, HRP-conjugated secondary antibody (Jackson

ImmunoResearch Laboratories, 115-035-174) was detected with a LumiGLO kit (Cell Signaling) according to manufacturer's instructions.

In vitro glucosyltransferase assay

Unless otherwise noted, 100 nM TcdB or TcdB glucosyltransferase mutants and 2 uM Rac1 were mixed with 20 mM UDP-[^{14}C]glucose (250 mCi/mmol, Perkin Elmer) in a total reaction volume of 10 uL. The buffer contained 50 mM HEPES pH 7.5, 100 mM KCl, 1 mM $MnCl_2$, 2 mM $MgCl_2$, and 0.1 mg/mL BSA. Reactions were incubated at 37 °C for 1 h and stopped with the addition of loading buffer and boiling. Proteins were separated by SDS PAGE, and glucosylation of Rac1 was detected by phosphorimaging.

Kinetic assays of cytotoxic and cytopathic events

HeLa cells were seeded in a black 96-well imaging plate (PerkinElmer) and incubated overnight. Cells were pretreated with live/dead cell imaging dyes (Molecular Probes, R37601) and then treated with multiple concentrations of wild-type and mutant TcdB proteins. Cells were imaged in an environment-controlled chamber (37 °C, 5% CO_2) every 10 minutes over a 2 hour time using an Opera High-Throughput Confocal Screening Microscope and Peltier-cooled, confocal CCD cameras. The percentage of dead cells and round cells was quantified over six fields for each concentration and time point using the Columbus Analysis software. Dead cells were defined as red cells with an intensity greater than 450 relative units, and round cells were defined as having an area less than 500 um^2 and a width-to-length ratio of less than 0.4.

Porcine colonic explants

Colonic tissue was harvested from purpose-bred 25-35kg, male or female, York-Landrace crossbred pigs. Following an overnight fast and immediately after euthanasia, a midline incision was performed and 15 cm of distal colon proximal to the rectum was excised and placed in PBS. The colon was opened, the luminal side was washed 3 x 5 min in 1 mM DTT to remove the mucus, and 3 x 5 min in PBS prior to dissection. Individual tissue sections were placed in wells of a 24-well plate. A nutrient buffer [132] containing (mM/liter): 122.0 NaCl, 2.0 $CaCl_2$, 1.3 $MgSO_4$, 5.0 KCl, 20.0 glucose, 25.0

$NaHCO_3$ (pH 7.5) was pre-conditioned with HeLa cells overnight at 37 °C and used to dilute the toxins. Explants were treated with wild-type TcdB, mutant TcdB, staurosporine (100 uM, Enzo Life Sciences, ALX-380-014-C250) or nutrient buffer for 5 hours at 37 °C. The tissues were fixed with formalin for 56 h, washed in PBS, and transferred to cassettes. The tissue blocks were then embedded in paraffin, and 4 μm sections were cut and stained with hematoxylin and eosin (H&E) by the Vanderbilt University Translational Pathology Shared Resource core. Stained sections were coded and evaluated by six individuals, using a semi-quantitative injury scale: 0- no damage; 1-superficial damage, damage limited to intact surface epithelial cells; 2-loss of up to 50% of surface epithelial cells or gland length, crypts intact; 3-loss of over 50% of surface epithelial cells and damage in greater than 50% of gland length. An injury score was calculated as the mean score for sections evaluated seven times by six individuals. Statistical analysis was performed using a two-way ANOVA and Bonferroni's test. For keratin and caspase staining, sections were de-paraffinized with Histo-clear (National Diagnostics) and antigens were retrieved by citric acid. The sections were blocked with Serum-free protein block (Dako), stained with a rabbit anti-pan cytokeratin or anti-active caspase-3 antibody (Santa Cruz Biotechnology, sc-15367; Abcam, ab13847), and diluted in Dako's antigen diluent with background reducing components overnight at 4˚C. The sections were washed with PBS and incubated for 1 hr at RT with an AlexaFluor 546 donkey anti-rabbit antibody (Invitrogen A10040). The sections were washed with PBS and mounted with Prolong Gold with DAPI (Invitrogen). H&E, pan-cytokeratin, and caspase-3 stained sections were imaged using an Ariol SL-50 (Epithelial Biology Center Imaging Core).

Results

TcdB induces necrosis in cultured epithelial cells

The objective at the outset of this project was to conduct a high-throughput screen for small molecules that inhibit TcdB-mediated cell death. Our first goal was, therefore, to establish conditions for an assay that was sensitive and homogeneous. HeLa cells were seeded into 384 well plates and treated with TcdB at multiple

concentrations for varying lengths of time. Cells were then simultaneously assayed for caspase-3/7 activation and ATP levels using fluorescent and luminescent indicators, respectively. At all concentrations and time points tested, TcdB failed to activate caspase-3 and -7, central regulators in apoptotic cell death (Figure 2.1A). Conversely, staurosporine, a known inducer of apoptosis, triggered significant caspase-3/7 activation at a 5 hour time point. Since the result appeared to be in conflict with a previous report showing that TcdB-treatment of HeLa cells induced an increased rate of caspase-3 activity [150], we performed additional experiments using lower toxin concentrations, a 48 hour time point, and TcdA. We did not observe caspase-3/7 activation in any of the cells treated with TcdB and only saw TcdA-induced caspase-3/7 activation when the toxin was applied at concentrations of 100 nM (Figure 2.2A). While our initial experiments were performed with TcdB purified from a recombinant *Bacillus megaterium* expression system, we did not observe caspase-3/7 activation when we tested TcdB purified from *C. difficile* culture supernatants (Figure 2.2B).

Despite the lack of caspase-3/7 activation, the TcdB treatments had a significant impact on cellular ATP levels (Figure 2.1B). Decreases in ATP were observed after only 2.5 hours in cells treated with 1, 10, and 100 nM TcdB suggesting that these cells were no longer viable. The effect is specific to TcdB, as TcdA only impacted the viability at concentrations of 100 nM at 24 hours (Figure 2.3A). While lower concentrations of TcdB can induce cell death after a 48 hour application, the effect does not appear to be dose dependent at the 48 hour time point (Figure 2.3A).

In an attempt to correlate the viability indicators with cytopathic events, mock and TcdB treated cells were visualized by light microscopy. At concentrations of 10 pM, a characteristic cytopathic (cell rounding) effect was observed. In contrast, cells treated with 10 nM TcdB for 2.5 hours had completely lost their membrane integrity (Figure 2.1C). The rapid loss of ATP and membrane integrity suggested that cells treated with nM concentrations of TcdB were dying by necrosis. To further test this hypothesis, we assessed the effect of TcdB on LDH and HMGB1 release. LDH release was apparent 2.5 hours after intoxication and at an increased level after 8 hours (Figure 2.1D). Similar values for LDH release are observed when the cells are treated with TcdB from *C. difficile* supernatants (Figure 2.3B). Notably, LDH release is only detectable at toxin

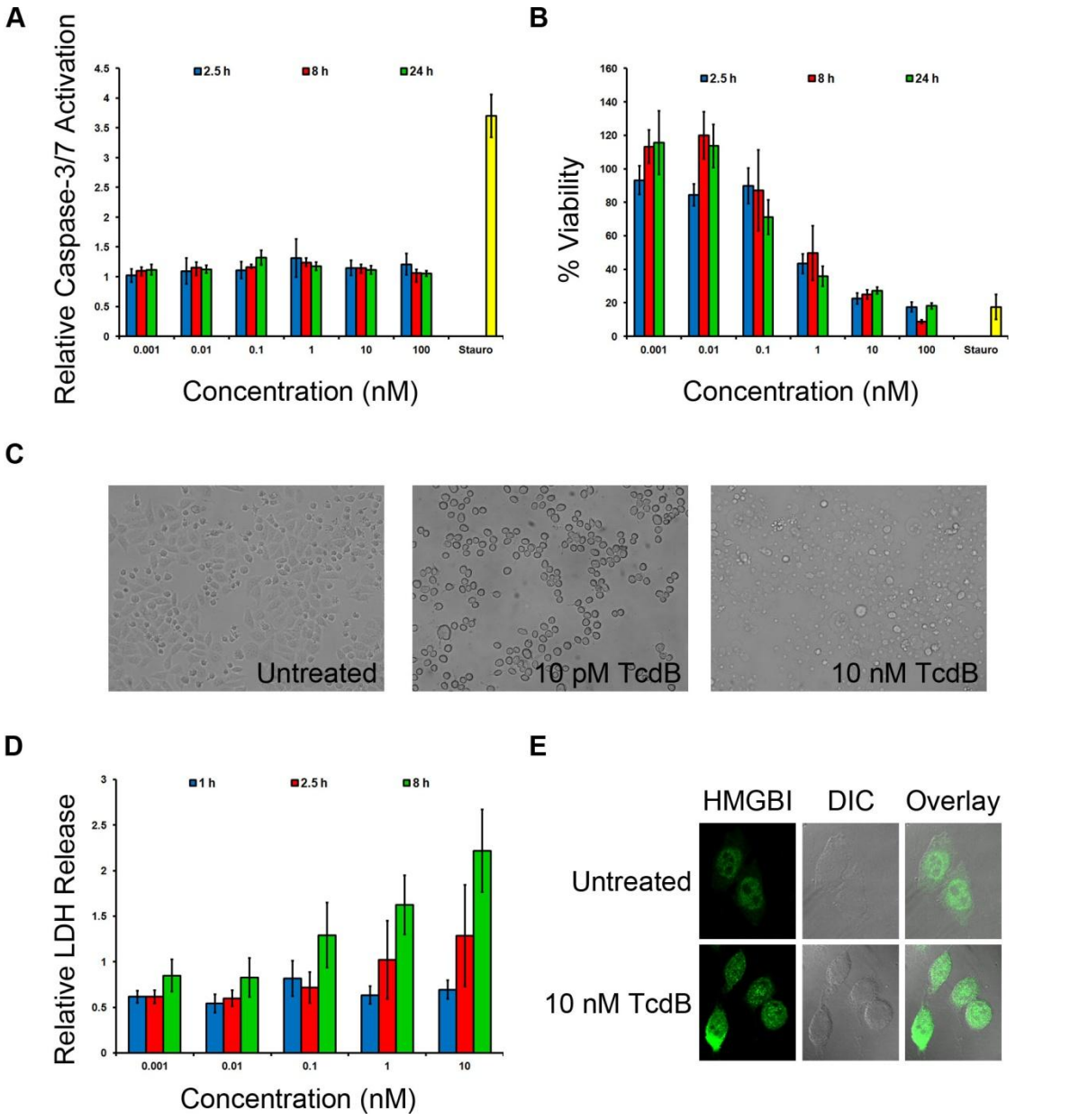

Figure 2.1. TcdB induces necrosis in epithelial cells. *A*, TcdB does not induce caspase-3/7 activation in HeLa cells, as detected by a fluorescent indicator, Apo-One. *B,* TcdB induces rapid death in HeLa cells, as detected by a luminescent indicator, CellTiterGlo. Caspase-3/7 activation and viability values represent the average of three experiments in which each condition was tested in triplicate. The error bars indicate the standard deviation between three experiments. *C,* HeLa cells were synchronized and incubated with or without TcdB for 2.5 hours at 37 °C. A representative image obtained by light microscopy indicates rounding in cells treated with 10 pM TcdB and a loss of membrane integrity in cells treated with 10 nM TcdB. *D*, Extracellular LDH was detected in TcdB-treated HeLa cells after 2.5 hours using a luminescence-based indicator, Cytotox-Glo. Increased levels of LDH release were apparent after 8 hours. LDH release values represent the average of three experiments in which three replicates were averaged. Error bars indicate the standard deviation between the values obtained from the three experiments. *E*, HeLa cells were treated with a buffer control or 10 nM TcdB for 1 h and then fixed with 4% formaldehyde. Cells were stained with an antibody specific for HMGB1 and an Alexa Fluor 488 anti-mouse antibody. The cells were visualized with a LSM510 Confocal microscope. The representative images show that HMGBI is released from the nucleus of HeLa cells when treated with 10 nM TcdB and remains nuclear in the untreated cells.

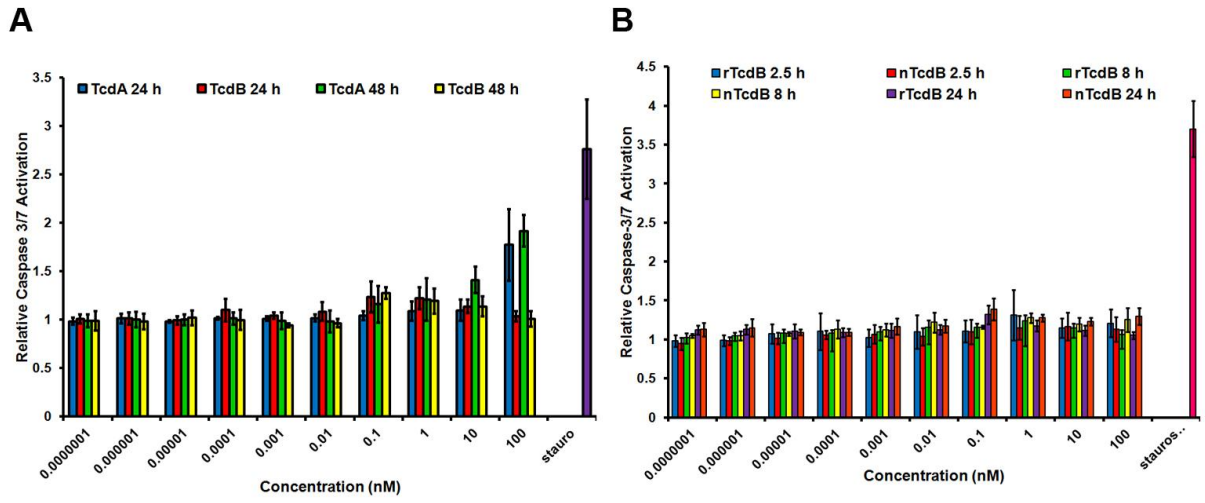

Figure 2.2. TcdA activates caspase-3/7 while both recombinant and native TcdB do not. *A*, TcdB does not induce caspase-3/7 activation in HeLa cells, as detected by a fluorescent indicator, Apo-One, at 24 or 48 h. TcdA, however, does induce caspase-3/7 activation at a concentration of 100 nM at 24 h and 10 and 100 nM at 48 h. *B*, TcdB purified from *C. difficile* supernatant looks similar to TcdB purified from *B. megaterium* in that neither induce caspase-3/7 activation. Values represent the average of 3 independent experiments in which each condition was tested in triplicate. Error bars represent the standard deviation of the average of the three independent experiments.

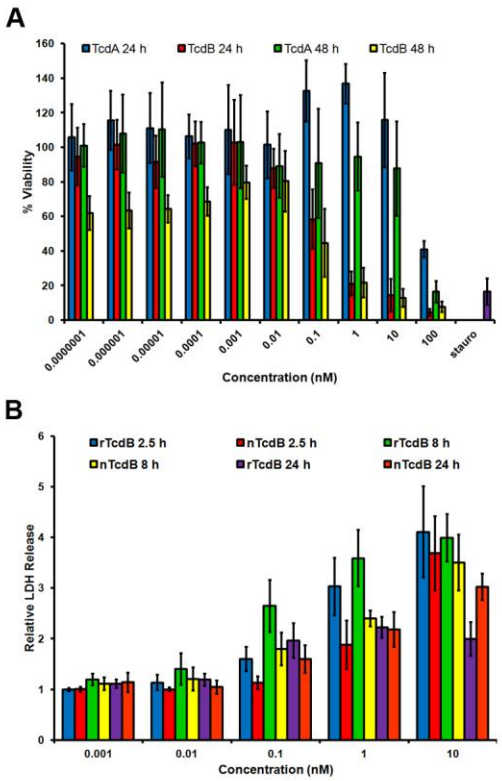

Figure 2.3. TcdB is more cytotoxic than TcdA, and the effects of native and recombinant TcdB on LDH release are similar. *A*, TcdB induces significant HeLa cell death, as detected by CellTiterGlo, in 24 h at concentrations of 1, 10, and 100 nM. At 48 h, a loss of cell viability was observed at lower concentrations in a dose-independent fashion. TcdA induces significant cell death at 24 h and 48 h at a concentration of 100 nM. *B*, TcdB purified from *C. difficile* and *B. megaterium* induce release of LDH starting at 2.5 h, with increased levels apparent after 8 h of treatment. Values represent the average of 3 independent experiments in which each condition was tested in triplicate. Error bars represent the standard deviation of the three independent experiments.

concentrations above 0.1 nM, consistent with the cell death data obtained with an ATP indicator (Figure 2.1B). HMGB1 is a nuclear protein that is released into the cytoplasm when the cell is dying by necrosis. We found that at 10 nM TcdB, HMGB1 was released into the cytoplasm after 1 hour (Figure 2.1E). As a result of these studies, CellTiterGlo, the luminescent indicator of cellular ATP levels, was deemed the best indicator of cell viability for high throughput screening. The rapid loss of ATP and membrane integrity, the release of LDH and HMGB1, and the lack of caspase-3/7 activation all suggest necrosis is the mechanism of TcdB-mediated death in HeLa cells.

Mutations in the autoprocessing domain active site and the cleavage site result in TcdB proteins with impaired autoprocessing activity in vitro and in cells

We next generated autoprocessing-deficient mutants that could be used as negative controls in a secondary assay that would allow us to select for molecules that inhibit the autoprocessing activity of the toxin. Single amino acid point mutations were made in the TcdB autoprocessing active site (C698S, C698A, H653A, and D587N) and the cleavage site (L543A). Proteins were expressed in the *B. megaterium* expression system and purified to homogeneity. All mutants were tested for their *in vitro* autoprocessing activity (Figure 2.4A). TcdB autoprocessing can be induced with the addition of 1 uM InsP6, and the amount of processing increases as the concentration of InsP6 increases. At all concentrations of InsP6, TcdB C698S, TcdB C698A, and TcdB H653A were completely inactive in autoprocessing, as detected by Coomassie-stained SDS PAGE (Figure 2.4A) and densitometry (Figure 2.4B). TcdB D587N and TcdB L543A had residual cleavage activity, but were significantly cleavage-impaired. Cleavage of D587N was not induced until 100 uM InsP6 was added, and the amount of processed toxin was reduced.

We next wanted to confirm that the mutants were also defective for autoprocessing in the context of the cell. HeLa cells were treated with wild-type TcdB or autoprocessing deficient TcdB mutants for 50 min, lysed, and probed by Western blot using an anti-TcdBGTD antibody. Free GTD was detected in cells treated with wild-type TcdB but was not detected in cells intoxicated with TcdB mutants (Figure 2.4C). The same lysates were probed with an antibody specific for unglucosylated Rac1. Rac1 is

glucosylated even when the cells have been treated with autoprocessing mutants. These data suggest that in cells treated with TcdB autoprocessing mutants, the GTDs are being translocated into the cytosol, but they remain tethered to the endosome where glucosylation of Rac1 can still occur.

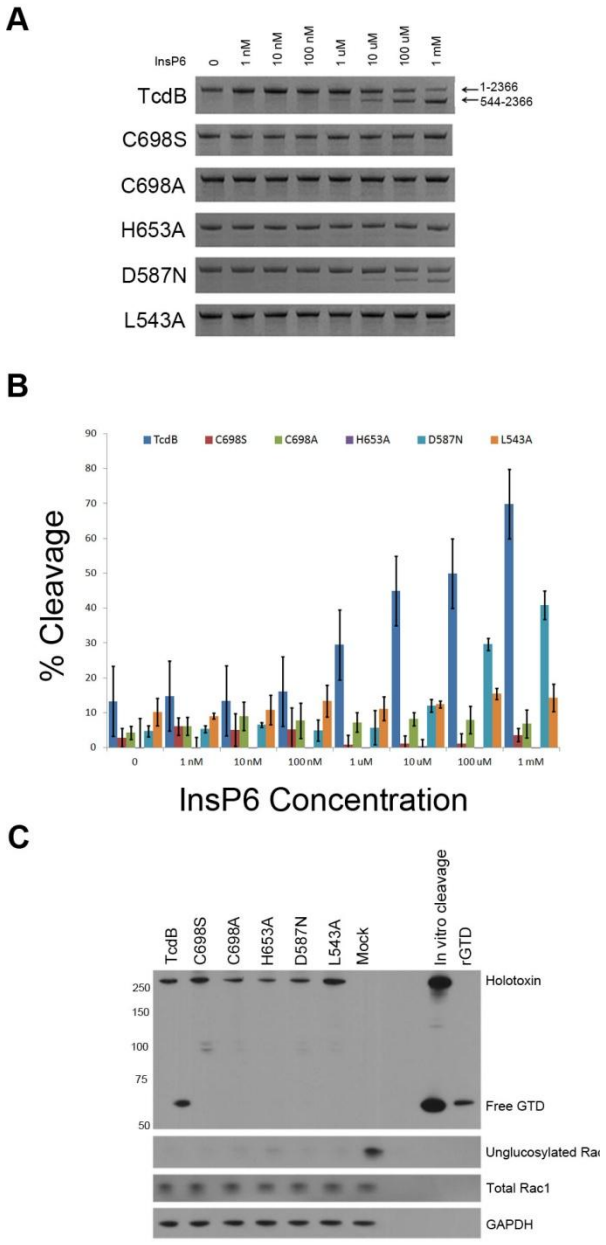

Figure 2.4. Mutations in the autoprocessing domain active site and the cleavage site result in TcdB proteins with impaired autoprocessing activity *in vitro* and in cells. *A,* Autoprocessing was induced *in vitro* by incubating wild-type TcdB and TcdB mutants with multiple InsP6 concentrations and 1 mM DTT at 37 °C. After 2 hours, the proteins were subjected to SDS-PAGE and visualized with Coomassie stain. A representative series of gels is shown from experiments performed in triplicate. *B,* Three replicates of the experiments shown in panel **A** were quantified by densitometry. Bands corresponding to TcdB 544-2366 were quantified and normalized to the band corresponding to TcdB 1-2366 without InsP6. Error bars reflect the standard deviation of the percent cleavage between three experiments. The data indicate that wild-type TcdB autoproteolysis can be detected at concentrations of 1 uM to 1 mM InsP6. By comparison, TcdB mutants C698S, C698A, and H653A were completely inactive for autoprocessing at all InsP6 concentrations. The TcdB D587N and L543A had some residual activity, but autoprocessing activity was impaired relative to wild-type. *D*, GTDs of autoprocessing mutants are not released in cells. HeLa cells were synchronized for 30 minutes at 4 °C, then intoxicated with 10 nM toxin. Intoxicated cells were incubated at 4 °C for an hour before being moved to 37 °C. Cells were harvested after 50 minutes and cell lysates were prepared for SDS PAGE and Western blot. The blot was probed with antibodies against the TcdB GTD, unglucosylated Rac1, total Rac1, and GAPDH. While release of the GTD in cells intoxicated with wild-type TcdB was detected, the free GTD was not detected in cells treated with autoprocessing deficient mutants. The absence of signal with an antibody that recognizes unglucosylated Rac1 suggests that the autoprocessing mutants are still able to modify Rac1 in cells.

Autoprocessing mutants induce necrosis in cultured epithelial cells

To test the hypothesis that small molecule inhibitors of TcdB autoprocessing could be detected in a cell based screen, we assessed cell viability in response to three of the TcdB autoprocessing mutants: TcdB C698S, TcdB C698A, and TcdB L543A. HeLa cells were treated for 2.5 hours with multiple concentrations of TcdB and the TcdB mutants, and viability was assessed using CellTiterGlo. Unexpectedly, the autoprocessing deficient mutants were found to induce cell death at concentrations comparable to TcdB (Figure 2.5A). To test whether this response was unique to HeLa cells, we performed similar experiments with Caco2 cells, an epithelial cell line derived from human colon. As with the HeLa cells, wild-type and autoprocessing deficient TcdB mutants induced a decrease in cellular ATP at similar concentrations in Caco2 cells (Figure 2.5B). Caspase-3/7 activation was not detected in HeLa cells treated for 25 hours with autoprocessing deficient TcdB mutants (Figure 2.5C), and the amount of LDH released in HeLa cells treated with wild-type TcdB and the TcdB C698S, C698A, and L543A autoprocessing mutants was equivalent (Figure 2.5D). Finally, HeLa cells were treated with 10 nM wild-type and mutant TcdB proteins in the presence of a live/dead cell indicator and imaged every 10 minutes over a 2 hour time course. A representative movie of what we observed is included in the supplemental material (Video S1). The percentage of dead cells quantified over six fields suggests that the kinetics of cell death are identical for the four proteins (Figure 2.6). Collectively, these data suggest autoprocessing is not required for TcdB-mediated necrosis in epithelial cells.

TcdB induced necrosis is a glucosyltransferase independent process

The idea that TcdB-induced necrosis did not require autoproteolytic release of the GTD suggested that the TcdB glucosyltransferase activity would also not be required for cytotoxicity. To test this hypothesis, single amino acid point mutations were made in the glucosyltransferase active site (D270N, D270A, Y284A, W520A, and N384A) based on the crystal structure of the TcdB GTD bound to UDP-glucose [10]. Proteins were expressed in the *B. megaterium* expression system and purified to

homogeneity. All mutants were tested for their *in vitro* glucosyltransferase activity in the presence of purified Rac1 and UDP[^{14}C]glucose, and all were impaired relative to wild-

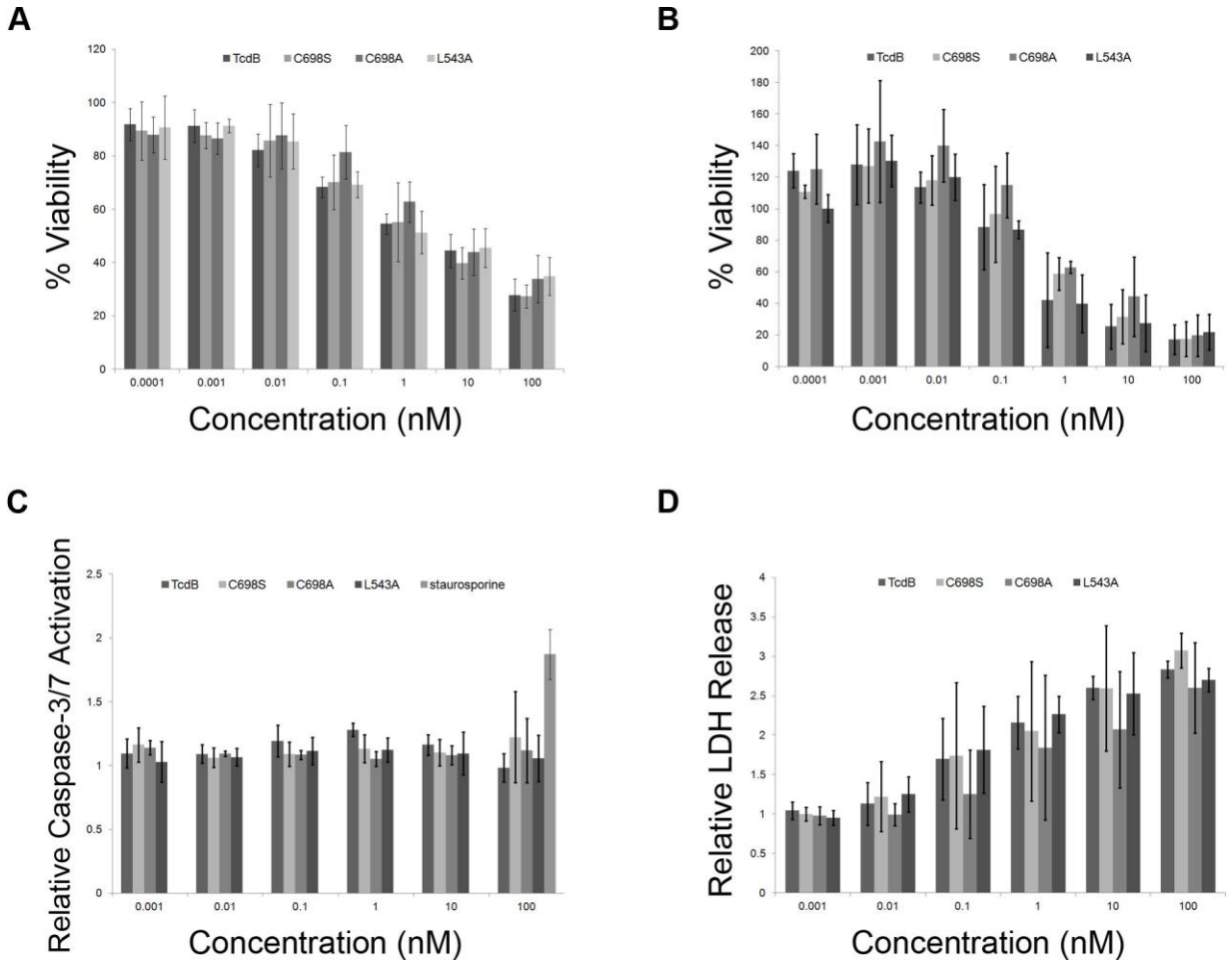

Figure 2.5. Autoprocessing mutants induce necrosis in epithelial cells. *A,* Toxins were applied to HeLa cells at concentrations ranging from 0.1 pM to 100 nM, and viability was measured after 2.5 hours with CellTiterGlo. *B,* Toxins were applied to Caco2 cells at concentrations ranging from 0.1 pM to 100 nM, and viability was measured after 18 hours with CellTiterGlo. Percent viability was determined by normalizing the signal from treated cells to the signal from untreated cells. Values reflect the average signal from three experiments in which each condition was tested in triplicate. Error bars correspond to the standard deviation in the percent viability from the three experiments. *C*, Autoprocessing mutants did not induce caspase-3/7 activation after 25 hours. *D*, Comparable levels of extracellular LDH were detected after 8 hours in HeLa cells treated with wild-type TcdB and TcdB autoprocessing mutants. Caspase and LDH values represent the average of three experiments in which three replicates were averaged. Error bars indicate the standard deviation between the values obtained from the three experiments.

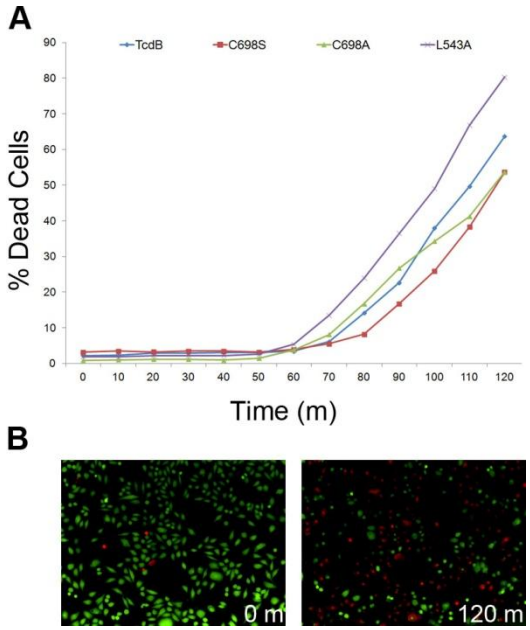

Figure 2.6. TcdB and TcdB autoprocessing mutants have the same cytotoxicity kinetics. *A*, TcdB, TcdB C698S, TcdB C698A, and TcdB L543A at 10 nM induce HeLa cell death at similar rates, as detected by Live/Dead Cell Imaging dyes. Values represent the number of red (dead) cells per total number of cells (red + green) over six image fields and were calculated using Columbus Analysis Software. Dead cells were defined as having a red intensity greater than 500 relative units. *B*, Representative pictures of TcdB treated cells at 0 and 120 minutes. Images were taken using an Opera High-Throughput Confocal Screening Microscope.

type (Figure 2.7A). Of the five mutants, the TcdB D270N mutant showed the greatest defect in *in vitro* glucosyltransfer, with residual activity only evident in the highest concentrations of enzyme and substrate (Figure 2.7B). Even with differences in the amount of residual activity, all five mutants were defective in the modification of Rac1 in cells (Figure 2.7C). Furthermore, all 5 mutants were capable of inducing a cytotoxic effect similar to that of wild-type TcdB when applied to HeLa cells (Figure 2.7D) and Caco-2 cells (data not shown). We interpret these data to mean that the TcdB cytotoxic effect does not require the glucosyltransferase activity of the toxin.

The low concentration cytopathic effect is functionally distinct from the high concentration cytotoxic effect

The observation that TcdB autoprocessing mutants were able to glucosylate Rac1 in cells (Figure 2.4C) suggested that they would induce rearrangements in the actin cytoskeleton that result in the cytopathic 'rounding' phenotype. To investigate this, HeLa cells were treated with multiple concentrations of wild-type and mutant TcdB proteins and imaged every 10 minutes over a 2 hour time course. The percentage of round cells was quantified over six fields for each concentration and time point. At a 10 pM concentration, we observed similar rounding kinetics for TcdB and the three TcdB autoprocessing-deficient mutants (Figure 2.8A). Differences in the kinetics of rounding

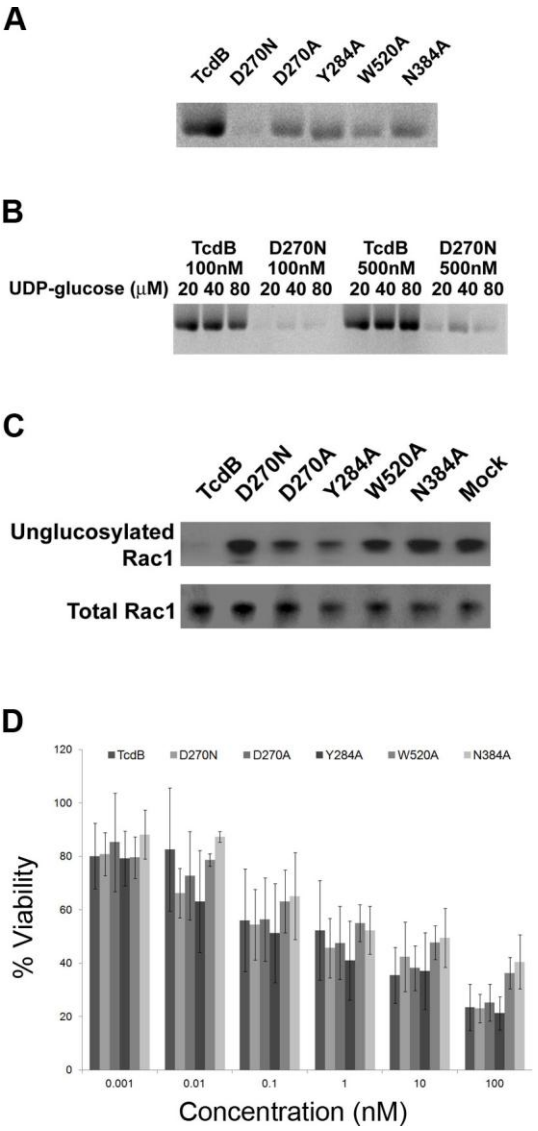

Figure 2.7. TcdB glucosyltransferase mutants cause epithelial cell death. *A,* TcdB and TcdB glucosyltransferase domain mutants (100 nM) were tested for their capacity to glucosylate purified Rac1 (2 uM) in the presence of 20 mM UDP-[^{14}C]-glucose over the course of 1 h. The proteins were resolved by SDS-PAGE, and the gels were analyzed by Phosphorimaging. *B,* TcdB D270N was tested with higher concentrations of both toxin and UDP-[^{14}C]-glucose. Only at the highest concentrations of both toxin and UDP-[^{14}C]-glucose is residual activity apparent. *C,* Glucosyltransferase activity in HeLa cells, as determined by Western and an antibody specific for unglucosylated Rac1, also showed that the glucosyltransferase mutants are deficient in Rac1 glucosylation, though levels of impairment are varied. Again, D270N was the most deficient of the mutants. *D,* Wild-type TcdB and the TcdB glucosyltransferase mutants induced comparable levels of HeLa cell death, as determined by CellTiterGlo, after 2.5 h of treatment. Percent viability was determined by normalizing the signal from treated cells to the signal from untreated cells. Values reflect the average signal from three experiments in which each condition was tested in triplicate. Error bars correspond to the standard deviation in the percent viability from the three experiments.

began to appear at a concentration of 100 fM (Figure 2.8B) but were not fully evident until the concentration of toxins was dropped to 1 fM (Figure 2.8C). The full dataset collected at concentrations spanning 8 orders of magnitude and a movie of what we observed with 10 fM wild-type TcdB is included in the supplemental material (Figure 2.9 and Video S2). While not required for cytotoxicity, autoprocessing and GTD release appear to be important for cytopathic processes that occur at very low concentrations. In HeLa cells, we see that at concentrations where cytopathic effects can be observed (1 fM-10 pM, Figure 2.8), the cells are not dead (Figure 2.5A). These data provide a clear distinction between the cytotoxic and cytopathic effects induced by TcdB.

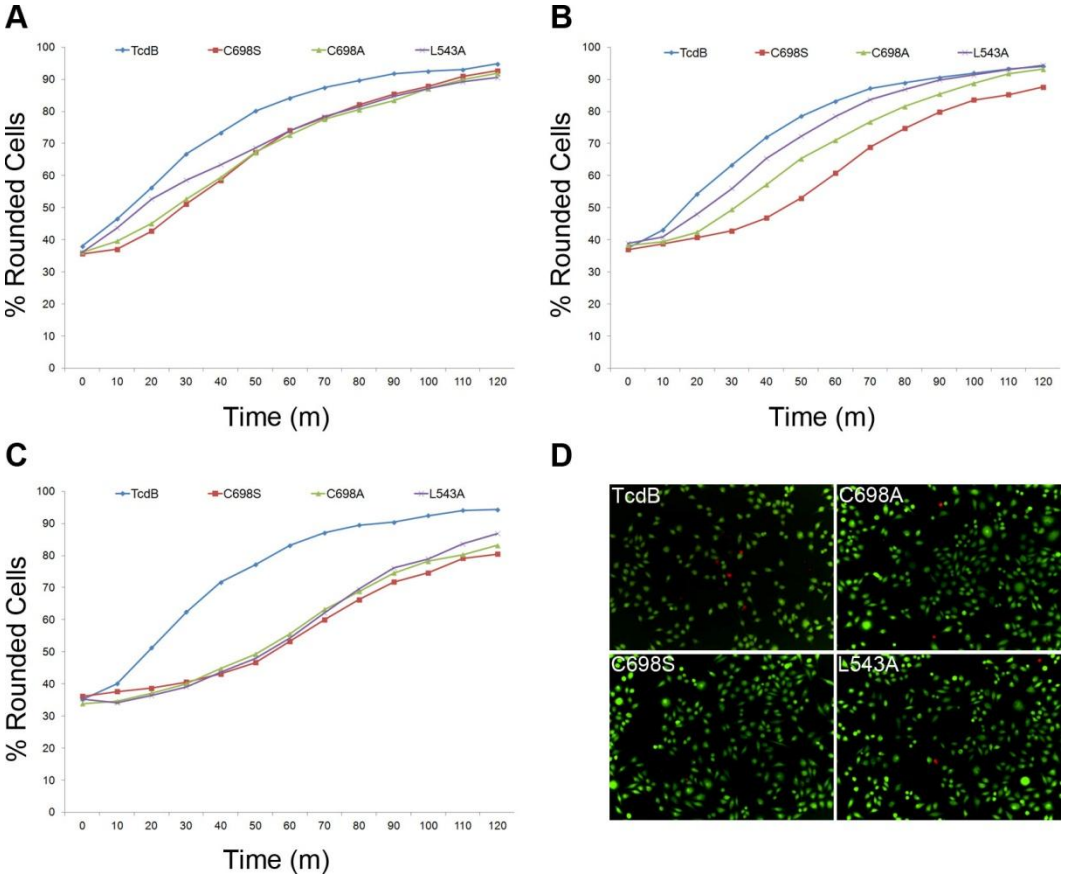

Figure 2.8. TcdB and TcdB autoprocessing mutants cause cell rounding with concentration dependent kinetics. HeLa cells were treated with multiple concentrations of wild-type and mutant TcdB proteins and imaged every 10 minutes over a 2 hour time course. The percentage of round cells was quantified over six fields for each concentration and time point. The kinetics of rounding induced by TcdB and the TcdB autoprocessing mutants is shown at concentrations of *A,* 10 pM. *B,* 100 fM and *C*, 1 fM. *D,* Representative images of cells treated with 1 fM TcdB and TcdB autoprocessing mutants for 50 minutes. Green cells are alive; red cells are dead. Images were collected with an Opera High-Throughput Confocal Screening Microscope in an environment-controlled chamber at 37 °C, 5% CO_2. Round cells were defined as having an area less than 500 um^2 and a width-to-length ratio of less than 0.4. Analysis was performed using Columbus Analysis software.

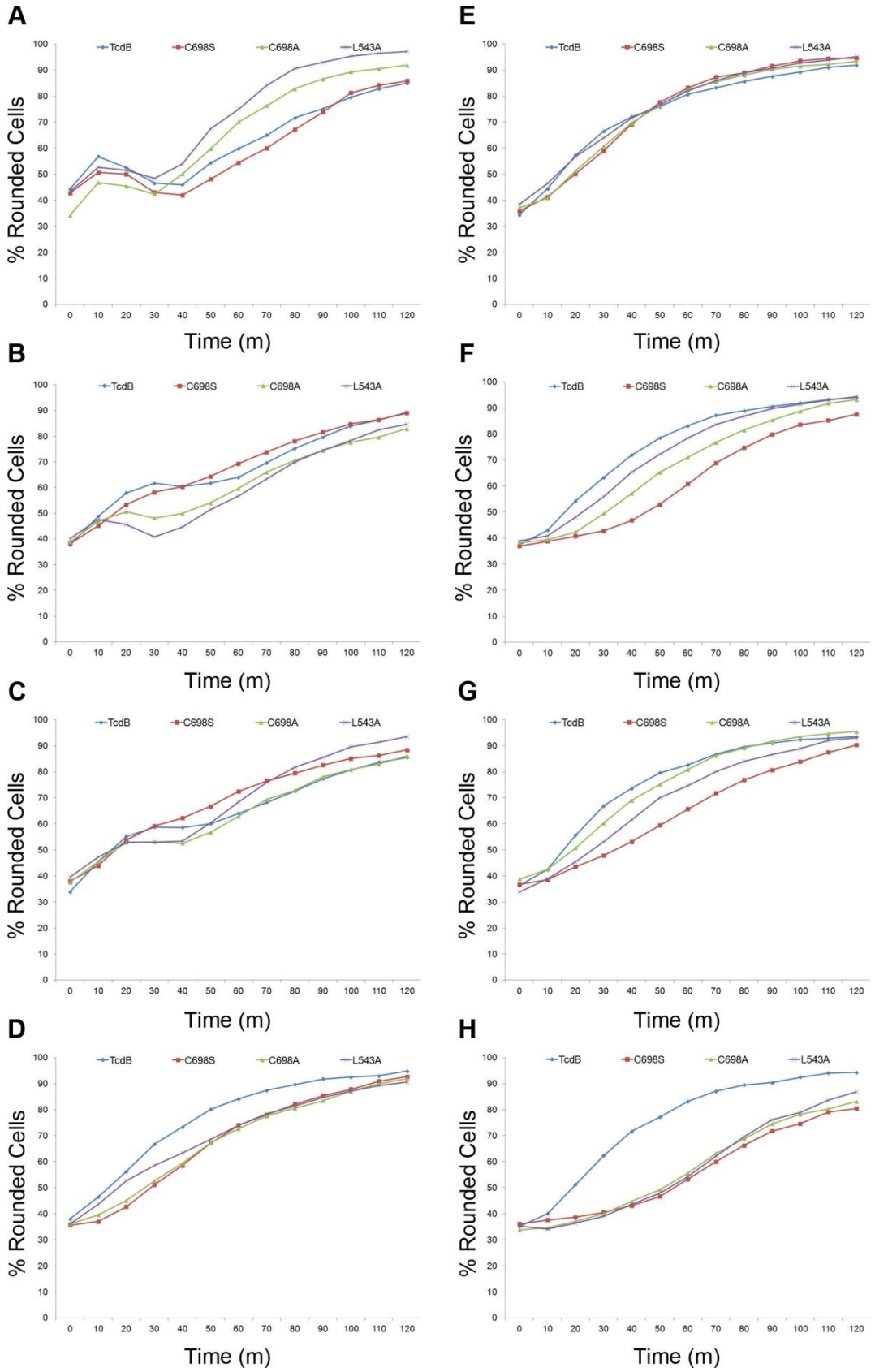
A
B
C
D
E
F
G
H
TcdB
C698S
C698A
L543A
% Rounded Cells
Time (m)
0
10
20
30
40
50
60
70
80
90
100
110
120

Figure 2.9. TcdB and TcdB autoprocessing mutants have different cytopathic kinetics at 1 fM. HeLa cells were treated with multiple concentrations of wild-type and mutant TcdB proteins and imaged every 10 minutes over a 2 hour time course. The percentage of round cells was quantified over six fields for each concentration and time point. Percent rounded cells induced by TcdB and autoprocessing mutants is shown at concentrations of *A,* 10 nM, *B,* 1 nM, *C*, 100 pM, *D*, 10 pM, *E*, 1 pM, *F*, 100 fM, *G*, 10 fM, and *H*, 1 fM. Differences in the rounding kinetics between TcdB and autoprocessing mutants begin to appear at a concentration of 100 fM and are clearly distinct at 1 fM. Images were collected with an Opera High-Throughput Confocal Screening Microscope in an environment-controlled chamber at 37 °C, 5% CO_2. Round cells were defined as having an area less than 500 um^2 and a width-to-length ratio greater than 0.4. Analysis was performed using Columbus Analysis software.

TcdB and TcdB C698A cause epithelial damage in porcine colonic explants

The distinction between cytopathic and cytotoxic events in cell culture led us to question if either event might correlate with disease pathology. Since the formation of necrotic lesions in the colon is a hallmark of CDI pathology, we sought to determine the concentration of toxin required to induce these effects and whether autoprocessing was required. Porcine colonic explants were incubated with multiple concentrations of toxin for 5 hours. The tissue was fixed with formalin, embedded in paraffin, and sections were stained with H&E (Figure 2.10A). The slides were scored in a blinded fashion and given a score (0-3) to reflect the level of epithelial damage (Figure 2.10B). Damage ranged from a mostly intact surface epithelium to mucosal loss of 50% or greater in the depth of colonic crypts. The scores indicated a loss of surface epithelium in tissue treated for 5 hours with 10 nM TcdB and TcdB C698A. There was little damage in tissues treated with a buffer control or in tissues treated with wild-type TcdB and TcdB C698A at a concentration of 10 pM. Statistical analysis by two-way ANOVA revealed a significant difference in scores for tissues treated with the toxins over the range of concentrations ($p < 0.001$), while there was no statistical difference between tissues treated with wild-type TcdB and TcdB C698A. A subsequent Bonferroni's test revealed that scores given to tissue treated with 10 nM TcdB and 10 nM TcdB C698A were significantly different from scores given to tissue treated with 10 pM TcdB and 10 pM TcdB C698A ($p < 0.001$). The tissues were stained with an anti-pan cytokeratin antibody to confirm the keratin positive cells at the luminal surface of the colon were disrupted (Figure 2.10C) and an anti-activated caspase-3 antibody to confirm that the toxin treatment did not induce an apoptotic response (Figure 2.10D). The data reveal a

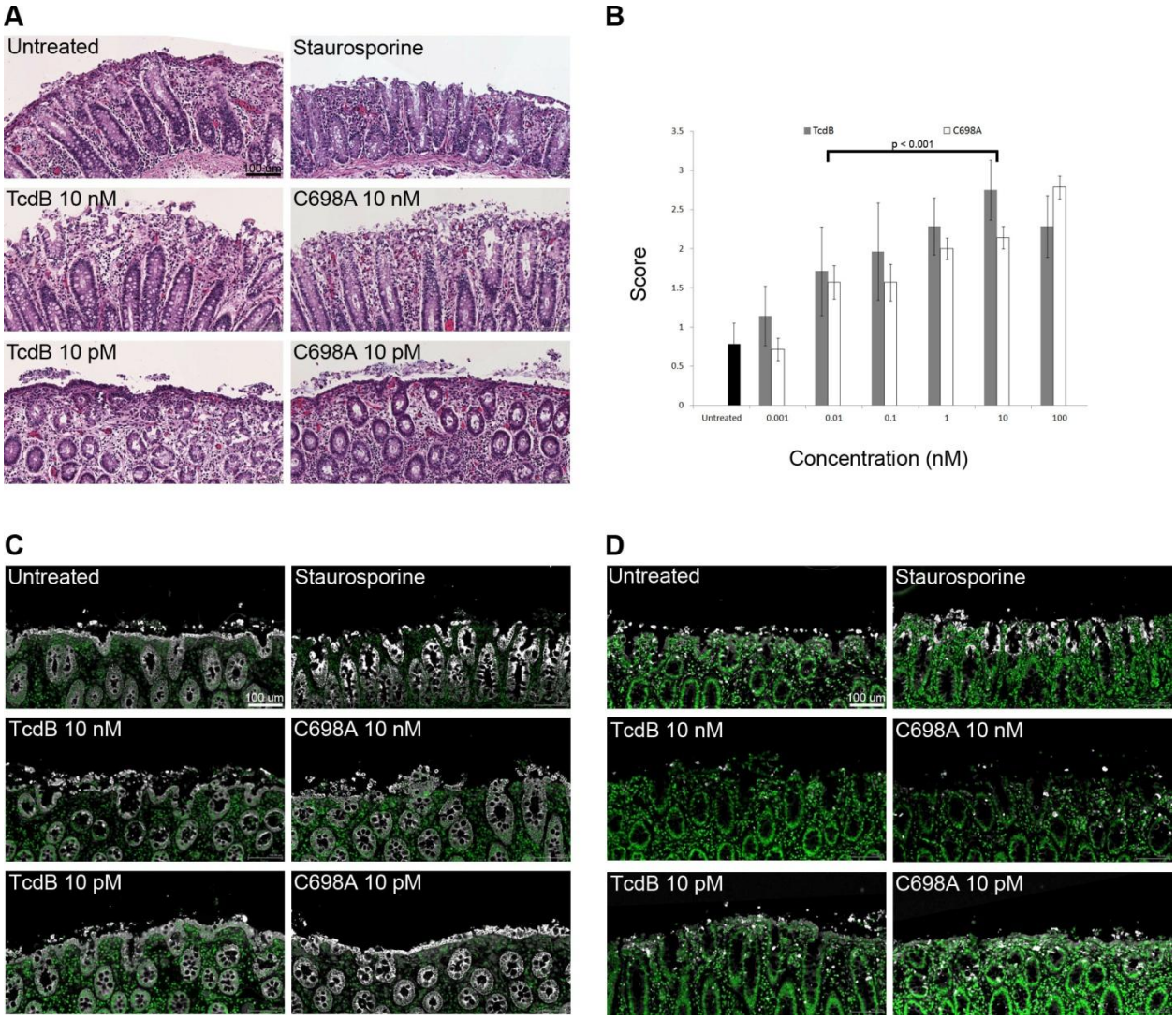

Figure 2.10. TcdB and TcdB C698A cause epithelial damage in porcine colonic explants. Porcine colonic explants were treated with 1 mM DTT to remove the mucus layer, washed with PBS, and incubated with toxin at 37 °C for 5 hours. *A,* Tissue sections were stained with H&E. *B,* The H&E slides were scored in a blinded fashion using a semi-quantitative injury scale: 0- no damage; 1-superficial damage, damage limited to intact surface epithelial cells; 2-loss of up to 50% of surface epithelial cells or gland length, crypts intact; 3-loss of over 50% of surface epithelial cells and damage in greater than 50% of gland length. An injury score was calculated as the mean score for sections analyzed seven times by six individuals. Statistical analysis was performed using a two-way ANOVA and post-hoc tests. These analyses revealed a significant difference in the scores given to tissues treated with the toxins over the range of concentrations ($p < 0.001$), while there was no statistical difference between tissues treated with TcdB and TcdB C698A. A subsequent Bonferroni's test revealed that scores given to tissue treated with 10 nM TcdB and 10 nM TcdB C698A were significantly different from scores given to tissue treated with 10 pM TcdB or 10 pM TcdB C698A ($p < 0.001$). Error bars correspond to the standard deviation between the seven scores. *C*, The sections were also stained with an anti-pan keratin and *D*, anti-active caspase-3 antibody. Representative images of H&E, pan-cytokeratin, and active caspase-3 staining (white – pan-cytokeratin/active caspase-3, green – DAPI) show significant damage to the epithelium of the colon at concentrations of TcdB and TcdB C698A that kill cells (10 nM). At concentrations that induce rounding but not death in cultured cells (10 pM), there was no significant damage to the tissue surface cells. Caspase-3 activation was not detected at levels above background in any of the TcdB-treated tissues.

correlation between the concentration of toxin required to kill epithelial cells in culture with the concentration required to disrupt epithelial integrity in colonic tissue and indicate that autoprocessing is not required for tissue damage.

Discussion

TcdB is a multi-functional protein with a central role in CDI pathogenesis. Our goal at the outset of this study was to conduct a screen for small molecule inhibitors that could aid in the dissection of the TcdB mechanism and the generation of new leads for therapeutic intervention. Our strategy was to combine a cell-based phenotypic screen with target-specific secondary assays. In the course of setting up our screening assays, we made two unexpected observations that warranted further investigation.

First, in contrast to a previous report [150], TcdB did not trigger the induction of apoptosis in cultured epithelial cells as measured by caspase-3/7 activation (Figure 2.1A, 2.2). Since there was an overlap in the cells, concentration of toxin, and timepoints used for analysis, we are left to speculate that the difference stems from advances in the detection reagent. The newer reagent for detecting caspase-3/7 activation allows one to directly quantitate the relative quantity of activated caspase-3/7 as opposed to the overall rate of caspase activity.

While TcdB-treatment did not induce the activation of caspase-3/7, the rapid ATP depletion observed in both HeLa (Figure 2.1B, 2.5A, 2.3A) and Caco2 (Figure 2.5B) cells suggested that the mechanism of TcdB-induced cell death was likely necrosis. The observed loss of membrane integrity (Figure 2.1C), rapid LDH (Figure 2.1D, 2.3B), and HMGB1 release (Figure 2.1E) support this conclusion.

We next questioned whether a cell-based assay for small molecule inhibitors of TcdB-induced necrosis would allow us to detect molecules that interfered with autoprocessing. We were particularly interested in targeting the autoprocessing activity of the toxin since, in theory, one could identify molecules that either activate (e.g. InsP6) or inhibit the function of the cysteine protease domain. We generated five TcdB point mutants in which key residues of the cysteine protease active site or cleavage site were

mutated. Three of these mutations, C698S, C698A, and L543A, rendered TcdB non-functional for InsP6-induced autoprocessing in an *in vitro* assay, even when InsP6 was added at a 1 mM concentration (Figure 2.4A, 2.4B). The mutants were also defective for autoprocessing in the context of cells since free GTD could be detected in cells treated with wild-type TcdB but not in cells treated with the autoprocessing mutants (Figure 2.4C). While we cannot rule out the possibility of an alternate cleavage mechanism that results in a quantity of free GTD that is less than the detection limit of the assay, the free GTD concentration generated from such a mechanism would be too small to account for the identical cytotoxicity profiles observed in Figures 2.5A and 2.5B.

The unexpected observation that cytotoxicity does not require autoproteolytic release of the GTD led us to directly test whether the glucosyltransferase activity of the toxin was required (Figure 2.7). We generated five single amino acid point mutants of TcdB that differed in their residual glucosyltransferase activities *in vitro* (Figure 2.7A, 2.7B). Despite the different enzyme activity levels, all were significantly impaired relative to wild-type TcdB in their capacity to modify Rac1 in cells (Figure 2.7C), and all were comparable to wild-type TcdB in their cytotoxic effects (Figure 2.7D). These data are consistent with the observation that autoprocessing is not required and suggest that the cytotoxic response to TcdB is triggered by an event upstream of GTD release.

While not required for cytotoxicity, autoprocessing and GTD release are important for cytopathic processes that occur at low concentrations [3,32,35,103,104]. Our data are consistent with these previous reports and indicate differences in rounding kinetics emerging at concentrations of 100 fM (Figure 2.8C and 2.9). While our Western experiment indicated TcdB autoprocessing mutants were still able to modify Rac1 in cells (Figure 2.4C), a similar observation has been made for a non-cleavable form of TcdA and is thought to reflect continuous vesicle trafficking and an exchange of membranous compartments that allow the uncleaved toxin to come into contact with the membrane-bound GTPases [105]. This capacity to modify Rac1 while still tethered to the endosomal membrane presumably accounts for the similar rounding kinetics that we observed when the TcdB autoprocessing mutants were applied to HeLa cells at concentrations of 1 pM and higher (Figure 2.8A, 2.9).

The concentrations of TcdB needed to induce cytopathic effects (≤ 1 fM, Figure 2.9) are significantly lower than what is required to induce the cytotoxic effect (1 nM, Figure 2.5). At a concentration of 10 pM TcdB, the cells are clearly round (Figure 2.8A) but not dead (Figure 2.5). The distinction between cytopathic and cytotoxic events in cell culture raises the question of whether either process correlates with mechanisms of pathology observed in the host. To address this question, we decided to test what concentration of toxin was required to induce epithelial cell damage in colonic tissue explants. Visual assessment of H&E stained colonic tissue integrity in a blinded fashion indicated damage with treatments of 10 nM TcdB but not with 10 pM TcdB (Figure 2.10). Similar observations were made with the TcdB C698A mutant suggesting that the damage that occurs to colonic tissue in response to TcdB does not depend on the autoprocessing activity. Pan-cytokeratin staining confirmed that the cells on the luminal surface of the tissue remained intact in the presence of 10 pM TcdB or TcdB C698A but were being disrupted in samples treated with 10 nM TcdB, 10 nM TcdB C698A, or 100 uM staurosporine. The staurosporine control revealed strong caspase-3 activation into the crypts (Figure 2.10D). The untreated control tissue demonstrated a low level of caspase-3 activation in the cells on the luminal surface and strong activation in single cells coming off the surface of the tissue. Tissues treated with 10 pM TcdB and TcdB C698A showed caspase-3 activation levels similar to those of the untreated tissue. Tissue treated with 10 nM TcdB or TcdB C698A demonstrated even lower levels of caspase-3 activation, presumably because the cells on the luminal surface have been shed. Unlike the untreated, staurosporine-treated, and 10 pM TcdB-treated tissues, caspase-3 activation was generally not observed in the cells that were in the process of being shed in tissues treated with 10 nM TcdB or TcdB C698A (Figure 2.10D). This suggests that tissue damage is not only independent of autoprocessing activity, but also not likely due to apoptosis.

The phenotypic differences with concentration led us to wonder what concentration of toxin is present in the colons of individuals experiencing the symptoms of CDI.

We found only one published report, where TcdB was quantitated using a real-time cell analysis system [168]. In this report, the TcdB concentrations in stool samples

from 10 patients experiencing mild to severe symptoms of CDI ranged from 4.9 pM to 413 pM with a mean concentration of 146 pM. Presumably, the concentration of TcdB would be much higher at the colonic epithelium prior to dilution by diarrhea. Of note, the average TcdB concentration in samples from 9 individuals who were not experiencing CDI symptoms was 1 pM, with a range of 0.1 pM to 3.3 pM. This analysis suggests that the cytotoxic effects observed in cells and tissues treated with 1 to 10 nM TcdB are better correlated with pathology than the cytopathic effects that are induced at 1 fM concentrations.

Our data suggest that inhibiting TcdB autoprocessing will not prevent the colonic tissue damage observed in *C. difficile* associated diseases. However, while the colonic epithelium is the primary barrier separating *C. difficile* from the host, it is possible that the autoprocessing function of TcdB is important in another setting relevant to pathogenesis. For example, the colonic explant model used in this study does not account for the impact of the toxins on inflammation or the potential impact of an anaerobic environment. Evaluating the effect of autoprocessing- and glucosyltransferase-deficient toxins in an animal model of *C. difficile* infection therefore represents a priority for future studies. In addition, it will be important to define the mechanism of TcdB-mediated necrosis in cells and tissue. Relevant comparisons may come from the study of other toxins. For example, the *Bordetella pertussis* adenylate cyclase (AC) toxin is known to have multiple mechanisms that contribute to cytotoxicity [169]. Identifying the autoprocessing- and glucosyltransferase-dependent and –independent aspects of TcdB-mediated pathology represents an exciting path for future study.

CHAPTER III

CLOSTRIDIUM DIFFICILE TOXINS A AND B CAUSE COLONIC TISSUE DAMAGE BY DISTINCT MECHANISMS

Introduction

Clostridium difficile is the most common cause of antibiotic-associated diarrhea in the United States and has been steadily increasing in prevalence and severity over the last 15 years [162,170,171]. Symptoms of *C. difficile* infection (CDI) can range from mild diarrhea to pseudomembranous colitis, and hallmarks of the disease include neutrophil infiltration, fluid release, and necrotic lesions in the colonic epithelium [34,172]. The bacteria produce two main virulence factors, large toxins called TcdA and TcdB [63,64].

The respective function and relative importance of each toxin in pathogenesis has been an active topic of investigation. Genetic knockout experiments in *C. difficile* have shown both toxins are important for disease pathology, although TcdB alone is sufficient to cause death in the hamster model [63,64]. For many years, TcdA and TcdB have been thought to act synergistically with TcdA acting as an enterotoxin and TcdB acting as a cytotoxin [123,129]. The general term enterotoxin refers to the capacity of TcdA to induce inflammation, cytokine release, and fluid secretion in animal intoxication models [67-69]. While TcdB does not always induce these same phenotypes in animal models, it has been shown to disrupt the integrity of the epithelial structure in both explant and xenograft models [132,133]. TcdB is also notably more potent as a cytotoxin in cell culture models [123,129-131].

The toxins have an N-terminal glucosyltransferase domain (GTD) that is delivered into the host cytosol by the C-terminal portion of the protein [102,163]. The GTD has been shown to target and inactivate a number of Rho-family GTPases, This inactivation has been linked to a cell ‘rounding’ or cytopathic effect (CPE) [108-110,173]

and to an apoptotic cytotoxic effect [9,20,21,126,142-145,150,151]. In most reports, the cytotoxic effects of TcdA in tissue culture models are not realized until more than 24 hours post intoxication [9,20,105,115,145,174]. TcdB also induces a glucosyltransferase-independent necrosis that is mediated by the assembly and activation of the NADPH oxidase (NOX) complex, subsequently producing high levels of reactive oxygen species (ROS) [100,174-177]. These observations were made at nanomolar concentrations in both tissue culture and colonic explant models.

In this study, we wanted to investigate the mechanisms and pathological outcome of both TcdA and TcdB intoxication under comparable conditions. Using a colonic explant model, we found that TcdA causes damage to tissue at the same concentrations as TcdB. Since we have previously been unable to recapitulate these observations in tissue culture systems, we reasoned that the anti-apoptotic mutations of transformed cell lines may be preventing pathologically relevant outcomes of TcdA intoxication. Therefore, we wanted to find a non-transformed cell line that would allow us to study TcdA mechanisms of cell death in a convenient, accurate, and relevant model system that recapitulated our observations in tissue. Young adult mouse colonic (YAMC) epithelial cells are derived from the Immortomouse which expresses a temperature sensitive simian virus 40 (SV40) T-antigen that suppresses p53 [178]. The cells can be carried as an anti-apoptotic cell line at the permissive temperature of 33 °C, and then upon shifting to the non-permissive temperature of 37 °C, YAMC cells behave as primary cells with an intact p53 pathway able to undergo normal apoptosis. Using this tool, we were able to investigate the effects of TcdA and TcdB side-by-side in the same cell line at the same time points with the same assay readouts. Our observations provide an opportunity to unify the many, seemingly conflicting, reports describing the mechanisms by which TcdA and TcdB cause cell death in epithelial cells.

Methods

Recombinant protein expression and purification

The glucosyltransferase domain double point mutation (TcdA D285/287N and TcdB D286/288N) plasmids were made using the TcdA and TcdB parent plasmids [5]

according to the QuickChange protocol (Stratagene). Recombinant TcdA, TcdA D285/287N, TcdB, and TcdB D286/288N proteins were expressed in *B. megaterium* and purified as previously described[5].

YAMC cell culture and viability assays

YAMC cells were maintained in RPMI-1640 supplemented with 5% FBS, 1 mg/ml insulin, 10 uM alpha-thioglycerol, 1 uM hydrocortisone, and 5 U/ml mouse interferon gamma. Cells were carried at 33 °C with 5% CO_2. For assays performed at 37 °C, cells were plated and incubated at 37 °C with 5% CO_2 overnight prior to intoxication. Viability was measured at the indicated concentrations and timepoints using the CellTiterGlo Luminescent Cell Viability Assay (Promega, G7573). LDH release indicative of necrosis was quantified using CytoToxGlo (Promega, G9290). Apoptosis was assessed by measuring active caspase 3 and 7 using Apo-ONE Homogeneous Caspase-3/7 Assay (Promega, G7792). ROS production was assayed with Carboxy-H2DCFDA (Life Technologies, C400) as previously described [175].

Colonic explants

Animal husbandry and experimental procedures related to the porcine colonic explants were performed in accordance with the Vanderbilt University Institutional Animal Care and Use Committee (IACUC) policy. Discarded colon tissues were obtained from pigs following euthanization at the end of IACUC-approved animal use protocols and prepared for intoxication as previously described[174]. Human colonic tissue was obtained by the Cooperative Human Tissue Network from consented, de-identified donors under IRB approved protocol 031078. Tissue was challenged with 10 nM TcdA, TcdB, TcdA D285/287N, or TcdB D286/288N for 5 h at 37 °C. Sections were cut by the Vanderbilt University Translational Pathology Shared Resource core. The H&E staining and scoring of tissues was performed as previously described [174]. H&E stained images were obtained with the Ariol SL-50 (Epithelial Biology Center Imaging Core). Caspase 3 and ROS staining of tissues were done as previously described [174,175]. All slides stained with fluorescent markers were analyzed with an LSM 510 Confocal microscope.

Statistical Analysis

Statistical analysis was performed using a two-way ANOVA and post-hoc test in GraphPad Prism. Two-tailed, paired student's t-tests were performed using Excel.

Results

TcdA causes damage to colonic tissue

Freshly excised colonic explants were intoxicated with TcdA and TcdB at a range of concentrations (10 pM to 100 nM) for 5 hours, and damage to the colonic epithelium was assessed in H&E stained tissue sections using a semi-quantitative injury scale (Figure 3.1A). The tissue damage induced by the toxins is dose-dependent and significant at concentrations ≥ 100 pM (Figure 3.1B). Statistical analysis by a two-way ANOVA revealed there was no significant difference between pathology scores of tissue intoxicated with TcdA and TcdB at any concentration tested (Figure 3.1B). These results demonstrate that TcdA causes damage to tissue within a five hour time frame at similar doses as TcdB.

TcdA induces a robust cell death in conditionally immortalized cells

The explant model is informative in that we can establish similar potencies between TcdA and TcdB, but H&E staining does not allow the delineation of mechanistic detail by which damage is occurring. For example, if the toxins cause damage with similar potencies in tissue, why do we not observe the same phenotype in tissue culture models? We hypothesized that the lack of rapid TcdA-induced cell death in typical tissue culture models was due to mutations in the apoptotic pathways of many transformed cell lines. In order to test our hypothesis, we obtained YAMC cells, a conditionally immortalized cell line with temperature-dependent p53 function. YAMC cells were challenged with the TcdA and TcdB toxins at both the permissive and non-permissive temperatures, and cell death was quantified using CellTiterGlo, an ATP sensitive viability indicator. Consistent with what is observed in transformed cell lines, TcdA does not induce appreciable cell death at the permissive temperature of 33 °C,

where p53 is inactivated (Figure 3.2A). TcdB does not cause cell death at concentrations ≤ 10 pM but kills cells efficiently at concentrations ≥ 100 pM, consistent with our previous observations in transformed HeLa and Caco2 cell lines [174].

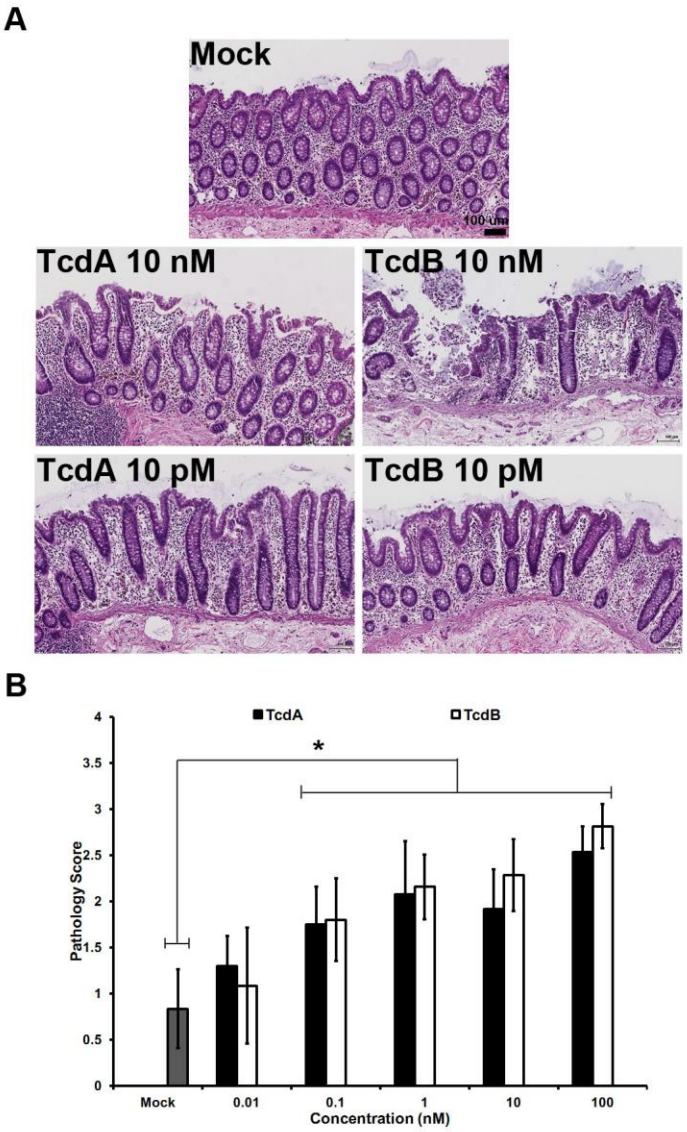

Figure 3.1. TcdA causes damage to colonic tissue. A, Porcine colonic explants were intoxicated with the indicated concentration of toxin and incubated at 37 °C for 5 hours. Slides were stained with H&E. B, Tissue sections were scored in a blinded fashion by 3 pathologists using a semi-quantitative injury scale: 0-no damage; 1-superficial damage, damage limited to intact surface epithelial cells; 2-loss of up to 50 % of surface epithelial cells or gland length, crypts intact; 3-loss of over 50% of surface epithelial cells and damage in greater than 50% of gland length. The scores represent the average of triplicate scores of at least 4 different experiments. Error bars represent the standard deviation of all scores given in all experiments. The data were analyzed by two-way ANOVA, and at all concentrations, TcdA and TcdB were not statistically different. Student's t-tests were performed between each toxin at each concentration and the mock treated tissue and found every concentration except 10 pM to have significant pathological damage at $p < 0.001$, represented by the asterisk.

Upon shifting to 37 °C and allowing normal p53 expression, however, we detected a drastically different phenotype. Consistent with observations in our colonic explant model, TcdA caused cytotoxicity in YAMC cells across a wide concentration

range (100 nM to 10 fM, Figure 3.2B). These results suggest that when cells are intoxicated with TcdA, the mechanism of cell death may be dependent on the p53 pathway.

Interestingly, we also observed differences in TcdB-induced cell death when comparing the two cellular states. In cells at 33 °C, where p53 function is disrupted, we detected significant cell death when we used higher concentrations (100 nM to 100 pM) of TcdB. At lower concentrations, starting at 10 pM, however, the cells were viable (Figure 3.2A). We do not observe this change in cell viability at 37 °C, where p53 function is not disrupted. TcdB causes cytotoxicity at all concentrations assayed at 37 °C, suggesting that the cell death induced by TcdB at lower concentrations (≤ 10 pM) is dependent upon the p53 pathway.

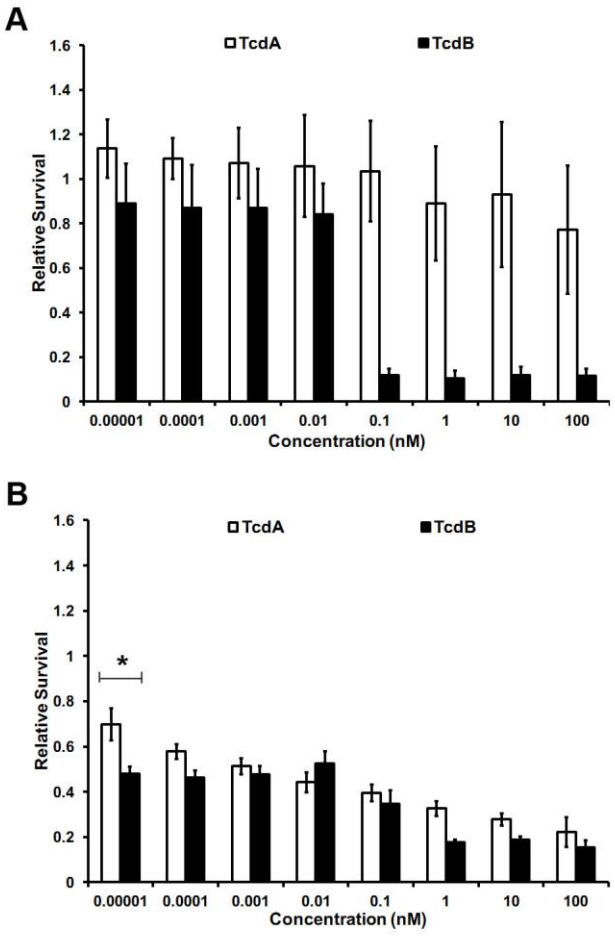

Figure 3.2. TcdA induced cell death of conditionally immortalized cells is p53 dependent. YAMCs were seeded in a 96 well plate and incubated overnight at either A, 33 °C or B, 37 °C. Cells were intoxicated as indicated and incubated at their respective temperatures for 18 h. Cell viability was determined using CellTiterGlo, an ATP sensitive, luminescent viability indicator. Relative survival was calculated by normalizing the treated samples to untreated samples. Data represent the average of three experiments performed in triplicate. Error bars represent the standard deviation of the averages of the 3 experiments. Asterisks represent a statistical difference between TcdA and TcdB with a p-value of $p < 0.0001$ by two-way ANOVA. There is no statistical difference between TcdA and TcdB between 10 pM and 100 fM by two-way ANOVA. At 10 fM, a significant difference in potency becomes apparent when analyzed by a student's t-test, paired, two-tailed, and a p-value < 0.0001.

TcdA induces cell death by a mechanism distinct from TcdB at higher toxin concentrations

The difference in killing induced by TcdA and TcdB observed at high concentrations suggests they are killing cells by distinct mechanisms. We expected TcdB to induce ROS-driven necrosis at these higher concentrations based on our previous work [175]. ROS production in response to each toxin was monitored in YAMC cells using a fluorescent ROS reporter (Figure 3.3A). TcdB induced the production of high levels of ROS at higher concentrations (≥ 100 pM), where we have previously observed necrosis, but not at toxin concentrations below 100 pM. This observation is consistent with the mechanistic switch noted in Figure 2 over the same concentration range. TcdA induced a small amount of ROS production at 100 nM, though it remains significantly different from the signal induced by TcdB (Figure 3.3A).

We next wanted to see if the cells were dying by a necrotic mechanism using a lactose dehydrogenase (LDH) indicator as a quantitative measure for the loss of cell membrane integrity, a hallmark of necrosis (Figure 3.3B,C). LDH signal in response to TcdA was not detected until 24 hours after intoxication (Figure 3.3B), which may reflect necrosis secondary to apoptosis. In contrast to TcdA, and consistent with our previous observations, we detected rapid necrotic cell death in response to TcdB at concentrations ≥100 pM (Figure 3.3C). We detected a loss of membrane integrity as early as 2 hours after cells were challenged with TcdB (Figure 3.3C). LDH signal increased in cells treated with high concentrations (100 pM to 100 nM) of toxin for up to 8 hours post intoxication (Figure 3.3C). At these higher concentrations, at 2, 4, and 8 hours, the LDH signal induced by TcdB was significantly different from that induced by TcdA. Concentrations below 100 pM did not demonstrate an appreciable rise in LDH levels at the 2, 4, or 8 hour time points assayed and were not significantly different from the signal produced from cells intoxicated with TcdA. However, an increase in LDH signal at lower concentrations was detected at 24 h post-intoxication with TcdB, again suggesting secondary necrosis (Figure 3.3C). Notably, there was no significant difference in the LDH signal in cells treated with TcdA and TcdB at any concentration at the 24 hour time point. The correlation of ROS production and LDH release in response

to higher concentrations (≥ 100 pM) of TcdB indicates a necrotic cell death. The absence of ROS and delayed LDH signal in response to TcdA intoxication suggests that TcdA is not inducing necrosis, demonstrating that TcdA at all concentrations and TcdB at concentrations 100 pM and above are causing cell death by different mechanisms.

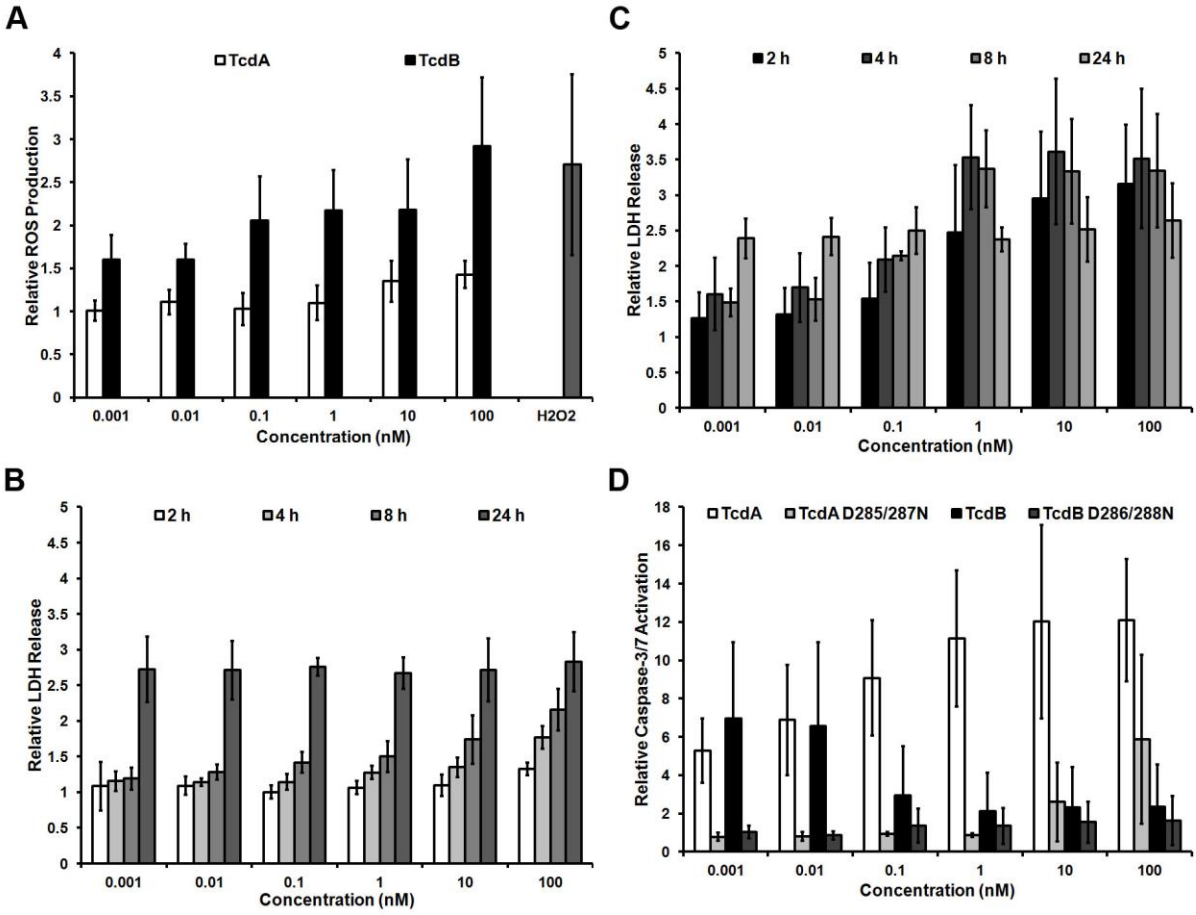

Figure 3.3. TcdA induces cell death by a mechanism different from TcdB. YAMC cells were seeded into multiwell plates and incubated at 37 °C overnight. The cells were then intoxicated with indicated concentrations of toxin and incubated at 37 °C. A, YAMCs were tested for ROS production in response to TcdA (white bars, 24 h) or TcdB (black bars, 6 h) using a fluorescent ROS reporter. Statistical analysis by two-way ANOVA revealed TcdA and TcdB were significantly different at all concentrations with $p < 0.0001$. The cells were then tested for LDH release, using CellToxGlo, in response to B, TcdA or C, TcdB at the indicated time points. Data in panels B and C were analyzed by two-way ANOVA at each time point. At 2, 4, and 8 h, there was a significant difference between TcdA and TcdB at concentrations ≥100 pM. There was no significant difference at concentrations ≤10 pM. At 24 h, two-way ANOVA revealed no significant difference between TcdA and TcdB at any concentration tested. D, YAMCs were also tested for activated caspase-3/7 using Apo-ONE, in response to TcdA (white bars), TcdA D285/287N (light gray bars), TcdB (black bars), or TcdB D286/288N (dark gray bars). Three separate two-way ANOVAs were used to analyze the data in panel D. The first revealed a significant difference between TcdA and TcdB at concentrations ≥100 pM with $p < 0.0001$. There was no significant difference at concentrations ≤10 pM. The second two-way ANOVA revealed a significant difference between TcdA and TcdA D285/287N at all concentrations with $p < 0.0001$. The third two-way ANOVA showed no significant difference between TcdB and TcdB D286/288N at concentrations ≥100 pM. At concentrations ≤10 pM, there was a significant difference between TcdB and TcdB D286/288N with $p < 0.01$. In all panels, data represent the average of 3 experiments performed in triplicate and error bars represent the standard deviation between the 3 experiments.

Given the importance of an intact p53 pathway (Figure 3.2), the absence of ROS production (Figure 3.3A), and the observation that TcdA and low concentrations of TcdB were not inducing early LDH release (Figure 3.3B and 3.3C), we chose to investigate apoptosis as a possible mechanism of cell death induced by TcdA and lower TcdB concentrations. While it is often reported that TcdA and TcdB induce an apoptotic cell death, we sought to provide a direct link between apoptotic markers and viability data. As reported in the literature, apoptosis in response to the toxins is thought to be dependent upon glucosyltransferase activity and subsequent GTPase inactivation [20,126,146-148,150,151,179,180]. To test this, we used an active caspase-3/7 indicator to detect apoptosis in YAMC cells challenged with TcdA, TcdB, and their respective glucosyltransferase mutants (Figure 3.3D). We detected a robust and dose-dependent caspase-3/7 activation in response to TcdA. The dose-dependence of caspase-3/7 activation correlates with the dose-dependent loss in cell viability we observed at 37 °C (Figure 3.2B). The glucosyltransferase mutant, TcdA D285/287N, seemed to have some residual activity at 100 nM, activating caspase-3/7, but showed very little activity at the other concentrations tested (Figure 3.3D). When the cells were challenged with higher, necrotic concentrations (≥ 100 pM) of TcdB, very little caspase activation was detected. At concentrations of 10 pM and lower, however, we begin to detect appreciable caspase-3/7 activation. Notably, the TcdB glucosyltransferase mutant, TcdB D286/288N, did not activate caspase-3/7 at any concentration tested (Figure 3.3D). These data are consistent with previous reports and suggest that TcdA induces a glucosyltransferase-dependent, apoptotic cell death. Also, at lower concentrations (≤ 10 pM) where necrosis is not observed, TcdB can induce a glucosyltransferase-dependent, apoptotic cell death, providing empirically derived support for TcdB utilizing a dose-dependent mechanistic switch.

TcdA induces glucosyltransferase-dependent caspase-3 activation, while TcdB induces glucosyltransferase-independent ROS production in colonic tissue

We next wanted to test whether our observations that TcdA and TcdB were inducing cell death by different mechanisms at higher concentrations in YAMC cells could also be observed in colonic explants. We intoxicated tissue with 10 nM TcdA and

TcdB and their corresponding glucosyltransferase deficient mutants and assessed epithelial damage in H&E stained sections (Figure 3.4A). Consistent with previous experiments, TcdA and TcdB cause epithelial damage at a concentration of 10 nM. TcdA D285/287N does not cause epithelial damage whereas TcdB D286/288N is equipotent to TcdB on colonic tissue. These data are congruent with our observations in YAMC cells (Figure 3.3). TcdA induced cell death and tissue damage is dependent upon the glucosyltransferase activity, while TcdB induced damage is independent of glucosyltransferase activity at a concentration of 10 nM.

We also wanted to test the colonic tissue for ROS production and evidence of an apoptotic cell death in response to the toxins, using a fluorescent indicator and an antibody specific for active caspase-3, respectively. Consistent with previous observations, we detected ROS in colonic explants treated with TcdB and TcdB D286/288N, but not in response to TcdA or TcdA D285/287N (Figure 3.4B). We detected a robust active caspase-3 signal in tissue treated with TcdA (Figure 3.4C). While there was a low amount of detectable signal in tissue treated with TcdA D285/287N, it is much less than that induced by TcdA. There was very little active caspase-3/7 signal in tissue treated with TcdB or TcdB D286/288N. Together, these data support our observations in YAMC cells and suggest that TcdA and TcdB induce cell death by different mechanisms. TcdA induces an apoptotic cell death while TcdB induces necrosis at concentrations ≥100 pM. At low concentrations (≤10 pM), TcdB also induces an apoptotic cell death. A cartoon model incorporating these data into a new intoxication model is shown in Figure 3.5.

Discussion

In order to fully elucidate the mechanisms toxins A and B utilize to drive disease pathology *in vivo*, it was important to design a study that allowed for the analysis of comparable doses of toxins at identical time points in the same tissue or cell type. The ability to directly compare the two toxins and catalytic mutants allowed a unique resolving power in terms of understanding the different cellular processes engaged by

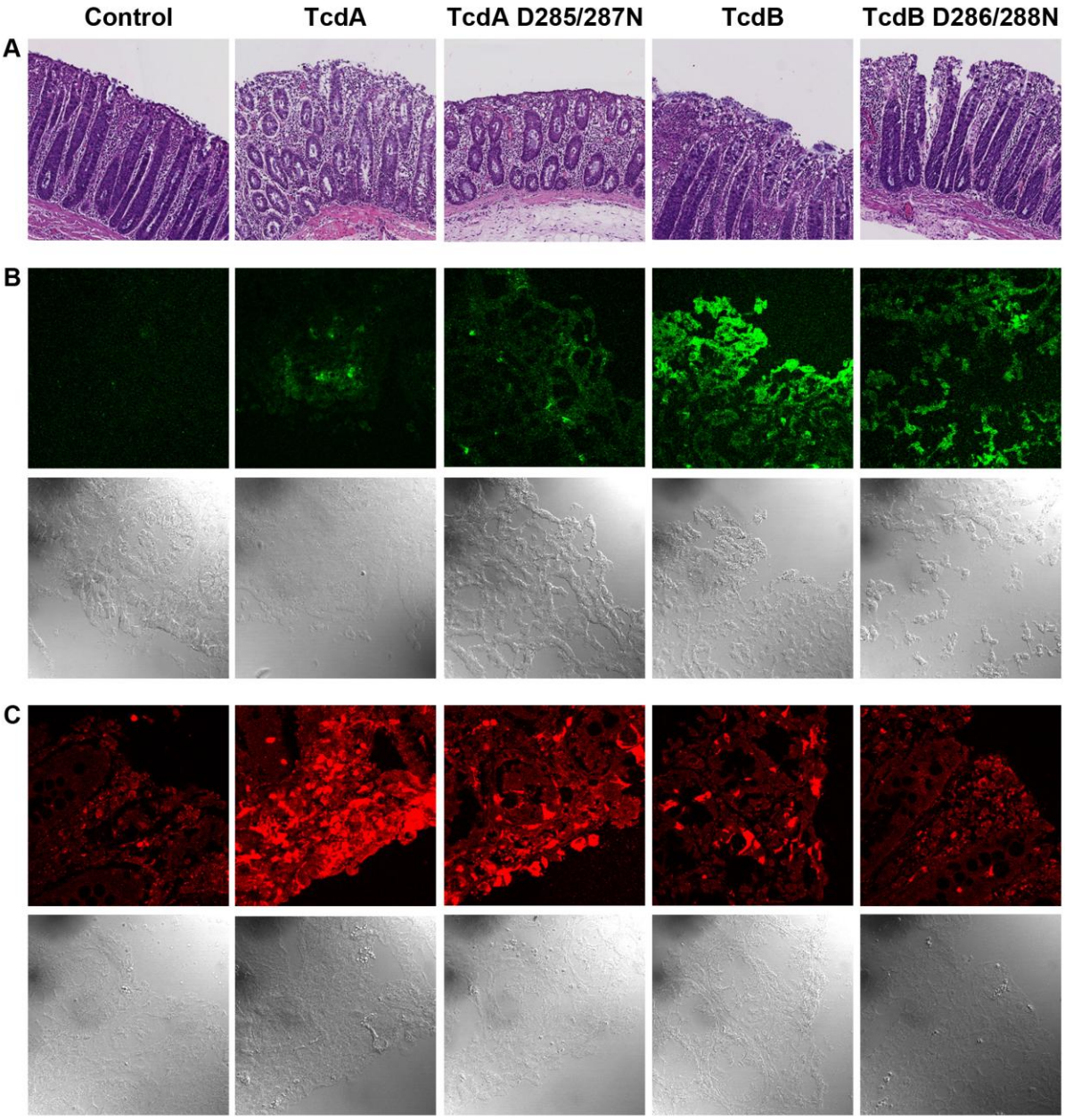

Figure 3.4. TcdA induces glucosyltransferase-dependent caspase-3 activation, while TcdB induces glucosyltransferase-independent ROS production in colonic tissue. A, Colonic explants were treated with 10 nM TcdA, TcdA D285/287N, TcdB, or TcdB D286/288N in incubated at 37 °C for 5 hours. Tissue sections were stained with H&E. B, Colonic explants were treated with ROS detection agent and incubated at 37 °C for 1 hour. Samples were then treated with toxin at 37 °C for 5 hours after which the tissue was flash frozen. Slides were prepared and immediately imaged. C, Tissue sections were stained with an active caspase-3 antibody (red). Fluorescent and bright field images in B and C were captured using confocal microscopy.

each toxin, the dose at which the toxin was capable of injuring the cell or tissue, and the relative contribution of the glucosyltransferase activity of the toxins. Initially, we sought to establish the physiologically relevant concentrations of toxin by challenging colonic explants with a range of toxin concentrations. This dosing of the toxins led to two surprising observations. First, both toxins were capable of inducing damage at concentrations above 10 pM (Figure 3.1). This observation is consistent with the effects of TcdA intoxication in animal model systems such as hamsters, mice, rats, and rabbits [67-69,132,133]; although it was surprising given the difficulty of detecting TcdA induced death in tissue culture models [9,20,105,115,174]. Also of note, was the fact that the overall damage scores were highly similar. Taken together, these data suggest that cell death is a physiologically relevant consequence of TcdA intoxication and an important pathway to understand.

This observation led us to seek out a cell line where both toxins could be assayed for cytotoxicity, and delineate these as apoptotic or necrotic death events. TcdA has historically been described as an enterotoxin while TcdB has been known to be a potent cytotoxin, implying an intrinsic difference in cytotoxic potency[123,129]. YAMC cells, a conditionally immortalized cell line, are sensitive to TcdA as well as TcdB (Figure 3.2). Using YAMC cells, we could readily detect TcdA induced cell death at a wide range of concentrations (100 nM to 10 fM) in 18 hours (Figure 3.2). TcdB induced cell death was also readily detectable down to 10 fM at the same time point. In both the colonic explant and the YAMC experiments at the non-permissive temperature (37 °C), p53 is unperturbed and toxins cause similar damage (Figure 3.1 and 3.2B). Notably, TcdB does not require p53 function at concentrations ≥ 100 pM (Figure 3.2A). These data highlight the importance of working in model systems with intact apoptotic pathways when studying the death mechanism of TcdA, and sub-picomolar concentrations of TcdB (Figure 3.2). The observation that TcdB induces a p53-independent death at higher concentrations and a p53-dependent death at lower concentrations could readily explain the disparity in cell death events reported by many different groups over the years (Figure 3.2). Studies where TcdB is used at high picomolar to nanomolar concentrations report necrosis [100,174,175], while sub-

picomolar intoxication results in an apoptotic event consistent with the p53 dependence profile observed in YAMC cells [21,126,142,150,151].

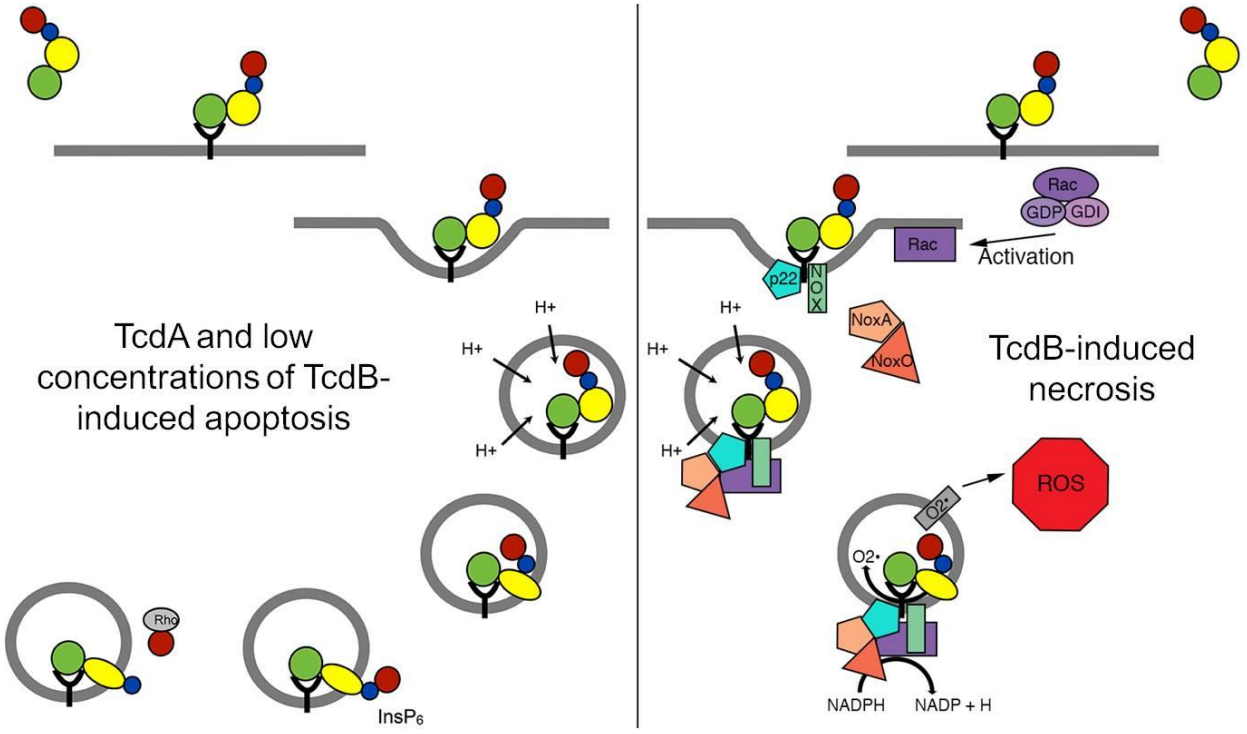

Figure 3.5. TcdA and TcdB intoxicate cells by distinct mechanisms. TcdA and low concentrations of TcdB intoxicate cells by ligating the host cell receptor, initiating endocytosis. As the endosome matures, the low pH induces a conformational change that allows endosomal membrane disruption and translocation of the APD and GTD to the cytosol. Upon encountering the cytosol, InsP6 binds the APD and allosterically activates the enzyme and induces cleavage. The GTD is then released into cell where it is trafficked to it target, membrane-bound Rho family GTPases. Glucosylation of GTPases leads to CPE and apoptosis. Higher concentrations of TcdB initiate the assembly and activation of the NOX complex leading to necrosis. Ligation of the host cell receptor initiates endocytosis and the recruitment of the cytosolic components of the NOX complex (activated Rac1, NOXO, and NOXA) to the membrane bound components (NADPH oxidase and p22). As the endosome matures, the NOX complex is activated producing and releasing large amounts of ROS into the cytosol. The aberrant production of ROS quickly leads to loss of membrane integrity and a necrotic cell death.

While TcdA and TcdB have been shown to have different effects on tissue and in animal models, they were thought to induce the same apoptotic cell death mechanism [9,20,21,126,142-145,150,151]. We have previously shown that TcdB induces a glucosyltransferase-independent necrotic cell death as a result of aberrant ROS production through the NADPH oxidase complex [174,175]. To further investigate the possibility that TcdB is inducing a concentration dependent mechanism that switches

from necrosis to apoptosis, we used indicators of necrosis or apoptosis to determine the death pathway activated at a given concentration. Here, we can clearly see in YAMC cells that TcdA induces an apoptotic cell death at all concentrations. Additionally, the induction of apoptosis by TcdA is completely dependent on a fully active glucosyltransferase. Most interestingly, we can observe two distinct cell death mechanisms occurring in response to TcdB. At higher concentrations (≥100 pM), we see clear indications of a necrotic cell death including ROS production, rapid LDH release, and minimal caspase activation. At lower concentrations (≤10 pM) where there are no indicators of necrosis, we see a rise in caspase activation indicating an apoptotic cell death. Also clearly demonstrated in Figure 3.3D, the activation of the apoptotic pathway at lower concentrations of TcdB mirrors TcdA in that it requires glucosyltransferase activity. This is the first report of TcdB inducing a bimodal cell death mechanism, dependent upon concentration of toxin, allowing the unification of the observations described by groups with seemingly opposing data (Figure 3.5).

We were able to extrapolate and confirm our findings in the colonic explant model. At a concentration of 10 nM toxin, TcdA induces a glucosyltransferase dependent apoptotic cell death while TcdB induces the glucosyltransferase independent production of ROS (Figure 3.4). We have demonstrated that a concentration of 10 nM TcdA and TcdB can induce a pathological response in tissue while intoxication with 10 pM toxin has minimal effect (Figure 3.1). We recognize that a 5 hour time point is not representative of the entire course of infection, and perhaps is more reflective of severe disease. Our current explant model system does not allow for longer time points, which may be useful for understanding the effects of lower concentrations of toxin. While it remains unclear how much toxin is present at the site of infection, we would hypothesize that both cell death mechanisms can be induced during the course of disease. It is also reasonable to hypothesize that both mechanisms of cell death should be targeted to effectively combat disease in a toxin-centric therapeutic strategy. The relative contribution of each toxin, and the respective mechanism of cell death induced, to overall pathology and disease represents an important question demanding future investigation.

CHAPTER IV

ZINC IS A REGULATOR OF *CLOSTRIDIUM DIFFICILE* TOXIN ENZYMATIC ACTIVITY

Introduction

Clostridium difficile is the leading cause of hospital-acquired diarrhea and secretes two large toxins, TcdA and TcdB [15,63,64,162]. *Clostridium difficile* infection (CDI) is a toxin-mediated disease that encompasses a wide range of disease symptoms from mild diarrhea to pseudomembranous colitis [29,161,181]. TcdA and TcdB are composed of four functional domains: receptor binding, delivery, an autoprocessing domain (APD) and a glucosyltransferase domain (GTD) [102,109,110,163]. The C-terminal combined repetitive oligopeptide (CROPS) region of the toxin is thought to be involved in host cell receptor binding [8]. The delivery domain is a large hydrophobic region thought to undergo a significant conformational change in the low pH of the endosome that allows for disruption of the endosomal membrane and translocation of the APD and GTD into the cytosol of the host cell [95,99]. The autoprocessing domain has been thought to engage in cysteine protease activity, cleaving the GTD upon binding of host-cell inositol hexakisphosphate (InsP6) [102]. Once released, the GTD has been shown to target Rho family GTPases [108]. Glucosylation of these small GTPases leads to both cytoskeletal rearrangements in which the cells round, known as the cytopathic effect (CPE), and an apoptotic cell death [9,142].

The autoprocessing activitiy is thought to be important for TcdA-induced cell death and the apoptotic cell death induced by lower concentrations of TcdB [32,103,104,174]. The domain is an attractive drug target because it contains a defined catalytic active site and an InsP6 binding pocket [4]. It is conceivable that either inhibition of autoprocessing or early activation of autoprocessing could provide

therapeutic benefit, making a detailed understanding of the allosteric and enzymatic mechanism of auotoprocessing is a priority. Here, we report new mechanistic insights into the regulation and function of TcdA and TcdB.

Transition metals are known to be essential cofactors in many cellular processes and the structure and function of proteins [182,183]. Metals are also known to be essential to the function of a number of bacterial effector proteins that cause disease [184-187]. In particular, the regulation and function of toxins secreted by at least two *Clostridial* species, botulinum neurotoxin (BoNT) and tetanus toxin (TeNT), is completely dependent upon zinc [188-190]. In this study, we describe the regulatory functions of zinc in the autoprocessing activity of TcdA and TcdB. These insights advance our understanding of the mechanism by which the toxins initiate and carry out autoprocessing of the GTD and may help guide drug development efforts.

Methods

Plasmid Construction and Point Mutants

Previously described plasmids for the recombinant expression of TcdA [2], $TcdA_{1-1832}$, and TcdB were used as templates for all mutant proteins generated for this study. Mutations were introduced by site-directed mutagenesis using the QuickChange protocol.

Protein Expression and Purification

Proteins were expressed and purified as previously described [191].

Cleavage assays

Cleavage assays were performed as previously described [191]. DTT, TCEP, and EDTA were added at the same time as InsP6. Protein was preincubated with TPEN at 37 °C for 2 hours before the addition of InsP6. Reactions were then incubated at 37 °C for an additional 2 hours.

Crystallization

$TcdA_{1\text{-}1832}$ and S1329C $TcdA_{1\text{-}1832}$ were concentrated to 10 mg/ml in 20 mM Tris, pH 8.0, 100 mM NaCl. Crystallization was performed using the hanging drop method at 21^{o} C with a 1:1 ratio of protein to mother liquor. The mother liquor formulation for WT crystals was 100 mM Bis-Tris, pH 6, 11% PEG 4000, 30-50 mM guanidium chloride (GuCl). The mother liquor formulation for the S1329C crystals was 100 mM Bis-Tris, pH 5.8, 8% PEG 4000, 50 mM GuCl. Crystals were exchanged into appropriate mother liquor containing 20% glycerol, mounted on cryo loops, and flash cooled in liquid nitrogen.

Heavy atom derivatives of $TcdA_{1831}$ were prepared by soaking crystals in the appropriate mother liquor containing either 1 mM gold(III) chloride hydrate for 40 min or 5 mM mercuric chloride for 1.5 h. Heavy atom derivatives of S1329C $TcdA_{1831}$ were prepared by soaking crystals in 5 mM mercuric chloride for 72 hours.

Structure Determination and Refinement

X-ray data were collected from single crystals on LS-CAT beamline 21 ID-D at the Advanced Photon Source (Argonne, IL) at 100^{o} K. Diffraction data were indexed, integrated, and scaled using XDS [192] or HKL2000 [193](Table 1). The two mercury datasets were compared to the native dataset using multiple isomorphous replacement with anomalous scattering in SHARP [194]. The analysis revealed five mercury sites in the two mercury datasets, differing only in their occupancies, and was consistent with the expectation that each protein monomer would have five free cysteine residues. The heavy atom positions were used to calculate initial phases, which were included in an auto-building protocol in PHENIX [195]. The fragments generated by auto-building guided manual placement of the apo-GTD structure (PDB ID 3SS1) [2]. Phases from the GTD model were combined with the phases from SHARP to calculate a new map and initiate a new round of autobuilding. The fragments generated through autobuilding allowed for manual placement of the CPD (PDB ID 3H06) [4]. Phases from the combined GTD and CPD model were combined with the phases from SHARP to calculate a new map and initiate new rounds of automated and manual building. Further phase improvement came from multi-crystal averaging. The working model

(consisting of the GTD, most of the CPD, and a series of unconnected fragments from the delivery domain) was used as search model for molecular replacement into the native, platinum, and gold datasets. The models and phases from each dataset were subjected to multi crystal averaging and density modification in PHENIX and resulted in excellent quality maps. One area of ambiguity was resolved through site specific introduction of a Hg atom: crystals of a S1329C TcdA1-1832 mutant were derivitized with mercuric chloride, and the sixth heavy atom site was identified using PHENIX. The model was generated through an iterative process of manual building in Coot [196] and refinement using Phenix [195]. The final model reflects the 50-3.25 Å native dataset (R_{cryst} = 22% , R_{free}= 26%) and contains residues 4-944 and 951-1806 along with 1 zinc atom.

X-ray absorption spectroscopy

X-ray absorption spectroscopy (XAS) experiments were carried at beamline X3B of the National Synchrotron Light Source, which was equipped with a sagitally focusing Si(111) double crystal monochromator and a Ni-coated mirror for harmonic rejection. A He Displex cryostat was used for temperature control (~15K typical sample temperatures). Fluorescence detection was provided by a 31-element solid-state germanium detector array (Canberra). Samples of $TcdA_{1-1832}$ (10 mg/mL) and buffer blanks were loaded into 30 µL polycarbonate cuvettes wrapped in 1 mil Kapton tape and then frozen by immediate immersion in liquid nitrogen. The Kα fluorescence emission spectra from $TcdA_{1831}$ and buffer samples in the X-ray beam (incident energy = 10 keV) were examined. There was a significant increase in the total Zn fluorescence counts for the $TcdA_{1831}$ sample compared to buffer, while fluorescence for the Mn - Cu series was unchanged. XAS measurements were therefore carried out at the Zn K-edge on $TcdA_{1831}$, over an energy range of 9.46 – 10.3 keV. Internal energy calibration was provided by simultaneous measurement of a Zn metal foil, with the first inflection point of the edge set to a reference energy of 9659 eV. Calibration and averaging of XAS data was carried out using Athena [197].

ICP-MS

Proteins were prepared as described above and dialyzed overnight into metal free buffer conditions as indicated. All buffers contained 50 mM NaCl; InsP6 was at a concentration of 10 mM, TPEN was at a concentration of 1 mM, $ZnCl_2$ was at a concentration of 10 μM. $ZnCl_2$ buffers also contained 1 mM TCEP. Samples dialyzed in TPEN and $ZnCl_2$ buffers were dialyzed at room temperature for 8 hours. All other samples were dialyzed at 4 °C for 18 hours. Protein samples were analyzed for metal content by utilizing 50 μL of the protein solution and diluting in 2.5% (v/v) nitric acid (Sigma-Aldrich, TraceSELECT quality) to a final volume of 3 mL for ICP-MS analysis. In samples with significant precipitation after acidification, the samples were centrifuged at 15,000 x g for 20 minutes to pellet any precipitate, and the solution transferred to a fresh tube for measurement. The diluted samples were analyzed for ^{66}Zn, ^{55}Mn, ^{63}Cu, and ^{60}Ni using a 1 – 30 ppb standard curve utilizing stock solutions (Perkin Elmer). Analyses were performed using a PerkinElmer ELAN DRCII ICP-MS. The instrument was equipped with a Microflow PFA-ST concentric nebulizer with a 100 μL/min self-aspiration capillary, a cyclonic spray chamber, a quartz torch and nickel sampler/skimmer cones. Germanium at 50 ppb was added as an internal standard using an EzyFit glass mixing chamber. Concentrations (in ppb) were corrected for the dilution factor and the molar concentrations and molar ratios (^{66}Zn/protein) were determined for each sample.

Results

TcdA autoprocessing is inhibited by a metal ion

We and others have observed the autoprocessing activity of TcdA is dependent upon the presence of a reducing agent (Figure 4.1A), as autocleavage of the GTD is not observed in reactions with InsP6 only. With the addition of 100 mM dithiothreitol (DTT), TcdA autoprocesses in an InsP6-dependent manner, as previously reported [104]. Curiously, TcdB holotoxin readily autoprocesses in the absence of reducing agent, indicating that the inhibitory mechanism present in TcdA is absent in TcdB (Figure

4.1A). In addition to reducing disulfide bonds, DTT can also coordinate metals. To begin to understand which chemical property of DTT was driving the induction of autoprocessing in TcdA, we tested other common chemical reagents with a similar chemical property to DTT. Tris(2-carboxyethyl)phosphine (TCEP) is another commonly used reducing agent of the phosphine family and does not coordinate metals. Ethylenediaminetetraacetic acid (EDTA) is an efficient metal chelator, but has no effect on disulfide bonds. We compared both of these reagents to the efficiency of DTT in the induction of an InsP6 dependent cleavage event. TCEP did not induce autocleavage of TcdA, whereas addition of EDTA to the reaction did result in autoprocessing (Figure 4.1B). These data indicate that the metal chelating properties of DTT and EDTA promote autoprocessing, suggesting a metal ion must be removed from TcdA before autoprocessing can occur.

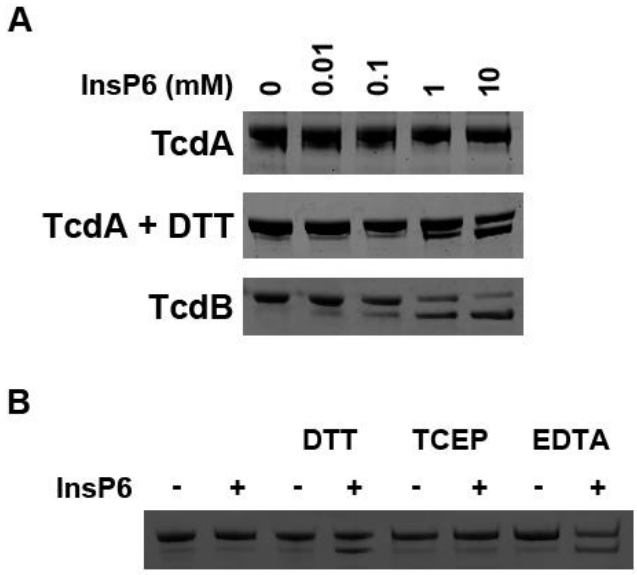

Figure 4.1. TcdA requires reducing agent to initiate cleavage. A, TcdB readily undergoes autoprocessing in an InsP6 dependent fashion. TcdA, however, does not autoprocess without the addition of 100 mM DTT. B, Initiation of autoprocessing was tested using different chemical additives, DTT, TCEP, and EDTA. 100 mM of the compound was added to the indicated reactions, and 10 mM InsP6 was added to the indicated reactions. All reactions were incubated at 37 °C for 2 hours before the reactions were stop with the addition of Laemmli buffer. The samples were analyzed by Coomassie stained SDS-PAGE

TcdA coordinates three zinc ions in different functional domains

We next sought to identify the metal that was inhibiting autoprocessing of TcdA. We identified the metal in an X-ray absorption near edge structure (XANES) experiment with TcdA, where we observed a strong signal at the zinc edge (Figure 4.2A). The spectrum collected was consistent with zinc coordination by both cysteine and histidine residues. As a secondary and more quantitative method of identification, we also

assessed the occupancy of TcdA using inductively coupled plasma mass spectrometry (ICP-MS). In this experiment, we again identified zinc as the metal coordinated by the toxin. Surprisingly, we calculated a zinc:toxin molar ratio of 3.36 (Table 4.1, black). Tetanus toxin (TeNT), known to bind one zinc ion, was analyzed as a control in ICP-MS experiments. To determine where in the toxin the zincs were coordinated, we made a series of C-terminal truncations and determined the molar ratio of zinc:toxin. The molar ratio of zinc to protein for a toxin where the CROPS domain was deleted ($TcdA_{1-1832}$) was 1.93 (Table 4.1, black). The loss of one zinc with the deletion of the CROPS suggests that one zinc is either coordinated in the deleted domain or within the interface between the CROPS and another domain. The zinc coordinated by the CROPS is not the zinc that inhibits autoprocessing activity, however, as EDTA is still required to induce cleavage (Figure 4.2B). Further deletion of the delivery domain ($TcdA_{1-809}$) revealed a zinc:toxin ratio of 0.52 by ICP-MS (Table 4.1, black). The loss of a zinc ion suggests the second zinc is coordinated within the delivery domain, leaving the third zinc coordinated somewhere in the APD or GTD. Importantly, the zinc coordinated by the delivery domain is the metal ion that inhibits autoprocessing activity. Loss of this zinc resulted in the loss of requirement for EDTA to induce cleavage (Figure 4.2B), indicating the inhibitory zinc is coordinated by residues either within the delivery domain or at an interface between the delivery domain and another domain.

To further define the binding site of the inhibitory zinc, we made two additional C-terminal deletion mutants in the delivery domain: $TcdA_{1-1809}$ and $TcdA_{1-1795}$. When we tested these truncation mutants for their dependence on EDTA for autoprocessing activity, we found that the $TcdA_{1-1809}$ protein still required EDTA which indicated that the inhibitory zinc was still coordinated (Figure 4.2C). The $TcdA_{1-1795}$ protein did not require the addition of EDTA to initiate cleavage, indicating the inhibitory zinc was no longer coordinated (Figure 4.2C). These data suggest the coordinating residues for the zinc ion that inhibits autoprocessing activity are located between residues 1795 and 1809. There are four potential metal coordinating residues within this 14 amino acid stretch: E1803, E1805, D1807, and D1809. Importantly, three of the four (E1805, D1807, and D1809) are not conserved between TcdA and TcdB (Figure 4.2D). We would expect

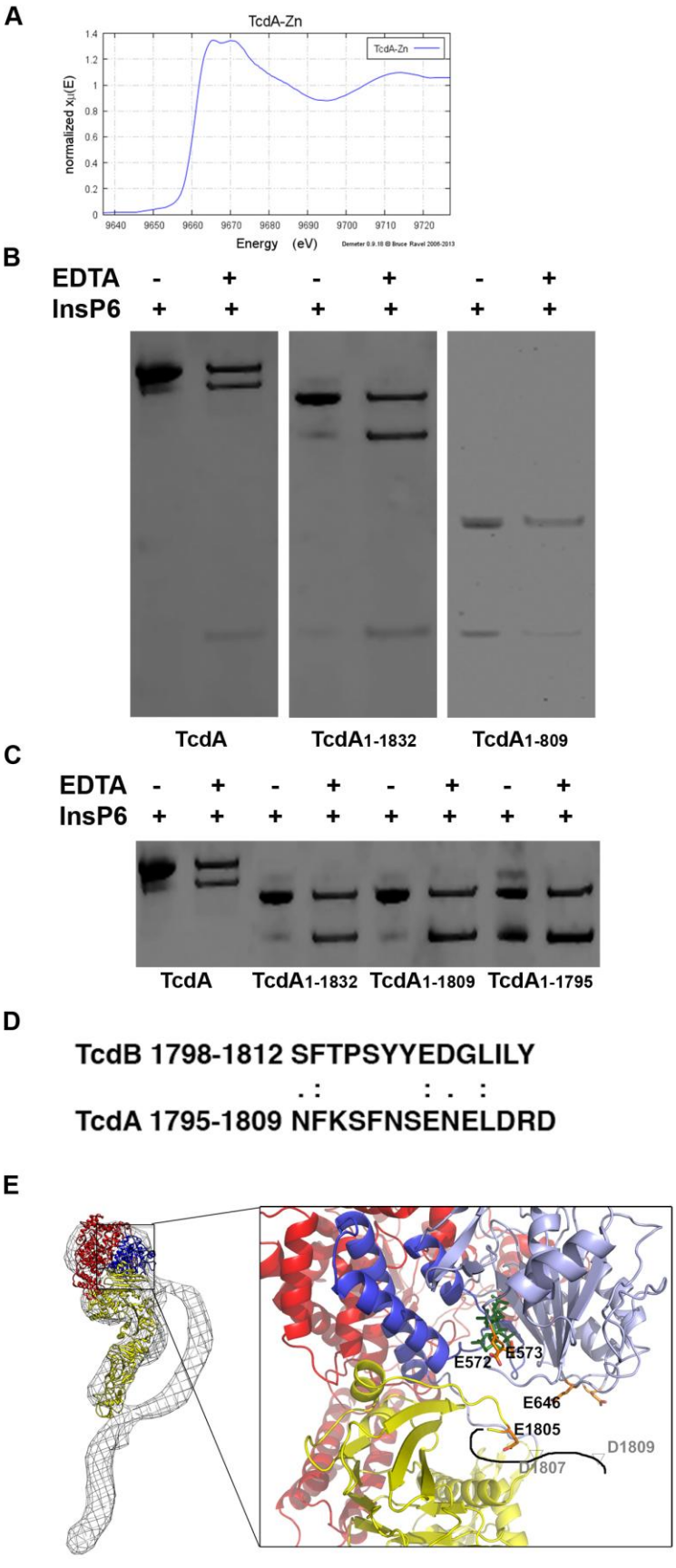

Figure 4.2. TcdA autoprocessing activity is inhibited by a zinc ion coordinated at the interface of the delivery domain and APD. A, XANES spectra of TcdA in solution. The shape of the X-ray absorption near-edge spectrum (XANES) supports a zinc site with mixed nitrogen/sulfur ligation. B, Cleavage assays with TcdA, $TcdA_{1\text{-}1832}$, and $TcdA_{1\text{-}809}$. C, Cleavage assays with the addition of $TcdA_{1\text{-}1809}$ and $TcdA_{1\text{-}1795}$. All reactions contained 10 mM InsP6. Indicated reactions contained 100 mM EDTA. Reactions were incubated at 37 °C for 2 hours. D, Sequence alignment of TcdA 1795-1809 and TcdB 1798-1812 with Expasy LALIGN. E, Crystal structure of TcdA1-1832 focused on the putative zinc coordination site. Putative coordinating residues, E572, E573, E646, E1805, E1807, and E1809 are highlighted.

Table 4.1. ICP-MS determination of zinc occupancy in *Clostridium difficile* toxins.

Sample	Zinc/Protein	Buffer
TcdA	3.36	20 mM HEPES pH 6.9
$TcdA_{1-1832}$	1.93	20 mM HEPES pH 6.9
$TcdA_{1-1832}$	0.72	100 mM BisTris pH 6.0
$TcdA_{1-809}$	0.52	20 mM HEPES pH 6.9
TeNT	0.75	20 mM HEPES pH 6.9
$TcdA_{1-1795}$	0.79	20 mM HEPES pH 6.9
C700A	0.08	20 mM HEPES pH 6.9
H655A	0.06	20 mM HEPES pH 6.9
H759A	0.3	20 mM HEPES pH 6.9
L542A	0.77	20 mM HEPES pH 6.9
$TcdA_{1-1795}$ + InsP6	0.54	20 mM HEPES pH 6.9
L542A + InsP6	0.45	20 mM HEPES pH 6.9
$TcdA_{1-1795}$ + TPEN	0.04	20 mM HEPES pH 6.9
$TcdA_{1-1795}$ + $ZnCl_2$	0.48	20 mM HEPES pH 6.9
TcdB	0.67	20 mM HEPES pH 6.9
C698A	0.09	20 mM HEPES pH 6.9
H653A	0.04	20 mM HEPES pH 6.9
H757A	0.31	20 mM HEPES pH 6.9
L543A	0.67	20 mM HEPES pH 6.9
TcdB + InsP6	0.5	20 mM HEPES pH 6.9
L543A + InsP6	0.47	20 mM HEPES pH 6.9
TcdB + TPEN	0.05	20 mM HEPES pH 6.9
TcdB + $ZnCl_2$	0.38	20 mM HEPES pH 6.9

the zinc coordinating residues to not be conserved in TcdB as there is no inhibitory zinc ion by both ICP-MS and cleavage assays.

Stacey Seeback crystallized the $TcdA_{1-1832}$ protein. The residues involved in the putative coordination site for the inhibitory zinc are localized to the base of the globular head domain at the interface of the delivery domain and the APD (Figure 4.2E). It is reasonable to hypothesize that residues in the APD could also be involved in the inhibitory zinc coordination site. Potential coordinating residues located at the interface include Glu572, Glu573, Glu646, and Glu694. Also of note, the InsP6 binding site is located 'behind' the putative coordination site (Figure 4.2E). Occluding the allosteric binding site of the enzyme may be one mechanism of regulation employed by the inhibitory zinc.

Low pH releases the inhibitory zinc

We wondered how this inhibitory zinc would be released in the context of cellular intoxication and hypothesized it may occur when the toxin encounters the low pH of the endosome. To test this, we performed a pH titration resembling the maturation cycle of an endosome and assessed the ability of the toxin to undergo autoprocessing with the addition of InsP6. As seen in Figure 4.3A, autoprocessing does not occur at neutral pH which the toxin may encounter on the cell surface. Cleavage begins at a pH of 6.0 and increases at pH 5.5, suggesting that low pH does release the inhibitory zinc and allow autoprocessing to occur. These pHs resemble that of an early endosome. Autoprocessing continues to occur down to pH 4.5, the pH of the lysosome (Figure 4.3A).

Interestingly, when we docked the $TcdA_{1-1832}$ structure into the EM structure, at both neutral and low pH [5], we noticed that the point of rotation for the large conformational change appears to be near the putative inhibitory zinc binding site (Figure 4.3B). Together, these data demonstrate that pH dependent release of the zinc and conformational change may be another mechanism by which zinc regulates autoprocessing activity.

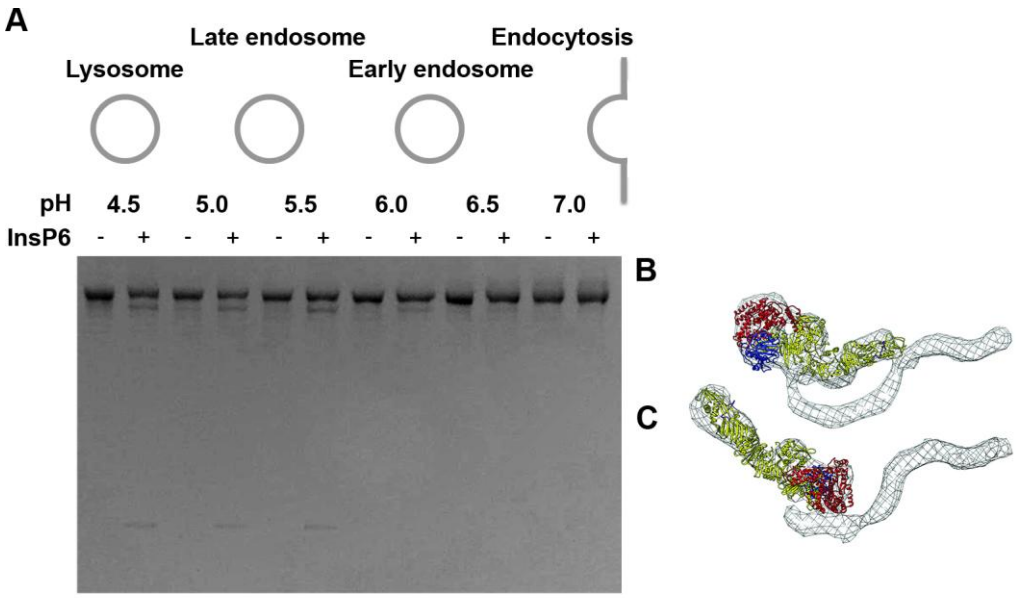

Figure 4.3. The inhibitory zinc is released upon exposure to low pH. A, Cleavage assays in 20 mM MES buffer at pHs 4.5 to 7.0. Indicated reactions contained 10 mM InsP6. The pHs tested resemble that of the pH of a maturing endosome. The $TcdA_{1-1832}$ structure was placed in the 20 Å EM structures of TcdA holotoxin at B, neutral (upper) and C, acidic (lower) pH. The EM structures were calculated by single particle averaging and random conical tilt as previously described [5]. The crystal structure was fit in each map using Chimera [11].

A second zinc is coordinated in the autoprocessing active site

We were able to collect zinc anomalous data with the $TcdA_{1-1832}$ crystals, in which we detected one zinc. Unexpectedly, the zinc, colored in green, was coordinated in the catalytic active site of the APD, colored in blue (Figure 4.4A). The protein was crystallized in the absence of InsP6, unlike other structures of the APD alone, revealing a new active site conformation. In the $TcdA_{1-1832}$ active site, in addition to the known catalytic residues Cys700 and His655, we see His759 also coordinating the zinc (Figure 4.4B). The structure of $TcdA_{1-1832}$ was determined at a moderate resolution of 3.25 Å, preventing the visualization of water molecules. Though we cannot see a water molecule, there is space for a water to be hydrogen bonded to Glu544/Asp545 and complete a tetrahedral coordination of the active site zinc (Figure 4.4B).

To confirm the presence of the zinc in the active site was not an artifact of crystallization, we analyzed the point mutants C700A, H655A, and H759A for the presence of zinc by ICP-MS (Table 4.1, blue). ICP-MS experiments investigating the active site zinc were performed using the $TcdA_{1-1795}$ protein, which does not coordinate

the inhibitory zinc, to simplify data and interpretation. This analysis demonstrated that Cys700 and His655 are clearly zinc coordinating residues. His759, however, is more ambiguous with a zinc:protein molar ratio of 0.3 (Table 4.1, blue). It is possible that His759 is a coordinating residue, but in its absence another residue may donate electrons needed to complete coordination of the zinc resulting in the signal we detect by ICP-MS (Figure 4.4B). We would hypothesize that the binding of this modified site is significantly less tight, resulting in the lower occupancy we detect by ICP-MS (Table 4.1, blue). The presence of a zinc ion in the H759A mutant was confirmed upon the determination of a $TcdA_{1\text{-}1832}$ H759A crystal structure at the zinc anomalous wavelength.

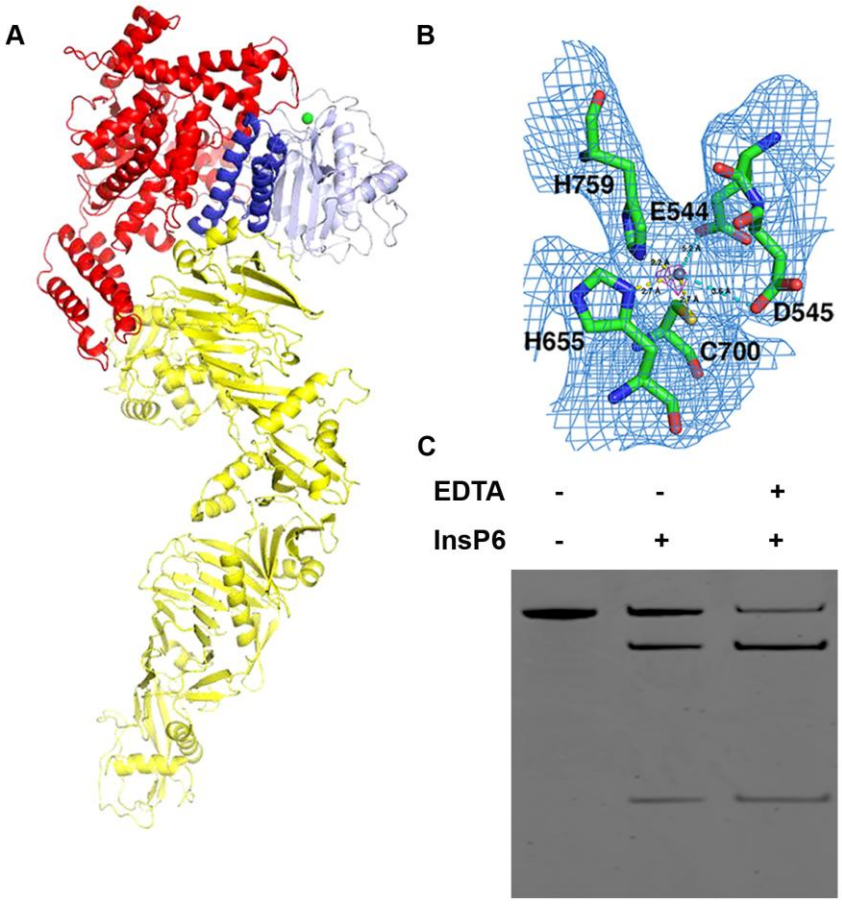

Figure 4.4. A zinc ion is coordinated in the APD active of TcdA and TcdB. A, A cartoon representation of the $TcdA_{1\text{-}1832}$ crystal structure colored as in Figure 1.1. The GTD is red, APD is blue, delivery domain is yellow, and a zinc atom is indicated in green. B, Analysis of the anomalous zinc signal, reveals a single peak, shown here in purple at 7 sigma, located in the APD active site. The zinc is coordinated by H655 (2.7 Å), C700 (2.7 Å), and H759 (2.2 Å) and may have indirect contacts with E544 or D545. The blue mesh depicts a 2Fo-Fc map contoured around the 5 active site amino acids at 1 sigma. C, Cleave assays in the crystallization buffer, 100 mM BisTris pH 6.0, 50 mM GuCl, used to obtain the structure of $TcdA_{1\text{-}1832}$. Reactions contained 100 mM EDTA and 10 mM InsP6 as indicated.

It is important to note that there is a zinc coordinated in the active site of TcdB, also. We demonstrated this by analyzing the active site mutants, C698A, H653A, and H759A for zinc content. The zinc:protein molar ratio of each sample was similar to the equivalent mutation in the TcdA truncation. The Cys698 and His653 residues are clearly coordinating the active site zinc, as the zinc:protein molar ratio approached zero. Similar to TcdA, the His757 residue has an intermediate phenotype in which the molar ratio of zinc:protein is ~0.3 (Table 4.1, blue).

We were perplexed as to why we did not see a second zinc coordinated in the delivery domain by anomalous scattering, as was suggested by our previous ICP-MS data with the $TcdA_{1-1832}$ protein. The crystallization conditions included a BisTris pH 6.0 buffer, which we hypothesized may release the inhibitory zinc. If this were true, we would expect the toxin to autoprocess with the addition of InsP6 alone without the presence of EDTA. We performed this experiment and found that the BisTris pH 6.0 buffer was sufficient to remove the inhibitory zinc (Figure 4.4C), allowing autoprocessing to occur in the absence of chelator and preventing visualization by X-ray crystallography (Figure 4.4A). The loss of this zinc was confirmed by ICP-MS (Table 4.1, black).

His759 is an essential residue in allosteric regulation by InsP6

To begin to understand the function of the active site zinc, we first investigated the effect that mutating the His759/757 residue, previously unknown to be involved in catalysis, would have on autoprocessing activity. When we assessed the cleavage activity of $TcdA_{1-1795}$ H759A and TcdB H757A, we noticed that initiation of catalysis still required the presence of InsP6, but was no longer dependent upon InsP6 concentration, suggesting that this residue is a key regulator of InsP6 allostery in both TcdA and TcdB, respectively (Figure 4.5A). There is structural evidence for this hypothesis. When we compare the structure of the APD from the $TcdA_{1-1832}$ structure in the absence of InsP6 and the structure of the APD alone with InsP6 bound, we see an impressive 19 Å movement out of the active site (Figure 4.5B). The residue sits at the base of the β-flap, previously described as the secondary structure communicating the allosteric regulation of InsP6-induced autoprocessing (Figure 4.5B).

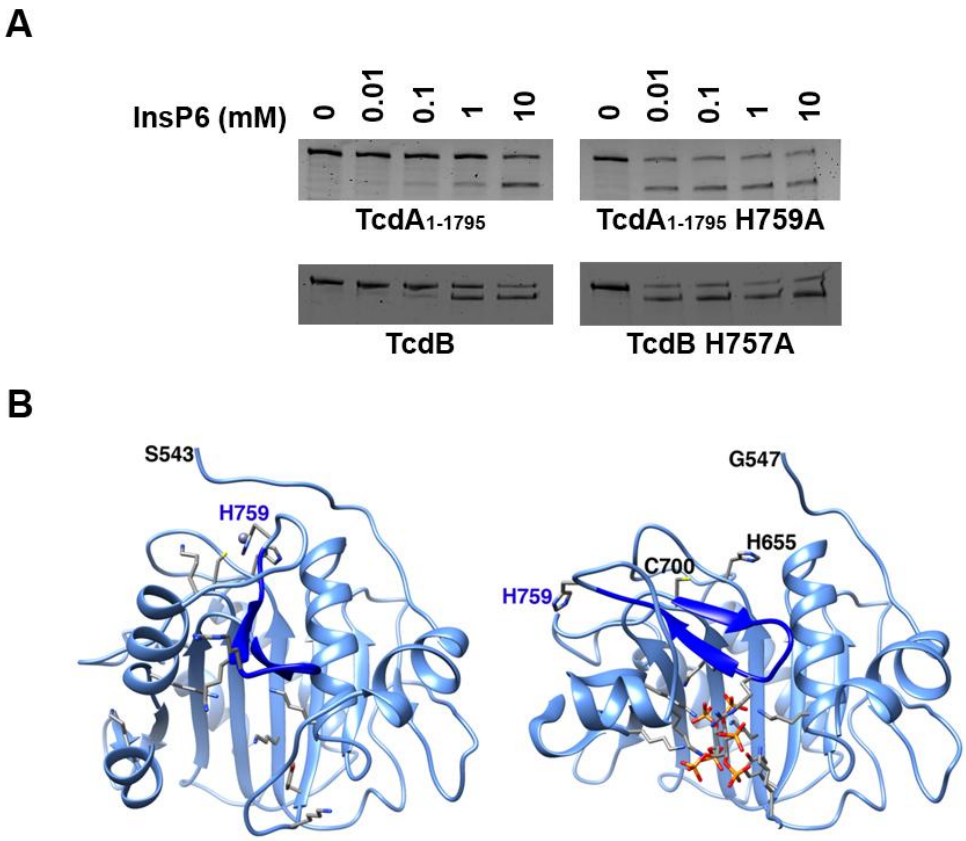

Figure 4.5. His759/757 is a key residue is the allosteric regulation TcdA and TcdB induced by InsP6. A, Cleavage assays comparing autoprocessing activity of wild type $TcdA_{1-1795}$ and TcdB to their respective mutants, H759A and H757A. B, The APD and three-helix bundle from the $TcdA_{1-1832}$ structure is depicted on the left with residues 543-745 in white, the 746-765 β-flap in light blue, and the three helix bundle (766-841) in dark blue and yellow. A zinc atom (green) is bound in the CPD active site by H655, C700, and H759. Four lysines form the initial binding site for InsP6: K602, K649, K754, and K777. Comparison to the InsP6-bound structure of the TcdA APD (right) suggests significant structural changes occur with InsP6 binding: the accumulation of 8 lysines and 1 arginine in the InsP6-binding site, a rearrangement of the β-flap and elements of the three-helix bundle, and displacement of H759 from the active site.

The active site zinc is required for enzymatic function

An obvious question upon the discovery of a zinc in the catalytic active site is the function of the zinc in catalysis. We could think of two reasonable possibilities. The active site zinc could inhibit catalysis, as has been reported for caspase family members. If this were true, we would expect zinc to no longer be coordinated by the toxin after InsP6 binding. To test this, we dialyzed $TcdA_{1-1795}$ and TcdB in the presence of InsP6 and analyzed these samples by ICP-MS. We conducted a similar experiment

with the cleavage site mutants L542A and L543A, in $TcdA_{1-1795}$ and TcdB, respectively. These mutants should bind InsP6, but not cleave. We found that zinc was present in every sample, indicating that the zinc ion is not displaced upon InsP6 binding (Table 4.1, red). Alternatively, the zinc could be required for catalysis acting as an activator of a water molecule as in a metalloprotease. We used N,N,N',N'-tetrakis(2-pyridylmethyl)ethane-1,2-diamine (TPEN), a chelator specific for zinc, to test this hypothesis. We pretreated both $TcdA_{1-1795}$ and TcdB with TPEN for 2 hours at 37 °C, and then incubated the toxin with InsP6 for an additional 2 hours at 37 °C. We found that pretreatment of the toxin with TPEN resulted in a loss of zinc and a loss of autoprocessing activity, suggesting that the zinc is required for catalytic activity (Figure 4.6A). Importantly, we also pretreated $TcdA_{1-1795}$ H759A and TcdB H757A with TPEN to test whether we would see the same effect as in wild type TcdA and TcdB. We again observed a loss in all autoprocessing activity of the mutants, further suggesting zinc-dependent enzymatic activity (Figure 4.6B). To confirm we were extracting the zinc from the active site, we analyzed samples dialyzed with TPEN for their zinc content using ICP-MS (Table 4.1, red). In samples devoid of zinc, we observed a deficient autoprocessing (Figure 6C). We were also able to restore zinc binding, again confirmed with ICP-MS (Table 4.1, red), and restore activity (Figure 4.6C), further supporting the observation that *C. difficile* toxins require zinc for their autoprocessing activity.

Discussion

The autoprocessing activity of *C. difficile* toxins has been the subject of many investigations in the past. The enzymatic activity has been thought to be required for toxin-induced cell death, and has therefore been considered a viable drug target [3,102-104]. There is at least one report describing the observation that commonly used reducing agents, DTT and β-mercaptoethanol (BME), initiate autocatalytic activity in TcdA [104]. Another earlier study reported EDTA did not inhibit cleavage. DTT, BME, and EDTA have also all been described as metal chelators [198-200]. Here we demonstrated that DTT and EDTA can activate TcdA and allow autoprocessing to occur, whereas TCEP, another commonly used reducing agent that cannot chelate

metals, does not promote autoprocessing (Figure 4.1). This observation led us to determine the identity of the metal ion that was inhibiting autoprocessing. Using two independent methods of identification, XANES and ICP-MS, we discovered that TcdA coordinates at least 3 zinc ions (Figure 4.2A, Table 4.1).

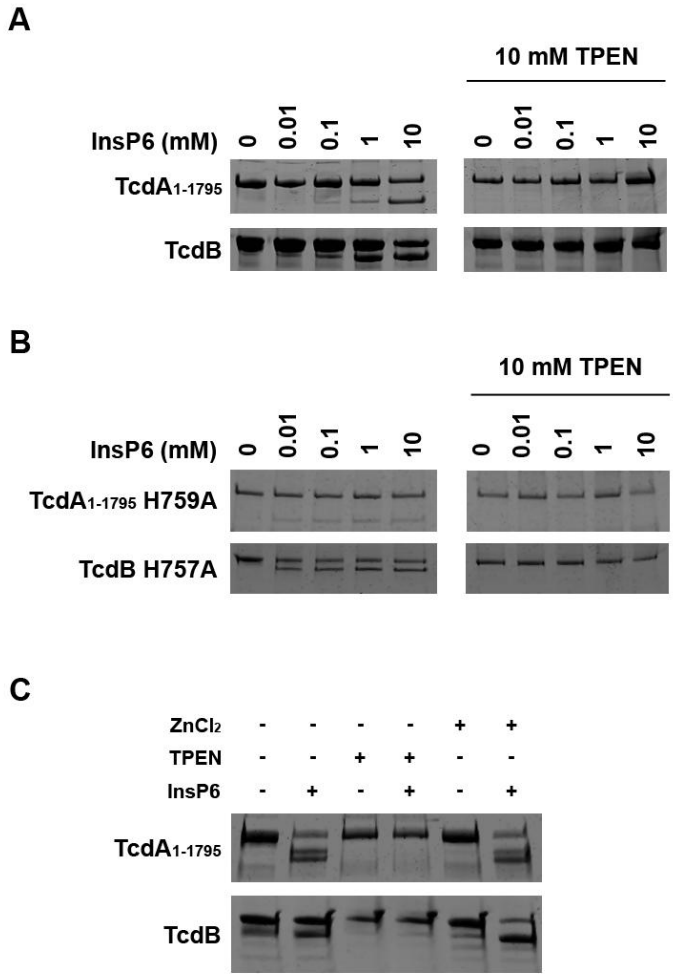

Figure 4.6. TcdA and TcdB are zinc-dependent proteases. Cleavage assays investigating the autoprocessing activity of A, $TcdA_{1-1795}$ and TcdB and B, $TcdA_{1-1795}$ H759A and TcdB in the presence of 10 mM TPEN. Reactions in the absence of TPEN were run in a control buffer containing 2.5% ethanol. C, Cleavage assays with samples analyzed by ICP-MS (Table 4.1). The reactions were run in each sample's dialyzate. Indicated reactions contained 100 µM InsP6 pretreated with 100 mM TPEN. Reactions were incubated at 37 °C for 2 hours and analyzed by Coomassie stained SDS-PAGE.

We localized at least one coordinating residue of the inhibitory zinc to the 14 amino acids between 1795 and 1809 using a series of truncation mutants analyzed by both ICP-MS and autoprocessing activity (Figure 4.2C, Table 4.1). There are four potential zinc coordinating residues within these 14 amino acids including two Glu residues and two Asp residues. Intriguingly, three of these residues are not conserved in TcdB. We might expect the residue(s) coordinating the zinc to be absent in TcdB, as

there is no inhibitory zinc binding at this site in the delivery domain (Figure 4.2D). Unfortunately, single point mutation of these four residues in TcdA has not abrogated the requirement for EDTA in autoprocessing. It may be that two or more mutations will be needed to eliminate zinc binding at this location. It is important to note that neither the inhibitory zinc nor its putative coordinating residues were visible in the crystal structure recently determined by our lab. The buffer conditions were shown to release the inhibitory zinc and allow autoprocessing. Taking note of the location of the last visible residue in the structure (1802), however, the next several residues, of interest, would likely reside at the interface of the delivery domain and APD (Figure 4.2E). It is, therefore, possible that residues on the APD side of the interface are also coordinating the inhibitory zinc. Using the positions of residues in the $TcdA_{1\text{-}1832}$ structure, we have mutated several residues in the APD potentially coordinating the zinc: Glu572, Glu573, Glu646, and Glu694 (Figure 4.2E). These mutants have not yet been tested by ICP-MS or cleavage assay to determine whether the residues are important for zinc coordination.

We hypothesize that the presence of the inhibitory zinc in TcdA and absence in TcdB has a functional consequence in the cellular intoxication mechanism. It is possible that the regulatory mechanism implemented by the inhibitory zinc is to ensure that autoprocessing occurs in the proper environment. We and others have shown that TcdA induces a GT-dependent apoptotic cell death, making pH dependent translocation of the GTD important for the intoxication mechanism of TcdA. We have shown that the zinc can be released upon exposure of TcdA to a pH of 6.0 or lower, resembling that of a maturing endosome (Figure 4.3). Perhaps the regulatory function of the inhibitory zinc is to allow cleavage of TcdA only upon progression into the late endosome to ensure proper translocation, cleavage, and trafficking of the GTD to its target GTPase. The putative binding site of the inhibitory zinc is positioned at the interface of the delivery domain and the APD (Figure 4.2E). Notably, this may also be the point of rotation for the conformational change induced by low pH observed by EM (Figure 4.3B) [5]. This observation provides structural support for hypothesis that the inhibitory zinc is important for the spatial regulation of TcdA autoprocessing activity.

The TcdA and TcdB APD were defined as a cysteine protease first by homology to the MARTx toxin from *Vibrio cholerae* (VcRTx) [104]. Subsequent mutagenesis of the homologous catalytic residues, Cys700, His655, and Asp589 in TcdA, resulted in deficient autoprocessing activity [4,32,104,158]. Chemical modification of the presumed catalytic cysteine with N-ethylmaleimide (NEM), iodoacetate, and novel substrate mimetics provided further evidence of cysteine protease activity [3,104]. In each case, the mutation or covalent modification of the catalytic cysteine would result in abrogation of zinc coordination, as demonstrated by the ICP-MS data with C700A (Table 4.1), which would result in loss of enzymatic activity. A more recent study describing the detectable nitrosylation of Cys700 also describes the modified toxin as deficient in catalytic activity [32]. Similarly, nitrosylation is a covalent modification that would interfere with zinc coordination [201]. Notably, the Asp589 is not in the catalytic active site in the $TcdA_{1\text{-}1832}$ structure (Figure 4.4B). It appears, instead, to act as a hydrogen bonding partner with His655, perhaps explaining the diminished but not abrogated autoprocessing activity observed upon its mutagenesis.

The crystal structure of $TcdA_{1\text{-}1832}$ revealed an unknown residue in the APD active site (Figure 4.4A and 4.4B). His759 contributes to the coordination of zinc, though its binding affinity appears to be significantly lower than the other residues in the active site, Cys700 and His655, based on ICP-MS data (Table 4.1). Mutating His759 results in autoprocessing activity that is independent of InsP6 concentration, demonstrating that this residue is important in the allosteric regulation of InsP6 binding (Figure 4.5A). This finding lends support to the reports that InsP6 binding is communicated through the β-flap, as His759 is positioned at the base of flap. In comparing the structure of $TcdA_{1\text{-}1832}$ in the absence of InsP6 and the TcdA APD alone bound to InsP6, we observe a large 19 Å displacement of InsP6 out of the active site (Figure 4.5B).

Our experiments with TPEN, a zinc specific chelator, suggest that TcdA and TcdB are zinc-dependent proteases (Figure 4.6). The dependence upon zinc is not new to Clostridial toxins, as both botulinum neurotoxin and tetanus toxin are known zinc proteases [188-190]. The catalytic active site of *C. difficile* toxins is unusual, however. Enzymatic coordination sites typically do not contain cysteine residues, though there are

examples such as alcohol dehydrogenase [201]. It is important to note that the conformation of the active site in the $TcdA_{1-1832}$ structure is likely not the conformation in which catalysis occurs. We have evidence that His759 moves out of the active site upon InsP6 binding (Figure 4.5), which is known to be required for autoprocessing to occur. We hypothesize that His759 provides steric hindrance and prevents the substrate from binding before InsP6 binds. Once His759 relocalizes, the substrate is then allowed to bind forming a new, unknown coordination site for the zinc. Perhaps this required relocalization of His759 before the enzyme is fully active is similar to the "cysteine switch" mechanism of activation first described in collagenase [202]. The identities of the residues involved in the coordination of the zinc are presumed to include either Cys700 or His655. Crystal structures of VcRTx and TcdB in the presence of InsP6 with the substrate or covalent inhibitor, respectively, bound indicate that the substrate lies in between Cys700 and His655 [1,3]. Our lab has also preliminarily determined the structure of the TcdA APD in the presence of InsP6 in which the substrate is bound, revealing a similar confirmation. Unfortunately, in each study, Cys700 was either mutated or covalently modified, resulting in loss of zinc coordination. Ideally, we could determine the structure of a mutant that did not ablate zinc binding such as the cleavage site mutant, L542A. Efforts to achieve this structure are ongoing, though thus far have been unsuccessful. For now, we can speculate based on the available substrate bound structures. There may be a possible coordination site on the Cys700 side of the substrate including Glu745 and Trp761. Efforts to determine the involvement of these residues by site-directed mutagenesis are underway.

In this study, we have demonstrated an essential and novel regulatory function of zinc in the enzymatic activity of *C. difficile* toxins. There are at least three zincs coordinated by TcdA, and we have described the functions of two here. One zinc is inhibitory and must be released before autoprocessing can occur. It is thought that this zinc is coordinated in the interface between the delivery domain and the APD. This coordination site may prevent InsP6 binding before the toxin has reached the low pH of a mature endosome. Another zinc is coordinated in the catalytic active site of the APD. This zinc has been shown to be required for catalytic activity and could activate a water molecule in a metalloprotease mechanism of action. Many details of the coordination

sites and the catalytic mechanism of the active site zinc remain unanswered and are active areas of investigation.

CHAPTER V

CONCLUSIONS AND FUTURE DIRECTIONS

Conclusions

When this project began, it was thought that TcdA and TcdB were homologous toxins that intoxicated cells by identical mechanisms and killed cells by inducing apoptosis. Additionally, autoprocessing and glucosyltransferase activity were thought to be required for toxin function and toxicity. As mediators of CDI, the toxins are viewed as drug targets where small molecule or biological inhibitors could provide novel treatment strategies for the disease. We conducted a high throughput small molecule inhibitor screen to identify compounds that protected cells from TcdB-induced cell death. In the process of this endeavor and the development of secondary assays, we discovered that TcdB induces a necrotic mechanism of cell death that is independent of both the autoprocessing and glucosyltransferase activities of the toxin (Chapter II). Dr. Melissa Farrow and I have since discovered that the necrosis induced by TcdB is a result of aberrant, NADPH oxidase (NOX)-derived reactive oxygen species (ROS) production. With a new understanding of the mechanism by which cells were dying, we returned to the confirmed hits identified from the small molecule inhibitor screen. 0449, one of the top hits from the screen, has been an invaluable tool in dissecting the NOX mechanism unique to TcdB. Our data demonstrate that calcium is a key component of the TcdB-induced NOX production of ROS (Appendix I).

Using a conditionally immortalized cell line, YAMCs, we observed for the first time a clear bimodal cell death induced by TcdB. At nanomolar concentrations, we observe GT-independent, NOX-driven necrosis, consistent with our observations in transformed cell lines. At low picomolar concentrations and below, however, we observe GT-dependent apoptosis that is likely occurring through a p53-dependent pathway. We were also able to directly compare the cell death mechanisms induced by

TcdA and TcdB side-by-side, in the same cell line and at the same time points. In doing so, we demonstrated that TcdA is a potent cytotoxin, killing cells and damaging colonic tissue in a concentration range and time frame similar to that of TcdB. This potency had not been observed in previous studies using transformed cell lines. We also supported previous observations that TcdA induces a GT-dependent, p53-dependent apoptotic cell death. Our mechanistic observations made in YAMC cells intoxicated with TcdA and TcdB were recapitulated in colonic tissue, providing evidence that the mechanisms of cell death observed in YAMC cells are relevant in pathogenesis. This report allowed for the unification of the field's differing observations (Chapter III).

We also discovered that TcdA autoprocessing activity is regulated by the coordination of at least two zinc ions (Chapter IV). One zinc acts as an inhibitor of enzymatic activity and must be extracted before cleavage is observed. This regulatory mechanism is not present in TcdB. The binding site of this inhibitory zinc includes at least one residue within the 14 amino acids between 1795 and 1809. The location of these residues within the $TcdA_{1\text{-}1832}$ crystal structure leaves room for the possibility that the zinc is coordinated at the interface of the delivery domain and the autoprocessing domain, blocking the InsP6 binding site. A second zinc is coordinated in the APD active site and is required for catalytic activity. Zinc represents a novel regulatory mechanism for the enzymatic activity of TcdA *in vitro*.

These data have advanced our understanding of the mechanistic actions of TcdA and TcdB but many unanswered questions remain. These questions and our efforts and ideas to investigate them are described in the next section.

Future Directions

What is the molecular target of 0449?

Our data suggest that the molecular target of 0449 is upstream of the initial calcium release from the endosome. Also, the similarities between the protective effects of bafilomycin A1 and 0449 suggest that 0449 may be targeting a molecule in the endosome. Similarities between the calcium release profiles of 0449 and known T-type calcium channel inhibitors indicate that an unidentified endosomal T-type calcium

channel may be involved in the TcdB induced NOX production of ROS. This hypothesis has been preliminarily supported by the calcium release profiles of siRNA knockdown of Tpcn1 and Trpml1, channels associated with endosomes, and Cav3.3, a known T-type calcium channel.

How is Ca^{2+} regulated in the NADPH oxidase (NOX) pathway initiated by TcdB?

One of the key discoveries our lab has made regarding the NOX pathway induced by TcdB is the importance of calcium release events. Based on kinetic assays investigating calcium release, we have observed a biphasic calcium release in response to TcdB. We consistently see a smaller, transient release early after intoxication followed by a much larger, sustained calcium release event. Inhibitor data combined with siRNA knockdown data have led us to hypothesize that upon internalization of TcdB, there is a small, localized calcium release from the endosome. This transient calcium burst results in undetermined signaling events that ultimately result in a much larger and sustained calcium release from the endoplasmic reticulum (ER). We speculate further that these calcium release events damage the mitochondria, resulting in mitochondrial release of ROS. These events may feed back into the NOX production of ROS creating a positive feedback loop that results in aberrant NOX-derived ROS production, ultimately leading to necrosis.

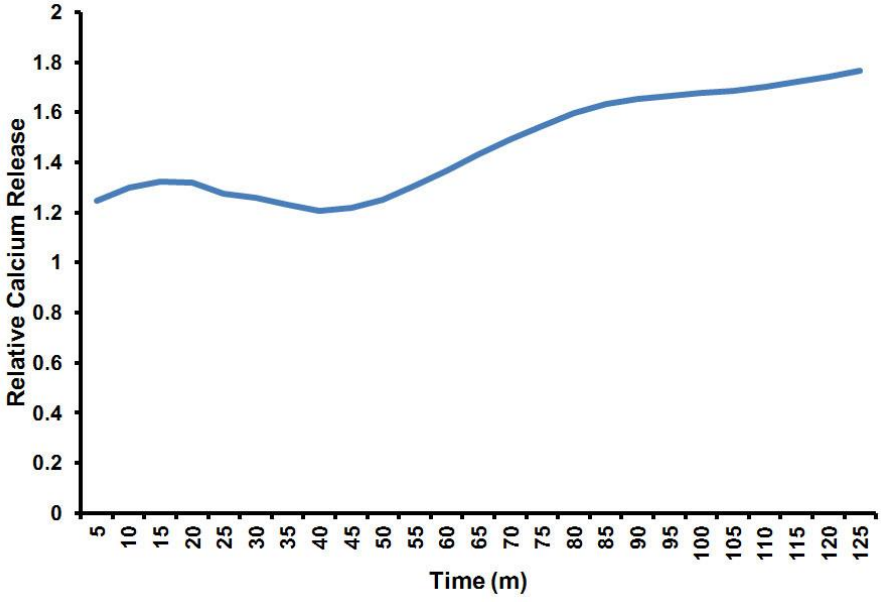

Figure 5.1. TcdB induces a biphasic calcium release from cells. HeLa cells were intoxicated were intoxicated with 10 nM TcdB and incubated at 37 °C. Calcium levels were assessed using a fluorescent calcium indicator, Fluoforte, every 5 minutes for 125 minutes. Data points represent the average relative signal of 3 experiments performed in triplicate.

Calcium release may be the property of TcdB initiated NOX activation that leads to the host cell's demise. IL-1 and TNF ligation to the cell surface also initiate NOX assembly and activation, but the result is low levels of ROS used by the cell as signaling molecules. Interestingly, we cannot detect a calcium release event in response to IL-1 or TNF treatment of cells in an endpoint assay. If calcium release is the disease state determinant of the NOX pathway, then understanding the mechanism by which calcium release occurs from the endosome is crucial to preventing the detrimental effects of NOX activation. Potential calcium channels in the endosome present novel drug targets in the treatment of not only CDI, but also other diseases in which aberrant NOX-derived ROS has been implicated. Such diseases include cardiovascular disease, neurodegenerative disease, and pancreatitis.

What are the unique properties of the interactions between TcdB and the redoxosome?

The redox active endosome, or 'redoxosome,' possesses several unique qualities that set it apart from normally maturing endosomes, including the regulation of ion transport. We have observed a toxin dependent interaction with the redoxosome that regulates the function of the NOX complex. Several point mutations in the delivery domain, spread out over the length of the domain, result in protection of the cell from necrosis. We do not detect any necrotic markers, calcium release, ROS production, or LDH release, in cells intoxicated with the delivery domain mutants tested. This phenotype is independent of pore formation, as the mutants have varying capabilities in forming pores as judged by rubidium release from liposomes and Rac1 glucosylation assays in cells. We hypothesize that the delivery domain of the TcdB interacts with some component of the redoxosome, such as the membrane, an ion channel, or another protein, that is important for proper function of the NOX complex. Dr. Fred Lamb, at Vanderbilt, has the capability to purify redoxosomes and investigate their unique components, such as associated proteins, ion channels, and lipids. We are hopeful that this collaboration will provide insight into the important interactions between TcdB and the redox active endosome.

How does TcdB-induced apoptosis contribute to pathogenesis?

We clearly detected TcdB-induced apoptosis in YAMC cells at concentrations lower than 100 pM. It remains unclear what the concentration of toxin is in the colon at the site of infection. Unfortunately, we cannot detect TcdB induced damage in our colonic explants model at concentrations where apoptosis is observed. It is possible that the absence of a damage phenotype is the result of the 5 hour time point used in our model system. The shorter time points are used, in part, to ensure the tissue remains healthy. Longer time points have resulted in damaged untreated tissue. We are collaborating with Frank McKeon's lab who has developed a system by which they can grow colonic tissue from human stem cells (manuscript under review at Nature). This very exciting new model system allows us to investigate the effects of lower concentrations of toxin at much longer time points post-intoxication. It may also be possible to develop an infection model in this system. Data from this model could potentially help to determine the concentration of toxin that is necessary to induce colonic damage and the respective mechanism that should be targeted to prevent damage from occurring.

Can we identify small molecule inhibitors of TcdA?

Now that we can detect TcdA-induced cell death in YAMC cells, a convenient model system that recapitulates what we observe in our tissue explant model, we can conduct a high throughput screen for compounds that protect cells from TcdA-induced cell death. The screen could be conducted in a manner similar to the screen against TcdB in which the readout for the assay is cell death. It is reasonable to expect to identify hits that are inhibitors of the GT activity of TcdA, as we have clearly observed a GT-dependent apoptotic cell death in response to TcdA intoxication. If the endpoint of the primary assay is cell death, it is equally reasonable to expect to find compounds that inhibit other steps of the intoxication mechanism that are thought to be required for cell death including host cell receptor binding, translocation, and autoprocessing activities. While the development of secondary assays identifying compounds that interact with the toxin directly may be more straight-forward, molecules that effect events downstream of GTPase glucosylation are also potential hits. Compounds that inhibit

TcdA-induced cell death are needed both as investigational tools and as candidates for novel therapeutics. Probes that can help define the downstream events that lead to apoptosis after GTPase modification could prove useful in understanding disease pathogenesis as a whole. Also, it is likely that targeting both cell death mechanisms, necrosis and apoptosis, will be necessary to effectively combat CDI in a toxin-centric therapeutic strategy.

Which residues in TcdA are coordinating the inhibitory zinc?

The residues that coordinate the inhibitory zinc remain unclear. Based on autoprocessing assays with the C-terminal truncations, we have narrowed possible residues to the 14 amino acids between 1795 and 1809. There are four acidic residues capable of coordinating a zinc ion at positions 1803, 1805, 1807, and 1809. Single point mutation of these residues did not have an impact on autoprocessing activity; all mutants still required EDTA to induce cleavage. It is possible that double mutants will be more informative. Also, these residues are located at the interface of the delivery domain and the APD. It is possible that the zinc is coordinated by residues in the APD as well. Point mutations have been made at residues E572, E573, E646, and E694 and will be investigated for autoprocessing activity in the absence of EDTA. Alternatively, we can attempt to find other crystallization conditions favorable for the inhibitory zinc to remain coordinated. Efforts to crystallize TcdA holotoxin could also pursued. The identification of the residues coordinating the zinc could be useful in determining the functional importance of this regulatory mechanism in the cell death pathway induced by TcdA.

Can we create a zinc binding site in TcdB?

Once we have identified the inhibitory zinc binding site, we would wonder if we could create a zinc binding site in TcdB by site-directed mutagenesis. If we did create a zinc binding site, and thereby creating an artificial regulatory mechanism, we would be very interested in the effects it would have on the intoxication and cell death mechanisms induced by TcdB. Would the presence of the inhibitory zinc make the apoptotic mechanism of cell death more prominent if there was tighter regulation of

translocation and autoprocessing? Would the inhibitory zinc affect the necrotic mechanism of cell death induced by TcdB?

What is the functional significance of the inhibitory zinc in cellular intoxication?

We hypothesized that the inhibitory zinc was, at least in part, stabilizing the neutral pH conformation and regulating the environment in which TcdA undergoes autocatalytic cleavage. To test this, cells were pretreated with known endosomal acidification inhibitors, bafilomycin A1, NH_4Cl, or mock conditions, and then intoxicated with TcdA or TcdB. The cells were lysed and Rac1 modification was assessed, using an antibody sensitive to unmodified Rac1 only, as a measure of toxin conformational change, pore formation, and GTD translocation. The glucosyltransferase mutants, TcdA D285/287N and TcdB D286/288N, were used as negative controls, as they should not modify Rac1. In cells pretreated with bafilomycin or NH_4Cl, subsequent intoxication with TcdA resulted in significantly less Rac1 glucosylation compared to the cells treated with toxin only. The lack of Rac1 modification when endosomal maturation is inhibited suggests that low pH of the endosome is required for the release of the inhibitory zinc and the conformational change necessary for translocation of the GTD. When cells were intoxicated with TcdB after bafilomycin or NH_4Cl pretreatment, however, there was no inhibition of Rac1 modification. This result suggests that the low pH of the mature endosome is less essential for TcdB translocation. One major difference between TcdA and TcdB is the presence of the inhibitory zinc in TcdA, which can be released upon exposure to low pH. These data suggest that the zinc is an important regulator of the pH dependent conformational change that promotes autoprocessing activity of TcdA in cells. We expect to be able to better delineate the specific functions of the inhibitory zinc once we have identified the coordination site of the inhibitory zinc and can construct point mutations.

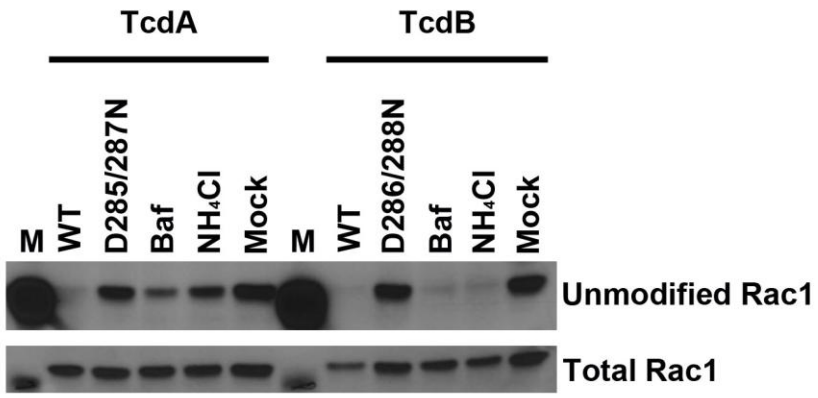

Figure 5.2. The inhibitory zinc may regulate pH dependent GTD translocation. HeLa cells were preincubated with 10 nM bafilomycin, 10 mM NH4Cl, or mock for 1 hour at 37 °C. Cells were then intoxicated with 10 nM toxin and incubated at 37 °C for with 1 or 3 hours (TcdB toxins or TcdA toxins, respectively). Cells were lysed as described previously, and lysates were probed for unmodified and total Rac1 as previously described.

What is the autoprocessing catalytic mechanism of action?

We have discovered that the catalytic mechanism of the APD is not that of a cysteine protease, but is rather a zinc-dependent protease. We hypothesize that His759 sterically hinders the substrate binding the active site until InsP6 binds. As the allostery is communicated through the β-flap, and His759 is pulled out of the active site, the substrate is then able to bind. Based on previous structures and our own preliminary structure, we further hypothesize that the substrate lies between two zinc coordinating residues, Cys700 and His655. This suggests that upon substrate binding, a new zinc coordination site is created. It is in this site that catalysis occurs. Unfortunately, we have no insight into the conformation or residues involved in this active site. We can speculate and propose possible coordination sites based on structural data. We have mutated Glu745 and Trp763 to test for defects in autoprocessing activity. Ideally, however, we will be able to determine the structure of substrate bound state with the zinc bound in the active site. We are actively pursuing this structure with a non-cleavable mutant, L542A, however, crystal trials have been unsuccessful thus far. We also plan to try to crystallize the protein in the presence of an active site peptide mimetic. Determining the mechanism by which autoprocessing occurs may help to guide therapeutic development.

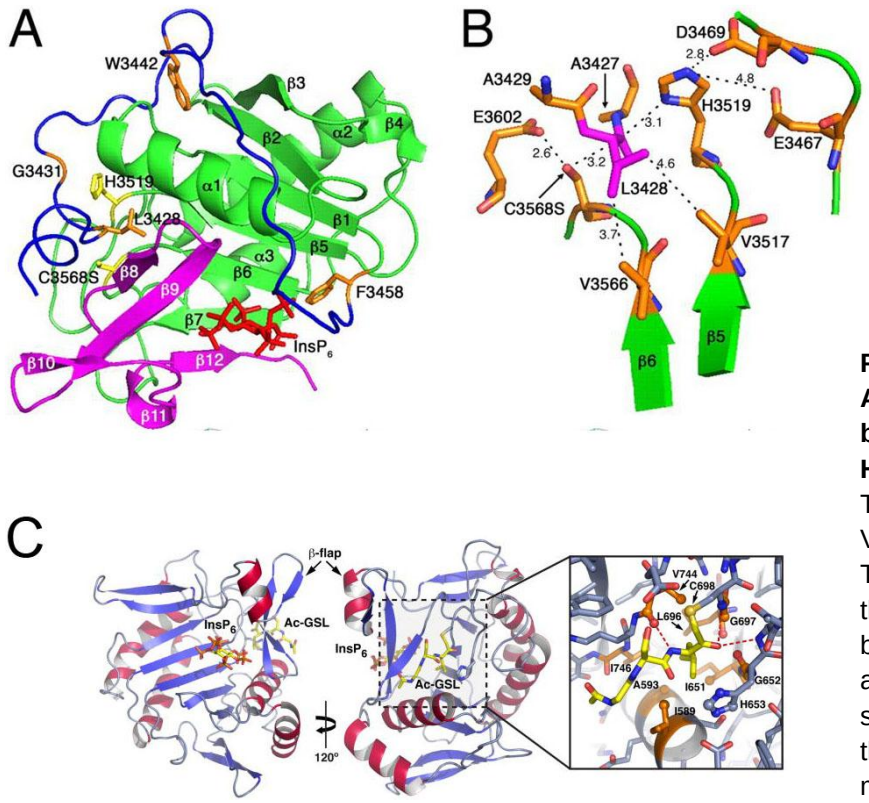

Figure 5.3. The TcdA APD substrate may lie between Cys700 and His655. The structures of TcdA homologues, A, VcRTx C3568S [1] and B, TcdB-As-OSL [3] suggest that the substrate lies between the catalytic Cys and His residues. These structures further suggest that the catalytic mechanism is unusual.

Can we test our hypotheses in a mouse model?

In collaboration with Dr. David Aronoff, we are beginning to test our hypotheses in a mouse infection model. Thus far, we can observe colonic tissue damage in mice treated with antibiotics prior to infection with spores from the 10643 strain of *C. difficile*. This is a laboratory strain that is known to produce high levels of toxin. We have preliminary data with NOX1 knockout mice infected with the 10643 strain that show significantly less colonic damage compared to control mice. This data suggests that the NOX pathway induced by TcdB intoxication of tissue culture cells is relevant in pathogenesis. We would also like to conduct experiments testing our hypothesis surrounding mechanistic differences between TcdA and TcdB and the importance of toxin regulation in the context of disease. In the future, we would like to create genetically altered *C. difficile* strains in which we can make single point mutations within toxin genes. This is possible using the newly developed ClosTron technology, though attempts by other groups at inserting single point mutations have not yet been successful. Single gene knockouts of each of the toxins, TcdA and TcdB, have been

successful, however, and we are collaborating with Dr. Dena Lyras who has isogenic knockout strains from an epidemic strain, M7404. We intend to exploit this technology to gain further insight into the relative functional contributions each of each toxin in disease.

Our goal is to understand the functional relevance of each toxin and the respective mechanisms they employ cause disease. The data presented here suggest that TcdA and TcdB initiate distinctly different mechanisms of cell death in cell culture and colonic explant models. Our compound, 0449, and use of chemical chelators have been useful tools in beginning to delineate differences between the mechanistic actions of the toxins. Moving into an infection model with 0449 and genetically modified strains of *C. difficile* will provide even more insight into disease pathogenesis.

APPENDIX I

Small molecule inhibition of TcdB induced necrosis

Successful treatment of CDI has proven to be a difficult task with recurrence and death rates continuing to increase. The medical challenge highlights the need for more effective therapeutics. Antibiotics are the standard course of treatment, but they have been shown to further disrupt the intestinal microbiota. While the immediate *C. difficile* infection may clear, antibiotic therapy may contribute to high recurrence rates. A novel therapeutic strategy has been put forth in which the toxins, TcdA and TcdB, are the targets of new drugs. CDI is a toxin mediated disease, and it is thought that preventing colonic damage by inhibiting the function of the toxins would provide the patient a window of opportunity to more effectively clear the infection, potentially reducing the risk of recurrence.

We performed a high throughput screen of 16,000 compounds in the Vanderbilt University High Throughput Screening Faciility using a robust cell viability assay (Z' = 0.8) to assess protection of Chinese Hamster Ovary (CHO) cells from TcdB induced cell death (Figure A1.1). CellTiterGlo, used as our screen assay readout, is a luminescent viability indicator that detects ATP in cells. Because our assay was a cell based assay involving the entire mechanism of intoxication, we thought it possible to identify compounds that not only inhibited TcdB directly, but that also inhibited host cell factors important in the death pathway. We wanted to focus on those compounds that inhibited the toxin directly, however, and began designing secondary assays to identify specific inhibitors of TcdB function. We recognized that any functional domain could potentially be inhibited, including host cell receptor binding, delivery, autoprocessing, or glucosyltransfer. Because the APD and GTD were thought to be required for TcdB induced cell death and contain defined active and allosteric binding sites, we anticipated identifying a number of compounds inhibiting these enzymatic activities.

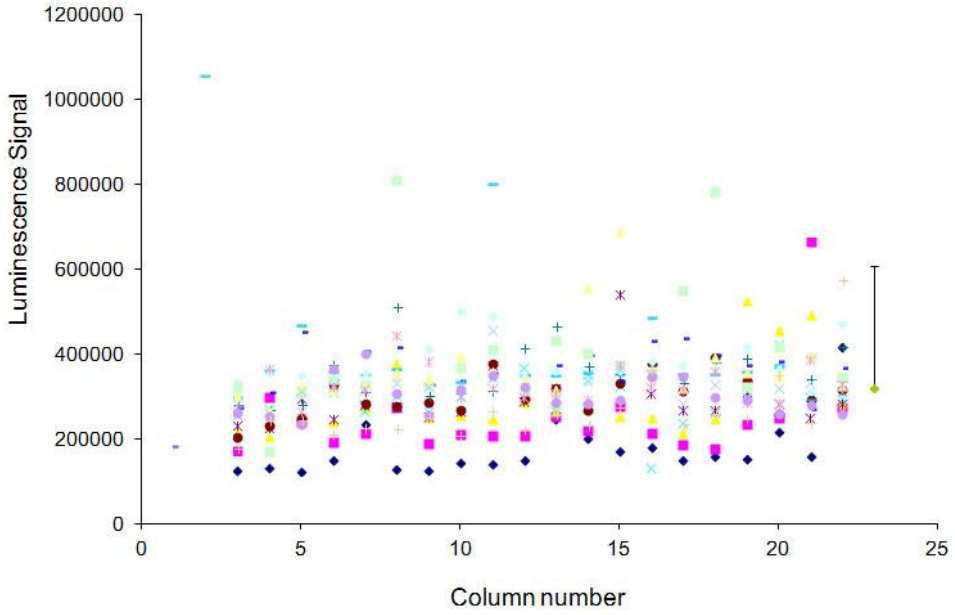

Figure A1.1. High-throughput screen to identify small molecule inhibitors of TcdB. Cells were pretreated with inhibitor at 37 °C for 1 h, intoxicated with 10 nM TcdB, and incubated at 37 °C for 6 h. Cell viability was measured using CellTiterGlo. A representative plate from the screen is shown with toxin and untreated controls in columns 1 and 2, respectively, which were used to calculate the Z' of each plate (Z' = 0.8). The bar in column 23 represents 3 standard deviations from the mean of the plate. Any compound protecting cells from TcdB-induced cell death more than 3 standard deviations from the mean was considered a hit. 176 hits were pulled and confirmed from a 16,000 compound screen. The 176 confirmed hits were classified into 3 groups: scavengers, non-scavengers, and dihydropyridines, based on their chemical structures.

We identified 176 hits that conferred protection against TcdB-induced cytotoxicity. Upon discovering autoprocessing and glucosyltransferase activities were not required for TcdB-induced necrosis, however, we no longer had a mechanistic context for understanding how these molecules were working. Once we discovered that TcdB activates the host NADPH oxidase (NOX) complex, resulting in aberrant production of reactive oxygen species (ROS) and necrosis in epithelial cells, we were able to return to the hits identified in our small molecule inhibitor screen and reevaluate how they might be conferring protection.

We were encouraged to find 16 compounds containing phenols or free thiols, capable of scavenging ROS. While these compounds are a satisfying confirmation for both our proposed mechanism of ROS dependent necrosis and our assay, we were not

interested in pursuing scavengers as therapeutics or mechanistic probes. Thus far, we have separated the hits into three categories based on their chemical properties: scavengers (16 compounds), non-scavengers (109 compounds), and dihydropyridines (51 compounds). The non-scavenger group of compounds is very chemically diverse. We would be very interested to find compounds that inhibit the assembly and activation of NOX. Assays to determine successful assembly of NOX to test the non-scavenging group are being optimized now. The dihydropyridine (DHP) scaffold has the potential to inhibit the pathogenic mechanism both as a scavenger of ROS and as a calcium channel inhibitor. Several DHP compounds used to treat hypertension, such as nifedipine, act by blocking calcium channels (Figure A1.2A). Together with siRNA knockdown data acquired by Dr. Melissa Farrow, this observation led us to investigate how calcium functions in NOX-dependent necrosis induced by TcdB and how our DHP scaffold is involved in protection.

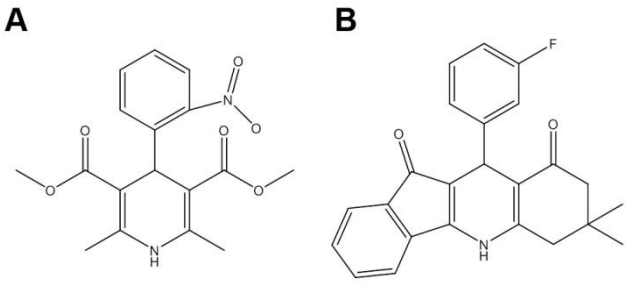

Figure A1.2. Chemical structures of dihydropyridines. A, Nifedipine, commonly prescribed to treat hypertension, is a known L-type calcium channel inhibitor. B, 0449 was a top hit from our small molecule inhibitor screen.

We decided to focus our studies on compound 0449 (Figure A1.2B), one of the most protective DHP compounds, and compare its inhibitory properties to those of nifedipine, defined as an L-type calcium channel inhibitor. First, we compared the protective effects of 0449 and nifedipine in a cell viability assay. As shown in Figure A1.3A, 0449 protects cells from TcdB induced necrosis more effectively and at lower concentrations than nifedipine. We observed a similar phenotype in our ROS assay.

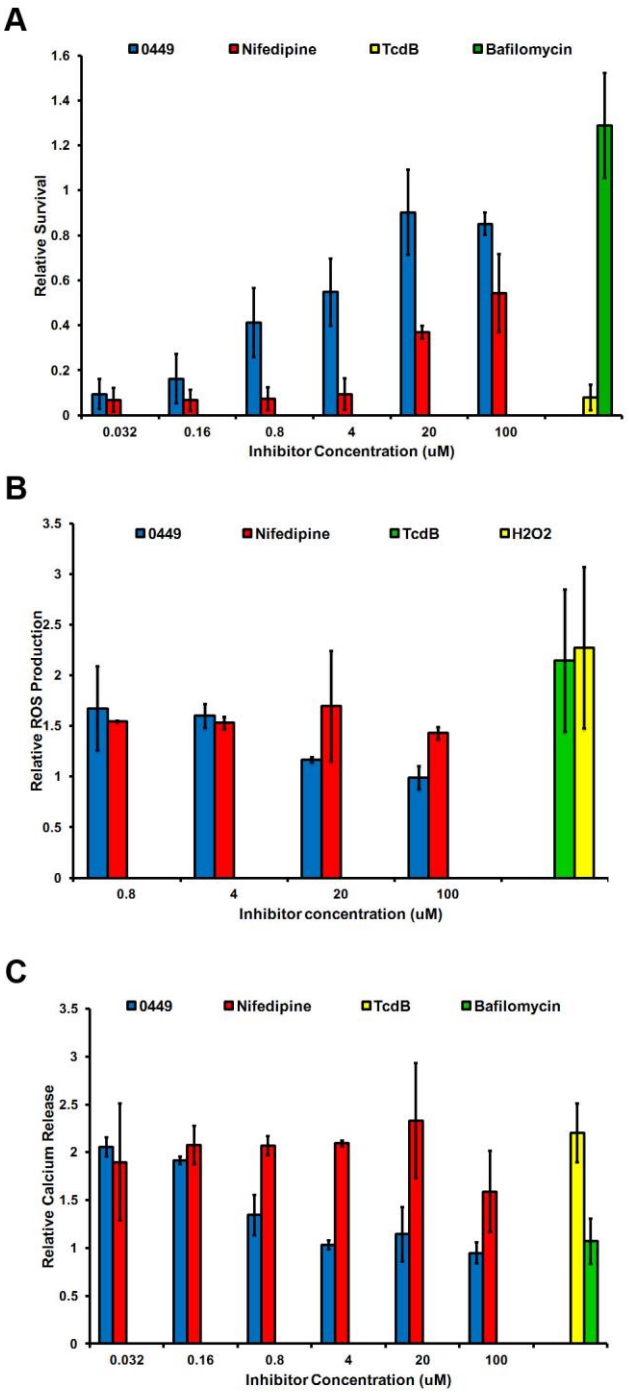

Figure A1.3. Nifedipine and 0449 prevent TcdB induced necrosis, ROS production, and calcium release. Cells were pretreated with inhibitor at 37 °C for 1 h, and then intoxicated with 10 nM TcdB and incubated at 37 °C overnight. A, Cell viability was measured using CellTiterGlo. B, ROS production and C, calcium release were measured using fluorescent indicators. The data in each graph represent the average of three experiments in which each condition was tested in triplicate. Error bars represent the standard deviation between experiments.

Both compounds provide reasonable inhibition of ROS production, though 0449 prevents the production of ROS at lower concentrations than nifedipine (Figure A1.3B). We next wanted to investigate whether TcdB induced a calcium response in the cell. We can detect a robust calcium release in response to TcdB intoxication, comparable to

that of ionomycin, a known ionophore (Figure A1.3C). 0449 inhibits the calcium release down to background cellular calcium levels at sub-micromolar concentrations of compound. Notably, nifedipine did not significantly inhibit the calcium release initiated by TcdB intoxication (Figure A1.3C). These data confirm that 0449 is an excellent inhibitor of TcdB-induced necrosis and is capable of directly or indirectly blocking TcdB induced calcium responses.

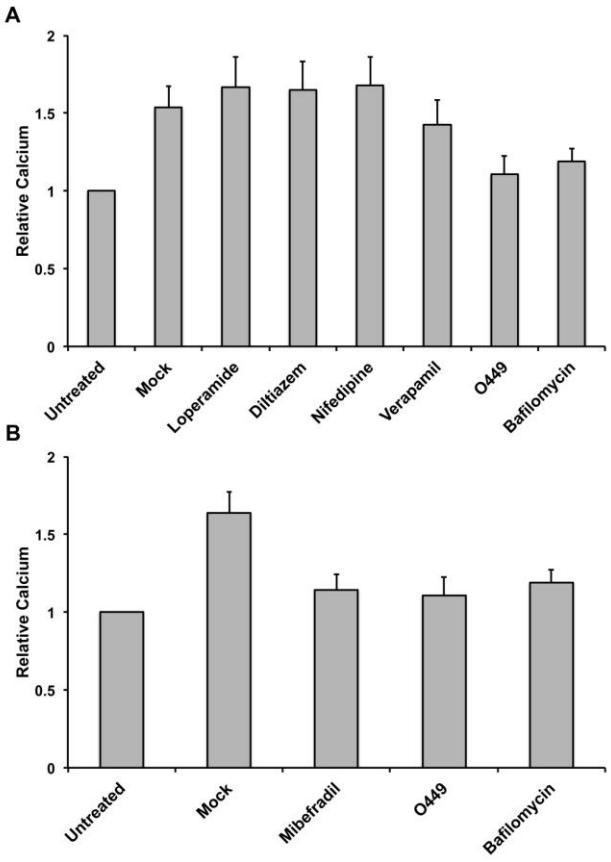

Figure A1.4. 0449 inhibits TcdB induced calcium release more similarly to T-type calcium channel inhibitors. A, Comparison of 0449 to structurally diverse L-type calcium channel inhibitors. Bafilomycin is a V-ATPase inhibitor. B, Comparison of 0449 to a T-type calcium channel inhibitor, mibefradil.

The superiority of 0449 inhibition of calcium release compared to nifedipine seemed curious to us. We thought it possible that 0449 is a more potent inhibitor of L-type calcium channels and wondered how it would compare to other, structurally diverse L-type calcium channels. In Figure A1.4A, calcium release data indicate that 0449 is more potent than all other L-type calcium channel inhibitors, leaving room for the possibility that the target of 0449 is not an L-type calcium channel. To test this, we compared 0449 to mibefradil, a T-type calcium channel inhibitor. Our preliminary data

show mibefradil inhibits TcdB induced calcium release to levels comparable to the inhibition of 0449 (Figure A1.4B). Though DHPs are known to inhibit L-type calcium channels, these data suggest that 0449 may inhibit a T-type calcium channel. These studies are in very early stages and require further investigation.

Interestingly, bafilomycin A1 inhibits calcium release in response to TcdB to levels comparable to 0449 (Figure A1.4). This suggests that the target of 0449 might reside in the endosome. We are in the preliminary stages of understanding the ion regulation of redox active endosomes and the channels that are involved. Dr. Melissa Farrow has identified, by siRNA knockdown, several endosomal ion channels that are important in TcdB induced necrosis. Our preliminary studies on both endosomal ion channels and the importance of calcium in the TcdB induced NOX pathway are discussed further in Chapter V.

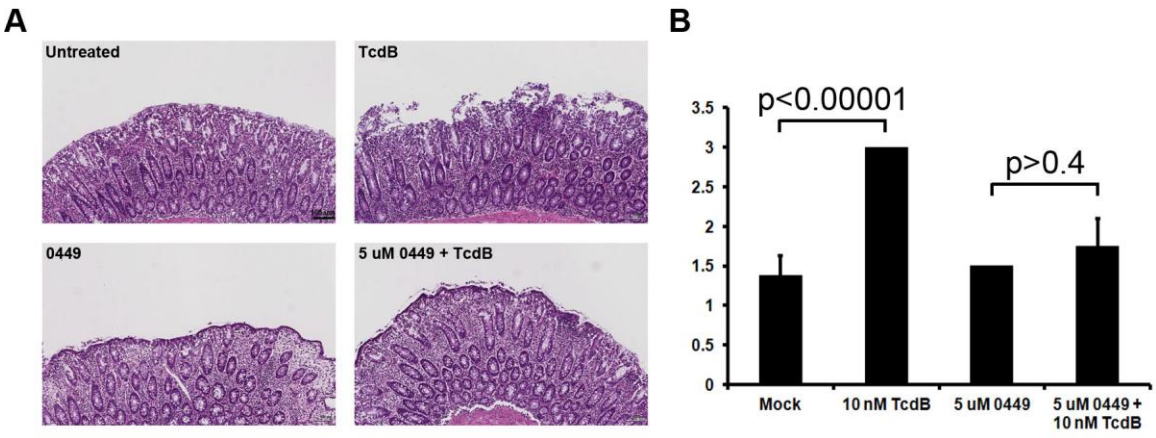

Figure A1.5. 0449 prevents TcdB induced tissue damage. Porcine colonic explants were mock or pretreated with 5 uM compound for 1 h at 37 °C and then intoxicated with 10 nM TcdB and incubated at 37 °C for 4 h. A, The tissue was fixed, and sections were stained with H&E. B, Pathology scores based on a semi-quantitative injury scoring system. Statistics were performed in Excel using a paired, two-tailed student's t-test.

We also tested the efficacy of 0449 in our colonic explant model. When we pretreated porcine colonic explants with 5 μM compound, the tissue was protected from TcdB induced damage (Figure A1.5A). Pathology scores demonstrated no significant difference between tissue that was treated with 0449 alone and tissue treated with 0449 and TcdB (Figure A1.5B). These data suggest that in addition to protecting cells from

TcdB induced damage, 0449 also provides protection from the effects of TcdB in the context of colonic tissue. We are encouraged by these data and we look forward to moving into a mouse infection model in the future.

Methods

Small molecule inhibitor screen

Compounds (final concentration of 10 μM) were put into 384 well plates using the VU HTS facility's robotic technology. CHO cells were seeded into the screen plates and incubated at 37 °C for 1 hour. Cells were then intoxicated with 30 nM TcdB and incubated at 37 °C for 6 hours. Viability of the cells was assessed using CellTiterGlo (Promega) as previously described. When analyzing the viability data, the Z' score of each plate was calculated and the average luminescence signal of each plate was calculated. A compound was considered a 'hit' if the signal from cells treated with that compound was more than 3 standard deviations above the average signal of the plate.

Viability, ROS, and Calcium assays

Viability and ROS assays were performed as previously described. For calcium assays, HeLa cells were preincubated with inhibitor for 1 hour at 37 °C. Cells were then intoxicated with 10 nM TcdB and FluorForte (Enzo) calcium indicator was used according to manufacturer's instructions.

Colonic explants

Colonic explants were prepared as previously described , and preincubated with with 5 μM 0449 or an equal volume of solvent at 37 °C for 1 hour. Explants were then intoxicated with either 10 nM TcdB or an equal volume of buffer and incubated at 37 °C for 5 hours. Tissue was fixed, prepared, and scored as previously described. Statistics were performed in Excel with a paired, two-tailed student's t-test.

APPENDIX II

Publications

Data presented in Chapter II

Chumbler NM, Farrow MA, Lapierre LA, Franklin JL, Haslam D, Goldenring JR, Lacy DB. *Clostridium difficile* Toxin B Causes Epithelial Cell Necrosis through an Autoprocessing-Independent Mechanism. PLoS Pathog. 2012 Dec;8(12):e1003072.
PMID: 23236283

Data presented in Chapter III

Chumbler, NM, Farrow, MA, Lapierre, LA, Franklin, JL, Lacy, DB. *Clostridium difficile* toxins TcdA and TcdB cause colonic tissue damage by distinct mechanisms. Manuscript in preparation.

Data presented in Chapter IV

Chumbler, NM*, Rutherford, SA*, Zhang, Z, Farrow, MA, Lisher, JP, Farquhar, E, Giedroc, DP, Spiller, BW, Melnyk, RA, Lacy, DB. Crystal structure of *Clostridium difficile* Toxin A. Under Review. Nature.

Other publications

DuMont AL, Yoong P, Liu X, Day CJ, Chumbler NM, James DB, Alonzo F 3rd, Bode NJ, Lacy DB, Jennings MP, Torres VJ. Identification of a crucial residue required for *Staphylococcus aureus* LukAB cytotoxicity and receptor recognition. Infect Immun. 2014 Mar;82(3):1268-76. doi: 10.1128/IAI.01444-13. Epub 2013 Dec 30.
PMID: 24379286

Farrow MA, Chumbler NM, Lapierre LA, Franklin JL, Rutherford SA, Craven RE, Goldenring JR and Lacy DB. *Clostridium difficile* toxin B induced necrosis is mediated by reactive oxygen species. Proc Natl Acad Sci U S A. 2013 Nov 12;110(46):18674-9. doi: 10.1073/pnas.1313658110. Epub 2013 Oct 28. PMID: 24167244

Slater L, Hett E, Mark K, Chumbler NM, Patel D, Lacy DB, Collier RJ, Hung D. Identification of Novel Host-Targeted Compounds That Protect From Anthrax Lethal Toxin-Induced Cell Death. ACS Chem Biol. 2013 Apr 19;8(4):812-22. PMID: 23343607

Pruitt RN, Chumbler NM, Rutherford SA, Farrow MA, Friedman DB, Spiller B, Lacy DB. Structural determinants of *Clostridium difficile* toxin A glucosyltransferase activity. J Biol Chem. 2012 Mar 9;287(11):8013-20. PMID: 22267739

REFERENCES

1. Prochazkova K, Shuvalova LA, Minasov G, Voburka Z, Anderson WF, et al. (2009) Structural and molecular mechanism for autoprocessing of MARTX toxin of Vibrio cholerae at multiple sites. J Biol Chem 284: 26557-26568.
2. Pruitt RN, Chumbler NM, Rutherford SA, Farrow MA, Friedman DB, et al. (2012) Structural determinants of Clostridium difficile toxin A glucosyltransferase activity. J Biol Chem 287: 8013-8020.
3. Puri AW, Lupardus PJ, Deu E, Albrow VE, Garcia KC, et al. (2010) Rational design of inhibitors and activity-based probes targeting Clostridium difficile virulence factor TcdB. Chem Biol 17: 1201-1211.
4. Pruitt RN, Chagot B, Cover M, Chazin WJ, Spiller B, et al. (2009) Structure-function analysis of inositol hexakisphosphate-induced autoprocessing in Clostridium difficile toxin A. J Biol Chem 284: 21934-21940.
5. Pruitt RN, Chambers MG, Ng KK, Ohi MD, Lacy DB (2010) Structural organization of the functional domains of Clostridium difficile toxins A and B. Proc Natl Acad Sci U S A 107: 13467-13472.
6. Pruitt RN, Lacy DB (2012) Toward a structural understanding of Clostridium difficile toxins A and B. Front Cell Infect Microbiol 2: 28.
7. Hall IC, O'Toole E (1935) Intestinal flora in new-born infants with a description of a new pathogenic anaerobe, *Bacillus difficilis*. Am J Dis Child 49: 390-402.
8. Ho JG, Greco A, Rupnik M, Ng KK (2005) Crystal structure of receptor-binding C-terminal repeats from Clostridium difficile toxin A. Proc Natl Acad Sci U S A 102: 18373-18378.
9. Brito GA, Fujji J, Carneiro-Filho BA, Lima AA, Obrig T, et al. (2002) Mechanism of Clostridium difficile toxin A-induced apoptosis in T84 cells. J Infect Dis 186: 1438-1447.
10. Jank T, Giesemann T, Aktories K (2007) Clostridium difficile glucosyltransferase toxin B-essential amino acids for substrate binding. J Biol Chem 282: 35222-35231.
11. Pettersen EF, Goddard TD, Huang CC, Couch GS, Greenblatt DM, et al. (2004) UCSF Chimera--a visualization system for exploratory research and analysis. J Comput Chem 25: 1605-1612.
12. Lessa FC, Mu Y, Bamberg WM, Beldavs ZG, Dumyati GK, et al. (2015) Burden of Clostridium difficile Infection in the United States. N Engl J Med 372: 825-834.
13. Ozaki E, Kato H, Kita H, Karasawa T, Maegawa T, et al. (2004) Clostridium difficile colonization in healthy adults: transient colonization and correlation with enterococcal colonization. J Med Microbiol 53: 167-172.
14. Bartlett JG (1994) Clostridium difficile: history of its role as an enteric pathogen and the current state of knowledge about the organism. Clin Infect Dis 18 Suppl 4: S265-272.
15. McFarland LV, Mulligan ME, Kwok RY, Stamm WE (1989) Nosocomial acquisition of Clostridium difficile infection. N Engl J Med 320: 204-210.
16. Warny M, Pepin J, Fang A, Killgore G, Thompson A, et al. (2005) Toxin production by an emerging strain of Clostridium difficile associated with outbreaks of severe disease in North America and Europe. Lancet 366: 1079-1084.

17. Merrigan M, Venugopal A, Mallozzi M, Roxas B, Viswanathan VK, et al. (2003) Human hypervirulent Clostridium difficile strains exhibit increased sporulation as well as robust toxin production. J Bacteriol 192: 4904-4911.
18. Akerlund T, Persson I, Unemo M, Noren T, Svenungsson B, et al. (2008) Increased sporulation rate of epidemic Clostridium difficile Type 027/NAP1. J Clin Microbiol 46: 1530-1533.
19. McDonald LC, Killgore GE, Thompson A, Owens RC, Jr., Kazakova SV, et al. (2005) An epidemic, toxin gene-variant strain of Clostridium difficile. N Engl J Med 353: 2433-2441.
20. Gerhard R, Nottrott S, Schoentaube J, Tatge H, Olling A, et al. (2008) Glucosylation of Rho GTPases by Clostridium difficile toxin A triggers apoptosis in intestinal epithelial cells. J Med Microbiol 57: 765-770.
21. Lica M, Schulz F, Schelle I, May M, Just I, et al. (2011) Difference in the biological effects of Clostridium difficile toxin B in proliferating and non-proliferating cells. Naunyn Schmiedebergs Arch Pharmacol 383: 275-283.
22. Vonberg RP, Reichardt C, Behnke M, Schwab F, Zindler S, et al. (2008) Costs of nosocomial Clostridium difficile-associated diarrhoea. J Hosp Infect 70: 15-20.
23. Dubberke ER, Reske KA, Olsen MA, McDonald LC, Fraser VJ (2008) Short- and long-term attributable costs of Clostridium difficile-associated disease in nonsurgical inpatients. Clin Infect Dis 46: 497-504.
24. Miller BA, Chen LF, Sexton DJ, Anderson DJ (2011) Comparison of the burdens of hospital-onset, healthcare facility-associated Clostridium difficile Infection and of healthcare-associated infection due to methicillin-resistant Staphylococcus aureus in community hospitals. Infect Control Hosp Epidemiol 32: 387-390.
25. Magill SS, Edwards JR, Bamberg W, Beldavs ZG, Dumyati G, et al. (2014) Multistate point-prevalence survey of health care-associated infections. N Engl J Med 370: 1198-1208.
26. Dubberke ER, Olsen MA (2012) Burden of Clostridium difficile on the healthcare system. Clin Infect Dis 55 Suppl 2: S88-92.
27. Sorg JA, Sonenshein AL (2008) Bile salts and glycine as cogerminants for Clostridium difficile spores. J Bacteriol 190: 2505-2512.
28. Hewlett P, Smith A, Lucas E (2009) Grazing, cognitive performance and mood. Appetite 52: 245-248.
29. Linscott LL, Osborn AG, Blaser S, Castillo M, Hewlett RH, et al. (2008) Pilomyxoid astrocytoma: expanding the imaging spectrum. AJNR Am J Neuroradiol 29: 1861-1866.
30. Hewlett SA, Luce CB, Servon LJ (2008) Stopping the exodus of women in science. Harv Bus Rev 86: 22-24, 139.
31. Wylde V, Blom A, Dieppe P, Hewlett S, Learmonth I (2008) Return to sport after joint replacement. J Bone Joint Surg Br 90: 920-923.
32. Savidge TC, Urvil P, Oezguen N, Ali K, Choudhury A, et al. (2011) Host S-nitrosylation inhibits clostridial small molecule-activated glucosylating toxins. Nat Med 17: 1136-1141.
33. Yaziji H, Taylor CR, Goldstein NS, Dabbs DJ, Hammond EH, et al. (2008) Consensus recommendations on estrogen receptor testing in breast cancer by immunohistochemistry. Appl Immunohistochem Mol Morphol 16: 513-520.
34. Kelly CP, Pothoulakis C, LaMont JT (1994) Clostridium difficile colitis. N Engl J Med 330: 257-262.

35. Lanis JM, Hightower LD, Shen A, Ballard JD (2012) TcdB from hypervirulent Clostridium difficile exhibits increased efficiency of autoprocessing. Mol Microbiol 84: 66-76.
36. Giblin JP, Hewlett LJ, Hannah MJ (2008) Basal secretion of von Willebrand factor from human endothelial cells. Blood 112: 957-964.
37. Fang AF, Damle BD, LaBadie RR, Crownover PH, Hewlett D, Jr., et al. (2008) Significant decrease in nelfinavir systemic exposure after omeprazole coadministration in healthy subjects. Pharmacotherapy 28: 42-50.
38. Hewlett S, Cockshott Z, Almeida C, Richards P, Lowe R, et al. (2008) Sensitivity to change of the Rheumatoid Arthritis Self-Efficacy scale (RASE) and predictors of change in self-efficacy. Musculoskeletal Care 6: 49-67.
39. Easley CJ, Karlinsey JM, Bienvenue JM, Legendre LA, Roper MG, et al. (2006) A fully integrated microfluidic genetic analysis system with sample-in-answer-out capability. Proc Natl Acad Sci U S A 103: 19272-19277.
40. Hehir M, Carr M, Davis B, Radford S, Robertson L, et al. (2008) Nursing support at the onset of rheumatoid arthritis: Time and space for emotions, practicalities and self-management. Musculoskeletal Care 6: 124-134.
41. Larchanche PE, Ultre V, Le Broc D, Ballandone C, Furman C, et al. (2015) 6-Sulfonylbenzothiazolones as potential scaffolds for the design of 5-HT ligands. Eur J Med Chem 92C: 807-817.
42. Melnyk P, Vingt-Deux V, Burlet S, Eddarkaoui S, Grosjean ME, et al. (2015) Chloroquine- and chloroquinoline-derivatives as models for the design of modulators of Amyloid Peptide Precursor metabolism. ACS Chem Neurosci.
43. Donnier-Marechal M, Carato P, Le Broc D, Furman C, Melnyk P (2014) Synthesis and pharmacological evaluation of benzannulated derivatives as potent and selective sigma-1 protein ligands. Eur J Med Chem 92C: 575-582.
44. Boll E, Drobecq H, Ollivier N, Blanpain A, Raibaut L, et al. (2015) One-pot chemical synthesis of small ubiquitin-like modifier protein-peptide conjugates using bis(2-sulfanylethyl)amido peptide latent thioester surrogates. Nat Protoc 10: 269-292.
45. Melnyk AD, Chak JD, Singh V, Kelly A, Cripton PA, et al. (2015) Characterization of the behavior of a novel low-stiffness posterior spinal implant under anterior shear loading on a degenerative spinal model. Eur Spine J.
46. Bezdrobna LK, Tarasenko LV, Tsyganok TV, Melnyk TV, Nosach YO, et al. (2014) Cytogenetic indices in blood lymphocites of individuals from the staff working on new confinement buildining in Chornobyl NPP zone. Probl Radiac Med Radiobiol 19: 203-212.
47. Ettaoussi M, Peres B, Errazani A, Boutin JA, Caignard DH, et al. (2015) Synthesis and pharmacological evaluation of dual ligands for melatonin (MT1/MT2) and serotonin 5-HT2C receptor subtypes (II). Eur J Med Chem 90: 822-833.
48. Donnier-Marechal M, Larchanche PE, Le Broc D, Furman C, Carato P, et al. (2015) Carboline- and phenothiazine-derivated heterocycles as potent SIGMA-1 protein ligands. Eur J Med Chem 89: 198-206.
49. Edgerton JD, Melnyk TS, Roberts LW (2014) Problem Gambling and the Youth-to-Adulthood Transition: Assessing Problem Gambling Severity Trajectories in a Sample of Young Adults. J Gambl Stud.

50. Cherepanov PV, Melnyk I, Andreeva DV (2015) Effect of high intensity ultrasound on Al(3)Ni(2), Al(3)Ni crystallite size in binary AlNi (50 wt% of Ni) alloy. Ultrason Sonochem 23: 26-30.
51. de Conti A, Tryndyak V, Churchwell MI, Melnyk S, Latendresse JR, et al. (2014) Genotoxic, epigenetic, and transcriptomic effects of tamoxifen in mouse liver. Toxicology 325: 12-20.
52. Ollivier N, Blanpain A, Boll E, Raibaut L, Drobecq H, et al. (2014) Selenopeptide transamidation and metathesis. Org Lett 16: 4032-4035.
53. Delmee M, Avesani V, Delferriere N, Burtonboy G (1990) Characterization of flagella of Clostridium difficile and their role in serogrouping reactions. J Clin Microbiol 28: 2210-2214.
54. Stabler RA, Gerding DN, Songer JG, Drudy D, Brazier JS, et al. (2006) Comparative phylogenomics of Clostridium difficile reveals clade specificity and microevolution of hypervirulent strains. J Bacteriol 188: 7297-7305.
55. Borriello SP, Davies HA, Kamiya S, Reed PJ, Seddon S (1990) Virulence factors of Clostridium difficile. Rev Infect Dis 12 Suppl 2: S185-191.
56. Karjalainen T, Waligora-Dupriet AJ, Cerquetti M, Spigaglia P, Maggioni A, et al. (2001) Molecular and genomic analysis of genes encoding surface-anchored proteins from Clostridium difficile. Infect Immun 69: 3442-3446.
57. Sebaihia M, Wren BW, Mullany P, Fairweather NF, Minton N, et al. (2006) The multidrug-resistant human pathogen Clostridium difficile has a highly mobile, mosaic genome. Nat Genet 38: 779-786.
58. Waligora AJ, Hennequin C, Mullany P, Bourlioux P, Collignon A, et al. (2001) Characterization of a cell surface protein of Clostridium difficile with adhesive properties. Infect Immun 69: 2144-2153.
59. Savariau-Lacomme MP, Lebarbier C, Karjalainen T, Collignon A, Janoir C (2003) Transcription and analysis of polymorphism in a cluster of genes encoding surface-associated proteins of Clostridium difficile. J Bacteriol 185: 4461-4470.
60. Bordeleau E, Purcell EB, Lafontaine DA, Fortier LC, Tamayo R, et al. (2015) Cyclic Di-GMP Riboswitch-Regulated Type IV Pili Contribute to Aggregation of Clostridium difficile. J Bacteriol 197: 819-832.
61. Popoff MR, Rubin EJ, Gill DM, Boquet P (1988) Actin-specific ADP-ribosyltransferase produced by a Clostridium difficile strain. Infect Immun 56: 2299-2306.
62. Perelle S, Gibert M, Bourlioux P, Corthier G, Popoff MR (1997) Production of a complete binary toxin (actin-specific ADP-ribosyltransferase) by Clostridium difficile CD196. Infect Immun 65: 1402-1407.
63. Lyras D, O'Connor JR, Howarth PM, Sambol SP, Carter GP, et al. (2009) Toxin B is essential for virulence of Clostridium difficile. Nature 458: 1176-1179.
64. Kuehne SA, Cartman ST, Heap JT, Kelly ML, Cockayne A, et al. (2010) The role of toxin A and toxin B in Clostridium difficile infection. Nature 467: 711-713.
65. Lyerly DM, Krivan HC, Wilkins TD (1988) Clostridium difficile: its disease and toxins. Clin Microbiol Rev 1: 1-18.
66. Rupnik M, Grabnar M, Geric B (2003) Binary toxin producing Clostridium difficile strains. Anaerobe 9: 289-294.
67. Mitchell TJ, Ketley JM, Haslam SC, Stephen J, Burdon DW, et al. (1986) Effect of toxin A and B of Clostridium difficile on rabbit ileum and colon. Gut 27: 78-85.

68. Lyerly DM, Lockwood DE, Richardson SH, Wilkins TD (1982) Biological activities of toxins A and B of Clostridium difficile. Infect Immun 35: 1147-1150.
69. Lyerly DM, Saum KE, MacDonald DK, Wilkins TD (1985) Effects of Clostridium difficile toxins given intragastrically to animals. Infect Immun 47: 349-352.
70. Kyne L, Warny M, Qamar A, Kelly CP (2001) Association between antibody response to toxin A and protection against recurrent Clostridium difficile diarrhoea. Lancet 357: 189-193.
71. Giannasca PJ, Warny M (2004) Active and passive immunization against Clostridium difficile diarrhea and colitis. Vaccine 22: 848-856.
72. Babcock GJ, Broering TJ, Hernandez HJ, Mandell RB, Donahue K, et al. (2006) Human monoclonal antibodies directed against toxins A and B prevent Clostridium difficile-induced mortality in hamsters. Infect Immun 74: 6339-6347.
73. Warny M, Vaerman JP, Avesani V, Delmee M (1994) Human antibody response to Clostridium difficile toxin A in relation to clinical course of infection. Infect Immun 62: 384-389.
74. Lyerly DM, Barroso LA, Wilkins TD, Depitre C, Corthier G (1992) Characterization of a toxin A-negative, toxin B-positive strain of Clostridium difficile. Infect Immun 60: 4633-4639.
75. Sambol SP, Merrigan MM, Lyerly D, Gerding DN, Johnson S (2000) Toxin gene analysis of a variant strain of Clostridium difficile that causes human clinical disease. Infect Immun 68: 5480-5487.
76. Heap JT, Cartman ST, Kuehne SA, Cooksley C, Minton NP (2010) ClosTron-targeted mutagenesis. Methods Mol Biol 646: 165-182.
77. Heap JT, Kuehne SA, Ehsaan M, Cartman ST, Cooksley CM, et al. (2010) The ClosTron: Mutagenesis in Clostridium refined and streamlined. J Microbiol Methods 80: 49-55.
78. Yang G, Zhou B, Wang J, He X, Sun X, et al. (2008) Expression of recombinant Clostridium difficile toxin A and B in Bacillus megaterium. BMC Microbiol 8: 192.
79. Dupuy B, Govind R, Antunes A, Matamouros S (2008) Clostridium difficile toxin synthesis is negatively regulated by TcdC. J Med Microbiol 57: 685-689.
80. Tan KS, Wee BY, Song KP (2001) Evidence for holin function of tcdE gene in the pathogenicity of Clostridium difficile. J Med Microbiol 50: 613-619.
81. Hundsberger T, Braun V, Weidmann M, Leukel P, Sauerborn M, et al. (1997) Transcription analysis of the genes tcdA-E of the pathogenicity locus of Clostridium difficile. Eur J Biochem 244: 735-742.
82. von Eichel-Streiber C, Sauerborn M (1990) Clostridium difficile toxin A carries a C-terminal repetitive structure homologous to the carbohydrate binding region of streptococcal glycosyltransferases. Gene 96: 107-113.
83. Jank T, Giesemann T, Aktories K (2007) Rho-glucosylating Clostridium difficile toxins A and B: new insights into structure and function. Glycobiology 17: 15R-22R.
84. von Eichel-Streiber C, Sauerborn M, Kuramitsu HK (1992) Evidence for a modular structure of the homologous repetitive C-terminal carbohydrate-binding sites of Clostridium difficile toxins and Streptococcus mutans glucosyltransferases. J Bacteriol 174: 6707-6710.
85. von Eichel-Streiber C, Laufenberg-Feldmann R, Sartingen S, Schulze J, Sauerborn M (1992) Comparative sequence analysis of the Clostridium difficile toxins A and B. Mol Gen Genet 233: 260-268.

86. Krivan HC, Clark GF, Smith DF, Wilkins TD (1986) Cell surface binding site for Clostridium difficile enterotoxin: evidence for a glycoconjugate containing the sequence Gal alpha 1-3Gal beta 1-4GlcNAc. Infect Immun 53: 573-581.
87. Tucker KD, Wilkins TD (1991) Toxin A of Clostridium difficile binds to the human carbohydrate antigens I, X, and Y. Infect Immun 59: 73-78.
88. Teneberg S, Lonnroth I, Torres Lopez JF, Galili U, Halvarsson MO, et al. (1996) Molecular mimicry in the recognition of glycosphingolipids by Gal alpha 3 Gal beta 4 GlcNAc beta-binding Clostridium difficile toxin A, human natural anti alpha-galactosyl IgG and the monoclonal antibody Gal-13: characterization of a binding-active human glycosphingolipid, non-identical with the animal receptor. Glycobiology 6: 599-609.
89. Pothoulakis C, Gilbert RJ, Cladaras C, Castagliuolo I, Semenza G, et al. (1996) Rabbit sucrase-isomaltase contains a functional intestinal receptor for Clostridium difficile toxin A. J Clin Invest 98: 641-649.
90. Na X, Kim H, Moyer MP, Pothoulakis C, LaMont JT (2008) gp96 is a human colonocyte plasma membrane binding protein for Clostridium difficile toxin A. Infect Immun 76: 2862-2871.
91. Yuan P, Zhang H, Cai C, Zhu S, Zhou Y, et al. (2015) Chondroitin sulfate proteoglycan 4 functions as the cellular receptor for Clostridium difficile toxin B. Cell Res 25: 157-168.
92. Papatheodorou P, Zamboglou C, Genisyuerek S, Guttenberg G, Aktories K (2010) Clostridial glucosylating toxins enter cells via clathrin-mediated endocytosis. PLoS One 5: e10673.
93. Barroso LA, Moncrief JS, Lyerly DM, Wilkins TD (1994) Mutagenesis of the Clostridium difficile toxin B gene and effect on cytotoxic activity. Microb Pathog 16: 297-303.
94. Olling A, Goy S, Hoffmann F, Tatge H, Just I, et al. (2011) The Repetitive Oligopeptide Sequences Modulate Cytopathic Potency but Are Not Crucial for Cellular Uptake of Clostridium difficile Toxin A. PLoS One 6: e17623.
95. Qa'Dan M, Spyres LM, Ballard JD (2000) pH-induced conformational changes in Clostridium difficile toxin B. Infect Immun 68: 2470-2474.
96. Barth H, Pfeifer G, Hofmann F, Maier E, Benz R, et al. (2001) Low pH-induced formation of ion channels by clostridium difficile toxin B in target cells. J Biol Chem 276: 10670-10676.
97. Giesemann T, Jank T, Gerhard R, Maier E, Just I, et al. (2006) Cholesterol-dependent pore formation of Clostridium difficile toxin A. J Biol Chem 281: 10808-10815.
98. Umata T, Moriyama Y, Futai M, Mekada E (1990) The cytotoxic action of diphtheria toxin and its degradation in intact Vero cells are inhibited by bafilomycin A1, a specific inhibitor of vacuolar-type H(+)-ATPase. J Biol Chem 265: 21940-21945.
99. Genisyuerek S, Papatheodorou P, Guttenberg G, Schubert R, Benz R, et al. (2011) Structural determinants for membrane insertion, pore formation and translocation of Clostridium difficile toxin B. Mol Microbiol 79: 1643-1654.
100. Zhang Z, Park M, Tam J, Auger A, Beilhartz GL, et al. (2014) Translocation domain mutations affecting cellular toxicity identify the Clostridium difficile toxin B pore. Proc Natl Acad Sci U S A 111: 3721-3726.
101. Pfeifer G, Schirmer J, Leemhuis J, Busch C, Meyer DK, et al. (2003) Cellular uptake of Clostridium difficile toxin B. Translocation of the N-terminal catalytic domain into the cytosol of eukaryotic cells. J Biol Chem 278: 44535-44541.
102. Rupnik M, Pabst S, Rupnik M, von Eichel-Streiber C, Urlaub H, et al. (2005) Characterization of the cleavage site and function of resulting cleavage fragments after

limited proteolysis of Clostridium difficile toxin B (TcdB) by host cells. Microbiology 151: 199-208.
103. Reineke J, Tenzer S, Rupnik M, Koschinski A, Hasselmayer O, et al. (2007) Autocatalytic cleavage of Clostridium difficile toxin B. Nature 446: 415-419.
104. Egerer M, Giesemann T, Jank T, Satchell KJ, Aktories K (2007) Auto-catalytic cleavage of Clostridium difficile toxins A and B depends on cysteine protease activity. J Biol Chem 282: 25314-25321.
105. Kreimeyer I, Euler F, Marckscheffel A, Tatge H, Pich A, et al. (2011) Autoproteolytic cleavage mediates cytotoxicity of Clostridium difficile toxin A. Naunyn Schmiedebergs Arch Pharmacol 383: 253-262.
106. Genth H, Aktories K, Just I (1999) Monoglucosylation of RhoA at threonine 37 blocks cytosol-membrane cycling. J Biol Chem 274: 29050-29056.
107. Aktories K, Just I (1995) Monoglucosylation of low-molecular-mass GTP-binding Rho proteins by clostridial cytotoxins. Trends Cell Biol 5: 441-443.
108. Just I, Selzer J, von Eichel-Streiber C, Aktories K (1995) The low molecular mass GTP-binding protein Rho is affected by toxin A from Clostridium difficile. J Clin Invest 95: 1026-1031.
109. Just I, Selzer J, Wilm M, von Eichel-Streiber C, Mann M, et al. (1995) Glucosylation of Rho proteins by Clostridium difficile toxin B. Nature 375: 500-503.
110. Just I, Wilm M, Selzer J, Rex G, von Eichel-Streiber C, et al. (1995) The enterotoxin from Clostridium difficile (ToxA) monoglucosylates the Rho proteins. J Biol Chem 270: 13932-13936.
111. Bishop AL, Hall A (2000) Rho GTPases and their effector proteins. Biochem J 348 Pt 2: 241-255.
112. Selzer J, Hofmann F, Rex G, Wilm M, Mann M, et al. (1996) Clostridium novyi alpha-toxin-catalyzed incorporation of GlcNAc into Rho subfamily proteins. J Biol Chem 271: 25173-25177.
113. Nagahama M, Ohkubo A, Oda M, Kobayashi K, Amimoto K, et al. (2011) Clostridium perfringens TpeL glycosylates the Rac and Ras subfamily proteins. Infect Immun 79: 905-910.
114. Hippenstiel S, Schmeck B, N'Guessan PD, Seybold J, Krull M, et al. (2002) Rho protein inactivation induced apoptosis of cultured human endothelial cells. Am J Physiol Lung Cell Mol Physiol 283: L830-838.
115. Nottrott S, Schoentaube J, Genth H, Just I, Gerhard R (2007) Clostridium difficile toxin A-induced apoptosis is p53-independent but depends on glucosylation of Rho GTPases. Apoptosis 12: 1443-1453.
116. Kim H, Kokkotou E, Na X, Rhee SH, Moyer MP, et al. (2005) Clostridium difficile toxin A-induced colonocyte apoptosis involves p53-dependent p21(WAF1/CIP1) induction via p38 mitogen-activated protein kinase. Gastroenterology 129: 1875-1888.
117. Nusrat A, Giry M, Turner JR, Colgan SP, Parkos CA, et al. (1995) Rho protein regulates tight junctions and perijunctional actin organization in polarized epithelia. Proc Natl Acad Sci U S A 92: 10629-10633.
118. Feltis BA, Wiesner SM, Kim AS, Erlandsen SL, Lyerly DL, et al. (2000) Clostridium difficile toxins A and B can alter epithelial permeability and promote bacterial paracellular migration through HT-29 enterocytes. Shock 14: 629-634.

119. Johal SS, Solomon K, Dodson S, Borriello SP, Mahida YR (2004) Differential effects of varying concentrations of clostridium difficile toxin A on epithelial barrier function and expression of cytokines. J Infect Dis 189: 2110-2119.
120. Raaijmakers JH, Bos JL (2009) Specificity in Ras and Rap signaling. J Biol Chem 284: 10995-10999.
121. Geissler B, Tungekar R, Satchell KJ (2010) Identification of a conserved membrane localization domain within numerous large bacterial protein toxins. Proc Natl Acad Sci U S A 107: 5581-5586.
122. Genth H, Dreger SC, Huelsenbeck J, Just I (2008) Clostridium difficile toxins: more than mere inhibitors of Rho proteins. Int J Biochem Cell Biol 40: 592-597.
123. Chaves-Olarte E, Weidmann M, Eichel-Streiber C, Thelestam M (1997) Toxins A and B from Clostridium difficile differ with respect to enzymatic potencies, cellular substrate specificities, and surface binding to cultured cells. J Clin Invest 100: 1734-1741.
124. Genth H, Hofmann F, Selzer J, Rex G, Aktories K, et al. (1996) Difference in protein substrate specificity between hemorrhagic toxin and lethal toxin from Clostridium sordellii. Biochem Biophys Res Commun 229: 370-374.
125. Chaves-Olarte E, Low P, Freer E, Norlin T, Weidmann M, et al. (1999) A novel cytotoxin from Clostridium difficile serogroup F is a functional hybrid between two other large clostridial cytotoxins. J Biol Chem 274: 11046-11052.
126. Huelsenbeck J, Dreger S, Gerhard R, Barth H, Just I, et al. (2007) Difference in the cytotoxic effects of toxin B from Clostridium difficile strain VPI 10463 and toxin B from variant Clostridium difficile strain 1470. Infect Immun 75: 801-809.
127. Mehlig M, Moos M, Braun V, Kalt B, Mahony DE, et al. (2001) Variant toxin B and a functional toxin A produced by Clostridium difficile C34. FEMS Microbiol Lett 198: 171-176.
128. Ball DW, Van Tassell RL, Roberts MD, Hahn PE, Lyerly DM, et al. (1993) Purification and characterization of alpha-toxin produced by Clostridium novyi type A. Infect Immun 61: 2912-2918.
129. Donta ST, Sullivan N, Wilkins TD (1982) Differential effects of Clostridium difficile toxins on tissue-cultured cells. J Clin Microbiol 15: 1157-1158.
130. Aktories K (1997) Bacterial toxins that target Rho proteins. J Clin Invest 99: 827-829.
131. Tucker KD, Carrig PE, Wilkins TD (1990) Toxin A of Clostridium difficile is a potent cytotoxin. J Clin Microbiol 28: 869-871.
132. Riegler M, Sedivy R, Pothoulakis C, Hamilton G, Zacherl J, et al. (1995) Clostridium difficile toxin B is more potent than toxin A in damaging human colonic epithelium in vitro. J Clin Invest 95: 2004-2011.
133. Savidge TC, Pan WH, Newman P, O'Brien M, Anton PM, et al. (2003) Clostridium difficile toxin B is an inflammatory enterotoxin in human intestine. Gastroenterology 125: 413-420.
134. Kuehne SA, Cartman ST, Minton NP (2011) Both, toxin A and toxin B, are important in Clostridium difficile infection. Gut Microbes 2: 252-255.
135. Kuehne SA, Collery MM, Kelly ML, Cartman ST, Cockayne A, et al. (2014) Importance of toxin A, toxin B, and CDT in virulence of an epidemic Clostridium difficile strain. J Infect Dis 209: 83-86.

136. Castagliuolo I, Keates AC, Wang CC, Pasha A, Valenick L, et al. (1998) Clostridium difficile toxin A stimulates macrophage-inflammatory protein-2 production in rat intestinal epithelial cells. J Immunol 160: 6039-6045.
137. Castagliuolo I, Riegler M, Pasha A, Nikulasson S, Lu B, et al. (1998) Neurokinin-1 (NK-1) receptor is required in Clostridium difficile- induced enteritis. J Clin Invest 101: 1547-1550.
138. Warny M, Keates AC, Keates S, Castagliuolo I, Zacks JK, et al. (2000) p38 MAP kinase activation by Clostridium difficile toxin A mediates monocyte necrosis, IL-8 production, and enteritis. J Clin Invest 105: 1147-1156.
139. Voth DE, Qa'Dan M, Hamm EE, Pelfrey JM, Ballard JD (2004) Clostridium sordellii lethal toxin is maintained in a multimeric protein complex. Infect Immun 72: 3366-3372.
140. Flegel WA, Muller F, Daubener W, Fischer HG, Hadding U, et al. (1991) Cytokine response by human monocytes to Clostridium difficile toxin A and toxin B. Infect Immun 59: 3659-3666.
141. Jiang ZD, DuPont HL, Garey K, Price M, Graham G, et al. (2006) A common polymorphism in the interleukin 8 gene promoter is associated with Clostridium difficile diarrhea. Am J Gastroenterol 101: 1112-1116.
142. Fiorentini C, Fabbri A, Falzano L, Fattorossi A, Matarrese P, et al. (1998) Clostridium difficile toxin B induces apoptosis in intestinal cultured cells. Infect Immun 66: 2660-2665.
143. Brito GA, Carneiro-Filho B, Oria RB, Destura RV, Lima AA, et al. (2005) Clostridium difficile toxin A induces intestinal epithelial cell apoptosis and damage: role of Gln and Ala-Gln in toxin A effects. Dig Dis Sci 50: 1271-1278.
144. Carneiro BA, Fujii J, Brito GA, Alcantara C, Oria RB, et al. (2006) Caspase and bid involvement in Clostridium difficile toxin A-induced apoptosis and modulation of toxin A effects by glutamine and alanyl-glutamine in vivo and in vitro. Infect Immun 74: 81-87.
145. Matte I, Lane D, Cote E, Asselin AE, Fortier LC, et al. (2009) Antiapoptotic proteins Bcl-2 and Bcl-XL inhibit Clostridium difficile toxin A-induced cell death in human epithelial cells. Infect Immun 77: 5400-5410.
146. Melnyk RA, Clark IC, Liao A, Coates JD (2014) Transposon and deletion mutagenesis of genes involved in perchlorate reduction in Azospira suillum PS. MBio 5: e00769-00713.
147. Rose S, Frye RE, Slattery J, Wynne R, Tippett M, et al. (2014) Oxidative stress induces mitochondrial dysfunction in a subset of autism lymphoblastoid cell lines in a well-matched case control cohort. PLoS One 9: e85436.
148. Li F, Deshaies EM, Singla A, Villwock MR, Melnyk V, et al. (2014) Impact of anesthesia on mortality during endovascular clot removal for acute ischemic stroke. J Neurosurg Anesthesiol 26: 286-290.
149. Hassdenteufel S, Klein MC, Melnyk A, Zimmermann R (2014) Protein transport into the human ER and related diseases, Sec61-channelopathies. Biochem Cell Biol 92: 499-509.
150. Qa'Dan M, Ramsey M, Daniel J, Spyres LM, Safiejko-Mroczka B, et al. (2002) Clostridium difficile toxin B activates dual caspase-dependent and caspase-independent apoptosis in intoxicated cells. Cell Microbiol 4: 425-434.
151. Matarrese P, Falzano L, Fabbri A, Gambardella L, Frank C, et al. (2007) Clostridium difficile toxin B causes apoptosis in epithelial cells by thrilling mitochondria.

Involvement of ATP-sensitive mitochondrial potassium channels. J Biol Chem 282: 9029-9041.
152. Kim H, Rhee SH, Kokkotou E, Na X, Savidge T, et al. (2005) Clostridium difficile toxin A regulates inducible cyclooxygenase-2 and prostaglandin E2 synthesis in colonocytes via reactive oxygen species and activation of p38 MAPK. J Biol Chem 280: 21237-21245.
153. Reinert DJ, Jank T, Aktories K, Schulz GE (2005) Structural basis for the function of Clostridium difficile toxin B. J Mol Biol 351: 973-981.
154. Mesmin B, Robbe K, Geny B, Luton F, Brandolin G, et al. (2004) A phosphatidylserine-binding site in the cytosolic fragment of Clostridium sordellii lethal toxin facilitates glucosylation of membrane-bound Rac and is required for cytotoxicity. J Biol Chem 279: 49876-49882.
155. Qasba PK, Ramakrishnan B, Boeggeman E (2005) Substrate-induced conformational changes in glycosyltransferases. Trends Biochem Sci 30: 53-62.
156. Prochazkova K, Satchell KJ (2008) Structure-function analysis of inositol hexakisphosphate-induced autoprocessing of the Vibrio cholerae multifunctional autoprocessing RTX toxin. J Biol Chem 283: 23656-23664.
157. Lupardus PJ, Shen A, Bogyo M, Garcia KC (2008) Small molecule-induced allosteric activation of the Vibrio cholerae RTX cysteine protease domain. Science 322: 265-268.
158. Shen A, Lupardus PJ, Gersch MM, Puri AW, Albrow VE, et al. (2011) Defining an allosteric circuit in the cysteine protease domain of Clostridium difficile toxins. Nat Struct Mol Biol 18: 364-371.
159. Santos MM, Moreira R (2007) Michael acceptors as cysteine protease inhibitors. Mini Rev Med Chem 7: 1040-1050.
160. Ascenzi P, Salvati L, Bolognesi M, Colasanti M, Polticelli F, et al. (2001) Inhibition of cysteine protease activity by NO-donors. Curr Protein Pept Sci 2: 137-153.
161. McFarland LV, Stamm WE (1986) Review of Clostridium difficile-associated diseases. Am J Infect Control 14: 99-109.
162. Kelly CP, LaMont JT (2008) Clostridium difficile--more difficult than ever. N Engl J Med 359: 1932-1940.
163. Hofmann F, Busch C, Prepens U, Just I, Aktories K (1997) Localization of the glucosyltransferase activity of Clostridium difficile toxin B to the N-terminal part of the holotoxin. J Biol Chem 272: 11074-11078.
164. Lima AA, Lyerly DM, Wilkins TD, Innes DJ, Guerrant RL (1988) Effects of Clostridium difficile toxins A and B in rabbit small and large intestine in vivo and on cultured cells in vitro. Infect Immun 56: 582-588.
165. Dove CH, Wang SZ, Price SB, Phelps CJ, Lyerly DM, et al. (1990) Molecular characterization of the Clostridium difficile toxin A gene. Infect Immun 58: 480-488.
166. Florin I, Thelestam M (1986) Lysosomal involvement in cellular intoxication with Clostridium difficile toxin B. Microb Pathog 1: 373-385.
167. Harlow EaL, D. (1988) Antibodies: a laboratory manual. Cold Spring Harbor, NY, Cold Spring Harbor.
168. Ryder AB, Huang Y, Li H, Zheng M, Wang X, et al. (2010) Assessment of Clostridium difficile infections by quantitative detection of tcdB toxin by use of a real-time cell analysis system. J Clin Microbiol 48: 4129-4134.

169. Hewlett EL, Donato GM, Gray MC (2006) Macrophage cytotoxicity produced by adenylate cyclase toxin from Bordetella pertussis: more than just making cyclic AMP! Mol Microbiol 59: 447-459.
170. Voelker R (2010) Increased Clostridium difficile virulence demands new treatment approach. JAMA 303: 2017-2019.
171. Cloud J, Kelly CP (2007) Update on Clostridium difficile associated disease. Curr Opin Gastroenterol 23: 4-9.
172. Bartlett JG, Gerding DN (2008) Clinical recognition and diagnosis of Clostridium difficile infection. Clin Infect Dis 46 Suppl 1: S12-18.
173. Giesemann T, Egerer M, Jank T, Aktories K (2008) Processing of Clostridium difficile toxins. J Med Microbiol 57: 690-696.
174. Chumbler NM, Farrow MA, Lapierre LA, Franklin JL, Haslam DB, et al. (2012) Clostridium difficile Toxin B causes epithelial cell necrosis through an autoprocessing-independent mechanism. PLoS Pathog 8: e1003072.
175. Farrow MA, Chumbler NM, Lapierre LA, Franklin JL, Rutherford SA, et al. (2013) Clostridium difficile toxin B-induced necrosis is mediated by the host epithelial cell NADPH oxidase complex. Proc Natl Acad Sci U S A 110: 18674-18679.
176. Tam J, Beilhartz GL, Auger A, Gupta P, Therien AG, et al. (2015) Small Molecule Inhibitors of Clostridium difficile Toxin B-Induced Cellular Damage. Chem Biol.
177. Donald RG, Flint M, Kalyan N, Johnson E, Witko SE, et al. (2013) A novel approach to generate a recombinant toxoid vaccine against Clostridium difficile. Microbiology 159: 1254-1266.
178. Whitehead RH, Joseph JL (1994) Derivation of conditionally immortalized cell lines containing the Min mutation from the normal colonic mucosa and other tissues of an "Immortomouse"/Min hybrid. Epithelial Cell Biol 3: 119-125.
179. Hamlin JC, Pauly M, Melnyk S, Pavliv O, Starrett W, et al. (2013) Dietary intake and plasma levels of choline and betaine in children with autism spectrum disorders. Autism Res Treat 2013: 578429.
180. Montales MT, Melnyk SB, Simmen FA, Simmen RC (2014) Maternal metabolic perturbations elicited by high-fat diet promote Wnt-1-induced mammary tumor risk in adult female offspring via long-term effects on mammary and systemic phenotypes. Carcinogenesis 35: 2102-2112.
181. Ha G, Roth A, Khattra J, Ho J, Yap D, et al. (2014) TITAN: inference of copy number architectures in clonal cell populations from tumor whole-genome sequence data. Genome Res 24: 1881-1893.
182. Finney LA, O'Halloran TV (2003) Transition metal speciation in the cell: insights from the chemistry of metal ion receptors. Science 300: 931-936.
183. Outten CE, Tobin DA, Penner-Hahn JE, O'Halloran TV (2001) Characterization of the metal receptor sites in Escherichia coli Zur, an ultrasensitive zinc(II) metalloregulatory protein. Biochemistry 40: 10417-10423.
184. Llamas MA, Imperi F, Visca P, Lamont IL (2014) Cell-surface signaling in Pseudomonas: stress responses, iron transport, and pathogenicity. FEMS Microbiol Rev 38: 569-597.
185. de Reuse H, Vinella D, Cavazza C (2013) Common themes and unique proteins for the uptake and trafficking of nickel, a metal essential for the virulence of Helicobacter pylori. Front Cell Infect Microbiol 3: 94.

186. Porcheron G, Garenaux A, Proulx J, Sabri M, Dozois CM (2013) Iron, copper, zinc, and manganese transport and regulation in pathogenic Enterobacteria: correlations between strains, site of infection and the relative importance of the different metal transport systems for virulence. Front Cell Infect Microbiol 3: 90.
187. Honsa ES, Johnson MD, Rosch JW (2013) The roles of transition metals in the physiology and pathogenesis of Streptococcus pneumoniae. Front Cell Infect Microbiol 3: 92.
188. Schiavo G, Poulain B, Rossetto O, Benfenati F, Tauc L, et al. (1992) Tetanus toxin is a zinc protein and its inhibition of neurotransmitter release and protease activity depend on zinc. EMBO J 11: 3577-3583.
189. Blasi J, Chapman ER, Link E, Binz T, Yamasaki S, et al. (1993) Botulinum neurotoxin A selectively cleaves the synaptic protein SNAP-25. Nature 365: 160-163.
190. de Paiva A, Ashton AC, Foran P, Schiavo G, Montecucco C, et al. (1993) Botulinum A like type B and tetanus toxins fulfils criteria for being a zinc-dependent protease. J Neurochem 61: 2338-2341.
191. Ollivier N, Raibaut L, Blanpain A, Desmet R, Dheur J, et al. (2013) Tidbits for the synthesis of bis(2-sulfanylethyl)amido (SEA) polystyrene resin, SEA peptides and peptide thioesters. J Pept Sci.
192. Kabsch W (2010) Xds. Acta Crystallogr D Biol Crystallogr 66: 125-132.
193. Otwinowski Z, Minor W (1997) Proceesing of X-ray Diffraction Data Collected in Oscillation Mode. Methods in Enzymology. New York: Academic Press. pp. 307-326.
194. Bricogne G, Vonrhein C, Flensburg C, Schiltz M, Paciorek W (2003) Generation, representation and flow of phase information in structure determination: recent developments in and around SHARP 2.0. Acta Crystallogr D Biol Crystallogr 59: 2023-2030.
195. Adams PD, Grosse-Kunstleve RW, Hung LW, Ioerger TR, McCoy AJ, et al. (2002) PHENIX: building new software for automated crystallographic structure determination. Acta Crystallogr D Biol Crystallogr 58: 1948-1954.
196. Emsley P, Cowtan K (2004) Coot: model-building tools for molecular graphics. Acta Crystallogr D Biol Crystallogr 60: 2126-2132.
197. Ravel B, Newville M (2005) ATHENA, ARTEMIS, HEPHAESTUS: data analysis for X-ray absorption spectroscopy using IFEFFIT. J Synchrotron Radiat 12: 537-541.
198. Kleinman JG, McNeil JS, Schwartz JH, Hamburger RJ, Flamenbaum W (1977) Effect of dithiothreitol on mercuric chloride- and uranyl nitrate-induced acute renal failure in the rat. Kidney Int 12: 115-121.
199. de Paula QA, Liu Q, Almaraz E, Denny JA, Mangrum JB, et al. (2009) Reactions of palladium and gold complexes with zinc-thiolate chelates using electrospray mass spectrometry and X-ray diffraction: molecular identification of [Pd(bme-dach)], [Au(bme-dach]+ and [ZnCl(bme-dach)]2Pd. Dalton Trans: 10896-10903.
200. Plumb RC, Martell AE, Bersworth FC (1950) Spectrophotometric determination of displacement series of metal complexes of the sodium salts of ethylenediaminetetraacetic acid. J Phys Colloid Chem 54: 1208-1215.
201. Gergel D, Cederbaum AI (1996) Inhibition of the catalytic activity of alcohol dehydrogenase by nitric oxide is associated with S nitrosylation and the release of zinc. Biochemistry 35: 16186-16194.
202. Springman EB, Angleton EL, Birkedal-Hansen H, Van Wart HE (1990) Multiple modes of activation of latent human fibroblast collagenase: evidence for the role of a Cys73 active-

site zinc complex in latency and a "cysteine switch" mechanism for activation. Proc Natl Acad Sci U S A 87: 364-368.